Bi_2O_3-Layered Double Hydroxide Nanocomposites and Their Adsorption and Photocatalytic Properties

A Thesis

Submitted for the fulfilment of the requirements for the award of thedegree of

Doctor of Philosophy

Submitted by

Pooja Kumari

(Regn. No. 901809019)

THAPAR INSTITUTE
OF ENGINEERING & TECHNOLOGY
(Deemed to be University)

Under the Supervision of

Dr. Bonamali Pal
Professor

Dr. Raj Kumar Das
Assistant Professor

SCHOOL OF CHEMISTRY AND BIOCHEMISTRY

THAPAR INSTITUTE OF ENGINEERING AND TECHNOLOGY, PATIALA-147004 PUNJAB (INDIA)

February-2023

Certificate

This is to certify that the thesis entitled **"Bi_2O_3-Layered Double Hydroxide Nanocomposites and Their Adsorption and Photocatalytic Properties"**, being submitted by Miss. Pooja Kumari in fulfillment of the requirement for the award of the degree of Doctor of Philosophy in the School of Chemistry and Biochemistry, Thapar Institute of Engineering and Technology, Patiala (Punjab) India. It is a record of candidates own independent and original research work carried out by her under our supervision and guidance. The material embodied in this thesis has not been submitted in part or full for the award of any degree in any other University or Institute.

Dr. Bonamali Pal
Supervisor
School of Chemistry and Biochemistry
TIET
Patiala-147004
Punjab (India)

Dr. Raj Kumar Das
Supervisor
School of Chemistry and Biochemistry
TIET
Patiala-147004
Punjab (India)

Dr. Satnam Singh
Professor and Head
School of Chemistry and Biochemistry
Thapar Institute of Engineering and
TechnologyPatiala-147004
Punjab (India)

Candidate's declaration

I, hereby declare that the work presented in the thesis entitled **"Bi_2O_3-Layered Double Hydroxide Nanocomposites and Their Adsorption and Photocatalytic Properties "**, in fulfillment of the requirement for the award of the Degree of Doctor of Philosophy, School of Chemistry and Biochemistry, Thapar Institute of Engineering and Technology, Patiala (Punjab) India, is an authentic record of my own work carried out under the supervision of Dr. Bonamali Pal (Professor) and Dr. Raj Kumar Das (Assistant Professor), School of Chemistry and Biochemistry, Thapar Institute of Engineering and Technology, Patiala, India. The matter embodied in this thesis has not been submitted in part or full to any other university or institute for the award of any degree in India or abroad.

Pooja Kumari

Dr. Bonamali Pal

(Professor)

Dr. Raj Kumar Das

(Assistant Professor)

Acknowledgements

First and foremost, thanks to the God, the Almighty, for his showers of blessings throughout my research work to complete the research successfully.

The completion of thesis would not have been possible without the support and encouragement of several special people. I have many people to thank with my open arms for their help and probably words will fall short.

I would first like to express my heartiest thanks to my research supervisor **Dr. Bonamali Pal** and **Dr. Raj Kumar Das** I am greatly indebted to them for their kind guidance, constructive criticism, valuable suggestions, discussions, and moral support. They mentored me at each and every point from the elementarily steps to complex experimental design. They have always been pillars of support and constant source of inspiration. Without their persistent help, the goal of this project would not have been realized.

I am also extremely thankful to the Director, Dean (Research & Sponsored Projects) **Dr. Rafat Siddique, and Dr. Satnam Singh**, Head, School of Chemistry & Biochemistry, Thapar University, for extending the opportunity to undertake this doctoral research. I am highly indebted to my doctoral committee members; **Dr. Soumen Basu** and **Dr. Davinder and Dr. S.D Tiwari** for their timely valuable suggestions. My sincere thanks also go to **Mr. Chander Thakur**, and office staff **Mr. Mayank** for their cooperation, support and help.

I would like to acknowledge **Dr. Sakshi Sharma, Dr. Samriti thakur, Dr. Aadil Bathla, Dr. Manpreet kaur**, **Miss. Manjusha**, **Miss. Harpreet, Miss Jemini , Miss Palak , Miss Preeti ,Miss Mehak and Miss Davinder** and all my juniors for their support and co-operation.

I am indebted to my parents, my father, **Mr. Bhushan Bansal** who had been a source of motivation and encouragement in my life. I would like to acknowledge my mother **Mrs. Kanta Bansal** for all the sacrifices she has made for me. I would also like to acknowledge constant love and support from my brother **Rahul Bansal**.

Words cannot express how grateful I am to my in-laws, my father-in-law **Mr. Arun Garg** and mother-in-law **Mrs. Meenakshi Garg** for their unconditional love, unending support and blessings when I needed the most during my difficult times. I would like to acknowledge my brother-in-law, **Mr. Mehul Garg** for his affection and love.

Last but not the least I would like to acknowledge my husband **Er. Sahil Garg** for his unquestioned faith and support, thank you for being my backbone throughout this entire journey. Love to my son ***Ayaan Garg*** , who has made me stronger ,better and more fulfilled.

Besides this, I am thankful to the persons who knowingly and unknowingly helped me during the successful completion of this work.

Pooja Kumari

Table of contents

Chapter 1

Introduction and literature survey

Chapter 2

Preparation and characterization of phase pure monoclinic α-Bi_2O_3 nanoparticles and influence of Ni^{2+} and Cu^{2+} impregnation on their photocatalytic properties

Chapter-3

Superior adsorptive removal of eco-toxic drug diclofenac sodium by Zn-Al LDH.xBi_2O_3 layer double hydroxide composites

Chapter 4

Enhanced photocatalytic degradation of eco-toxic pharmaceutical waste diclofenac sodium by anion loaded Cu-Al LDH·Bi_2O_3 composites

Chapter 5

Superior cooperative adsorption of methylene blue and naproxen by Ni-Al LDH.xBi_2O_3 layered double hydroxide composites

DEDICATED TO MY PARENTS

List of abbreviations

a.u.	Arbitrary unit
NP	Nanoparticles
LDH	Layered double hydroxide
Bi_2O_3	Bismuth trioxide
Nm	Nanometer
BET	Brunauer Emmett Teller
BJH	Barrett-Joyner-Halenda
DRS	Diffuse reflectance spectroscopy
EDS	Energy dispersive X-ray spectroscopy
UV	Ultraviolet spectroscopy
XRD	X-ray diffractometery
HRTEM	High resolution transmission electron Microscopy
JCPDS	Joint committee on powder diffraction Standards
L	Length
M	Metal
mL	Milli-litre
mM	Milli molar
Mol	Mole
UV	Ultra Violet
Vis	Visible
FTIR	Fourier Transform Infra-red
Pzc	Point of zero charge
DI	Distilled water
M^{n+}	Metal ion

List of symbols

%	Percentage
μ	Micron
L	Litre
M	Molar
K	Kelvin
v/v	Volume by volume
w/v	Weight by volume
β	Beta
°C	Degree Celsius
θ	Angle
C	Carbon
H	Hydrogen
N	Nitrogen
O	Oxygen
Al	Aluminium
Hg	Mercury
A	Alpha
Γ	Gamma
Cu	Copper
Fe	Iron
Ni	Nickel
Bi	Bismuth
Zn	Zinc
Ag	Silver
Au	Gold
Å	Amstrong
Cu	Copper
Π	Pi

Abstract

The present study in this thesis focus on the bismuth trioxide (Bi_2O_3) based nanoparticles and their nanocomposites with metal loaded ions or layered double hydroxides to know its applications in real life. Due to simpler synthesis and low cost of these nanoparticles and high efficiency these particles are modified with several other metals or LDHs to know its adsorption and photo catalytic performance. This complete thesis is divided into five chapters which are given below:

Chapter 1

This chapter signifies the modification of Layered double hydroxide and Bi_2O_3 by varying their molar/mass ratio in order to enhance its adsorption as well as photo catalytic properties. The importance of variation in the molar/mass ratio of Bi_2O_3 shifts the absorption spectra in visible region and their impact on surface and electrokinetic properties. Further, as LDH and metal ion loading on Bi_2O_3 surface improve surface area , zeta potential properties, hydrodynamic size and heterojunction behaviour of Bi_2O_3 has been discussed. In this respect, research gaps have been mentioned and various methodologies adopted to complete the objectives that have been presented.

Chapter 2

This chapter describes the introduction about bare Bi_2O_3 nanoparticles, metal ion loaded (Ni and Cu) Bi_2O_3 nanoparticles and their application in Naproxen and Fuschian Blue degradation under visible light irradiation. Introduction, literature review, research gap, objectives, and characterization techniques are discussed in this chapter.

Chapter 3

This Chapter signifies efficient removal of eco-toxic pollutant diclophenac sodium (DCF) from wastewater. However, low adsorption capacity, high cost of conventional adsorbents limits their

utility. In this context, Bi_2O_3 loaded Zn-Al layer double hydroxide (LDH) heterostructures (Zn-Al LDH. x Bi_2O_3, x= 0 to 3) have been investigated as a potential adsorbent for DCF removal .The XRD patterns confirm formation of both LDH and α-Bi_2O_3 phases. The flower-like morphology is evident by SEM, XPS and EDS confirm Bi_2O_3-LDH composite. Higher Bi_2O_3 loading leads to increase in the hydrodynamic sizes of the composite structure. The BET surface area and zeta potential also varies significantly with extent of loading. DCF adsorption of these composites obey the Langmuir adsorption isotherm model suggesting monolayer adsorption process whereas the intra-particle diffusion model indicates that the adsorption of DCF primarily occurs on the exterior surface. The heterostructure with x=1 exhibited ~10 times higher adsorption capacity compared to bare LDH owing to its highest surface area and positive zeta potential.

Chapter 4

This chapter describe the non-steroidal drug diclofenac sodium (DCF) has emerged as hazardous pollutant due to its eco-toxic nature and its efficient elimination from wastewater is emerging as crucial problem. But, low activity, high cost and instability of the conventional photocatalysts restrain their use. In this study, different anion impreganted Cu-Al layered double hydroxides (LDH) and Bi_2O_3 derived hetero-composites have been examined as plausible photocatalysts for degradation of DCF under visible light radiation. The BET sorption isotherms indicate that the anion loaded composites are having larger specific surface area than the pristine one. Also, upon anion impregnation the zeta potential values shift towards more negative values confirming absorption of anions. They show significantly higher (65% for carbonate and 83% for sulphate) photcatalytic activity compare to the parent hybrid (53%). Here, the anions act as efficient electron scavengers to suppress the electron-hole pair recombination. The individual photocatalytic reactions follow pseudo-first order kinetics. Due to low cost, simpler preparation, enhanced activity and recyclability the anion loaded derivatives can emerge as excellent catalysts.

Chapter 5

This chapter signifies the Ni-Al LDH–Bi_2O_3 (1:1) and Ni-Al LDH–Bi_2O_3 (1:2) LDHs have been prepared for the removal of multi-component system. These nano-catalysts were prepared by

simple co-precipitation method and characterized by XRD, FESEM, EDS, Mapping, XPS, zeta, DLS and HRTEM etc. The XRD spectra confirm the presence of Bi_2O_3 in the NiAl LDH. Sphere like morphology is evident by HRTEM analysis. XPS studies confirm that nickel is present in 2+ oxidation state. EDS spectra confirm the presence of Ni, Al, Bi and O elements in the sample. Particle size increases on Bi_2O_3 loading has been confirmed by HRTEM and hydrodynamic size. Multi-component (NPX+MB) system and bare ones follow freundlich adsorption isotherms. Moreover, NPX follows pseudo-second order kinetics and MB follow pseudo-first order kinetics. Larger adsorption capacity and cost effectiveness and high efficiency, these hetero-materials could act as good adsorbents for dye and pharmaceuticals from waste water.

Chapter 1 Introduction and literature

1.1 Introduction and literature survey

1.1.1 Metal-Bi_2O_3 nanocomposites show better and enhanced photocatalytic activities due to reduced recombination rates of generated charge carriers (e^-/h^+ pairs) and extended visible light absorptions [1-2]. At metal- Bi_2O_3 heterojunction, fermi level equilibration takes place due to work function difference between the metal and Bi_2O_3, enhancing the interfacial charge transfer process [3-5]. In this regard, Bi_2O_3 has been loaded/doped with various kind of metals or non-metals and their oxides [6-8]. Generally the photo-deposition and co-precipitation methods have been used for the preparation of metal loaded Bi_2O_3 nanoparticles (NP's). In the photodeposition method, metal ionic species having redox potential more positive than the conduction band (CB) potential of Bi_2O_3 act as electron scavangers and are reduced to lower or zero oxidation states in an inert atmosphere of argon and get adsorbed on the surface of Bi_2O_3[9]. Ag and CuO modified Bi_2O_3 nanoparticles have been investigated to have higher photocatalytic degradation rates for phenol and acetic acid than unmodified Bi_2O_3. Photo-catalysis is defined as the acceleration of a photoreaction by the presence of catalyst [10].When a photocatalyst is illuminated by an appropriate wavelength, electrons in the valence band are excited to conduction band to give an electron (e^-)-hole (h^+) pairs. These photogenerated charge carriers perform different redox reactions on the surface of semiconductor. Therefore combination of a photocatalyst and UV (visible light) can be used for the treatment of wastewater treatment. In order to reduce protons and oxidize oxygen ions, a photocatalyst should possess high band gap energy than the energy required for such process. Furthermore, the energy levels of the valence band and conduction band should be compatible for with those of the species to be oxidized or reduced and the

electrons promoted in the conduction band should have much negative potential than the substrate (X), and the holes left behind the valence band should possess higher positive potential than that particular system(Y) as shown in scheme 1. In the last three decades, a great number of semiconductors such as TiO_2, SnO_2, WO_3, RuO_3, Bi_2O_3, $BiVO_4$ and Fe_2O_3 have been investigated for overall photocatalytic process, out of which Bi2O3 is found to be attractive, safe, non-toxic and non-carcinogenic[11].

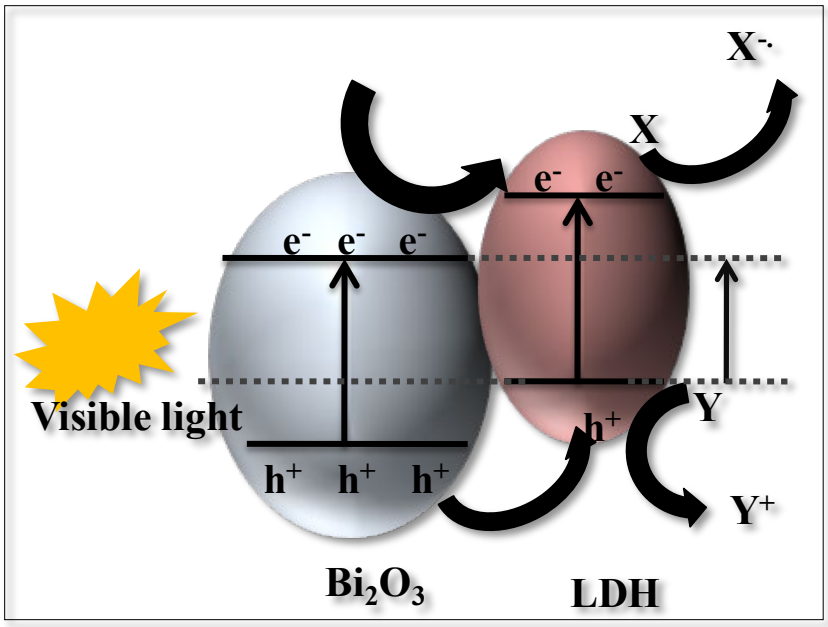

Scheme 1: Schematic Representation of the different redox reactions under light irradiation

In order to improve these problems LDH were utilized to modify the structure and properties of bismuth oxide-type semiconductor. Generally, heterostructured between a bismuth oxide type material and LDHs was synthesized by a layer-by-layer method [12], in which LDH was in-situ synthesized on a previous formed bismuth oxide type material, or in an opposite way. Besides, in order to accelerate the growth of heterostructured, the fabrication usually processed in a

hydrothermal environment [13-15].As for the application, heterostructured showed visible-light activities towards organic decompositions.

Literature revealed that if a particular (same) metal in its trivalent state is fixed by variation in the divalent metal (Ni^{2+}, Cu^{2+},Fe^{2+} etc) in LDHs, it will lead to different d-electronic states of the metal, different work functions, Lewis acidities, sizes, surface area and charge densities thus leading to different affinities for organic and inorganic molecules. For example if Ni^{+2} or Cu^{2+} with constant trivalent metal Al^{3+} are loaded with LDH, due to different ionic radii, zeta potential, optical absorption spectrum and redox potential values of different metal there is difference in the binding ability of substrate molecule that leads to variation in the photocatalytic or adsorption performance. Thus, the photocatalysts having high adsorption capabilities can be utilized for the separation and degradation of different kind of pollutants such as pharmaceuticals, disinfectants, pesticides, herbicides and waste water contaminants such as dye molecules that exhibit different ionic interactions. The combination of a photocatalyst and UV (visible light) can be used for the treatment of wastewater pollutants. When a photocatalyst is illuminated by an appropriate wavelength, various organic compounds are oxidized and mineralized on the surface of the photocatalyst or oxidized in the solution. During a photocatalysis process, the redox reaction [16-17] is associated with the electron–hole pairs and the adsorbed molecules on the surface of the catalyst. In comparison to single LDH photocatalysts, LDH-based hybrid [18] semiconductors possess significant advantages in terms of reduced recombination rate of electron–hole pairs due to various charge carrier transfer pathways. The efficient electron–hole transfer from one component to another with a suitable band edge position can facilitate the separation of the photo-induced electron–hole pairs and

increase the lifetime of charge carriers, and consequently, enhance the photocatalytic efficiency [19-20].

In order to improve the utilization efficiency of photo-excited electrons and holes in heterogeneous photocatalytic processes, the synthesis of hybrid LDHs would be a great strategy. Hybrid LDHs [21] improve the optical absorption and utilization of the visible light region for photocatalysts as well as enhancing the mobility and the separation rate of charge carriers. Since the initial work of Miyata, a large number of hybrid LDH materials have been developed as semiconductor photocatalysts for environmental purification. In any hybrid assembly, [22] the nature of the bond between two components is crucial. In LDHs, the foreign species interact with the hydroxide layer mainly by electrostatic and vander Waal's forces and the hydrated interlayer space becomes stabilized due to the development of an integrated hydrogen-bonding network among anions, water molecules, and OH groups of the host layers. In addition, hybrid LDHs can be prepared by different anion-intercalated LDHs as precursors. Further, active species can be intercalated into the interlayers of LDHs to form LDH intercalated [23-25] hybrid materials. In addition, LDH nanolayers can be employed to produce hybrids or heterostructured by restacking or layer-by-layer (LbL) assembly techniques.

1.2 LDH nanocomposites

Single LDH catalysts might not be able to meet the requirements of high-performance photo catalysis, for example, narrow band gap, large specific surface area, and effective electron–hole pair separation. However, most reported LDHs used for photocatalytic degradation of organic pollutants are mainly focused on trivalent cation-based transition metals, such as Cr and Ti. It was reported that a TiO_2/LDH [26] composite exhibited superior photocatalytic properties than

TiO_2 due to the presence of the TiO_2/LDH heterojunction, which facilitated the spatial separation between photo-generated electrons and holes. Garcia et al. synthesized Zn/Cr LDH for O_2 evolution [27] under visible light irradiation for the first time.

Although Zn-Cr LDH displays [28] a broad visible light absorption spectrum, its practical application in wastewater treatment still needs to be further modified. Graphene-based Zn Cr LDH hybrid nanocomposites facilitated the transportation and separation of photogenerated charge carriers and improved the photocatalytic degradation of rhodamineB (RhB). Novel a-Ag_2WO_4/ ZnCr-based LDH [29] composites were fabricated by an anion exchange precipitation reaction method, in which $AgNO_3$ solution was added into tungstate intercalated ZnCr LDH. The obtained nanocomposites exhibited superior visible light photocatalytic degradation efficiency toward RhB dye. Upon photon excitation, the electrons migrated from the CB of Zn-Cr LDH to the CB of a-Ag_2WO_4, whereas the photogenerated holes moved from the VB of a-Ag_2WO_4 to the VB of Zn-Cr LDH, thus inhibiting the recombination of photo-generated electron–hole pairs to achieve enhanced photo efficiency [30]. Parida et al. synthesized $LaFeO_3$ (LFO) and Zn-Cr LDH-based highly photoactive composites. Cu_2O is a narrow band gap semiconductor; therefore, it is a potential candidate for photocatalytic organic pollutant degradation [31]. MgAl LDH is inactive in the visible region due to wide band gap energy. However, Cu_2O/MgAl LDH composites manifested superior photocatalytic efficiency toward MB degradation. The minima of the CB for MgAl LDH and Cu_2O existed at −0.61 eV and −1.3 eV, respectively. Therefore, LDHs accepted photo-generated electrons and holes from Cu_2O and then reacted with OH^- to form $^{\cdot}OH$. Komarneni et al. prepared AgCl- BiOCl- NiFe LDH composites [32] from Ni Fe LDH precursors for RhB degradation under visible light irradiation. The electrons and holes were formed on the surfaces of the photocatalysts and AgCl effectively

prevented the recombination of electrons and holes. Bromide (Br)-based Ag/AgBr/Co-Ni-NO_3 LDH nanocomposites [33] were synthesized from CoNi LDH precursors by an anion-exchange precipitation method for photocatalytic applications. The composite was prepared by adding the $AgNO_3$ solution to the Co-Ni-Br LDH solution, and the Ag/AgBr nanoparticles were found to be highly dispersed on Co-Ni-NO_3 LDH sheets. The degradation activity of prepared nanocomposites was examined on MO, RhB, and phenol. In recent years, a large number of studies have been carried out on bismuth oxide (Bi_2O_3) nanocomposites [34]. Bi_2O_3 behaves like an anionic clay and usually has a favorable VB position formed by the Bi 6s orbital or a hybrid orbital of Bi 6s and O 2p; therefore, its narrow band gap facilitates the photocatalysis. However, the narrow band gap energy manifests excessive recombination rate of electron–hole pairs, low charge-carrier mobilities, and poor oxidative kinetics for dye degradation. Hence, a Bi_2O_3/LDH composite has been calcined and modified with Pd (II) for photocatalysis applications [35].

1.2 Research Gaps:

On the basis of literature studies, following research gaps have been realized which will be fulfilled in the present research proposal: There are reports available on the nanocomposites of layered double hydroxides (LDHs) with Bi_2O_3 nanocatalysts. However, there are no reports found on the interchange of a particular metal in its divalent states comparing the effects of variable metal on photocatalytic behaviours of $[M^{2+}_{1-x}\ Al^{3+}_{x}(OH)_2]^{\ q+}\ [A^{n}\text{-}_{q/n}\cdot mH_2O]$, LDH. where M^{2+} and M^{3+} are divalent and trivalent metal cations respectively. There are also reports on the study of electrochemical properties and surface properties such as surface area, zeta potential and of bismuth trioxide-layered double hydroxides nanocomposites of different shapes

and morphologies, but no reports are present on tuning these LDHs with Bi_2O_3 by interchanging divalent metal ion in LDHs or by variation in the ratios of particular LDH.

Based on the above mentioned research gaps, my research will focus on the synthesis of Bi_2O_3 NP's and their nanocomposites with layered double hydroxides by variable mass ratio or by changing the divalent metal ion in LDHs to tune its band energetic and study the effect of variable divalent metal on various electrochemical parameters of catalysts, adsorption isotherms and degradation kinetics for the photocatalytic degradations of some of the organic and inorganic water pollutants produced by pharmaceutical and dyeing industries. For example, M^{2+} (Ni^{2+},Zn^{2+},Cu^{2+}etc) can be used with Al^{3+} etc metal to evaluate its photocatalytic activities but on the other hand its various divalent metals can be utilised for manipulating different surface structural properties of nanocatalysts, adsorptions and effective photocatalytic degradation processes. The originality and novelty of this chapter is that the metal ion incorporation plays dual role. Due to different oxidation states of the metal ions impregnated into Bi_2O_3 the surface charge over Bi_2O_3 will change , surface structural properties of Bi_2O_3 will change after metal ion impregnation. As a result adsorption properties, zeta potential and surface structural properties will modify. Moreover,metal ion loading also prevent the e-hole recombination of the Ni^{2+}/Cu^{2+}composites during light irradiation thereby it will improve the photo catalytic property.

1.3 Objectives

1. Preparation and characterization of Bi_2O_3, LDHs (Zn-Al, Ni-Al, Cu-Al etc) and their nanostructures.

2. Influence of Bi_2O_3 loading on LDHs loading for surface structure and physiochemical properties.

3. To evaluate adsorption and photocatalytic properties of model pollutants by different as prepared nanostructures.

1.4 Methodology:

1.4.1 Preparation of Bi_2O_3 and M^{n+}-Bi_2O_3 nanocatalysts : Preparation of Bi_2O_3 was done by simple co-precipitation method and its procedure is given in brief in chapter 2 under heading (2.2.2 Synthesis of Bi_2O_3 nanoparticles). Metal-Bi_2O_3 nanoparticles (M^{+n}-Bi_2O_3) have been prepared by using different salts of a metal via wet impregnation method. Brief procedure is given in chapter 2, section b under heading 2.2.3 (Synthesis of M^{n+}-Bi_2O_3 nanocomposites M^{2+}= Ni, Cu)

1.4.2 Synthesis of Bi_2O_3 and Zn-Al LDHs nanoparticles: Zn-Al LDHs were synthesized by hydrothermal method (Scheme 2). Brief procedure is given in chapter 3, section under heading (3.2.3 Synthesis of Zn-Al layer double hydroxides (LDH). Zn-Al LDHs their nanocomposites with different mass ratios of Bi_2O_3 were detailed discussed in chapter 3, under heading 3.2.3.(Synthesis of Zn-Al LDH x.Bi_2O_3 x = 0.33, 0.5, 1, 2, 3 composite).

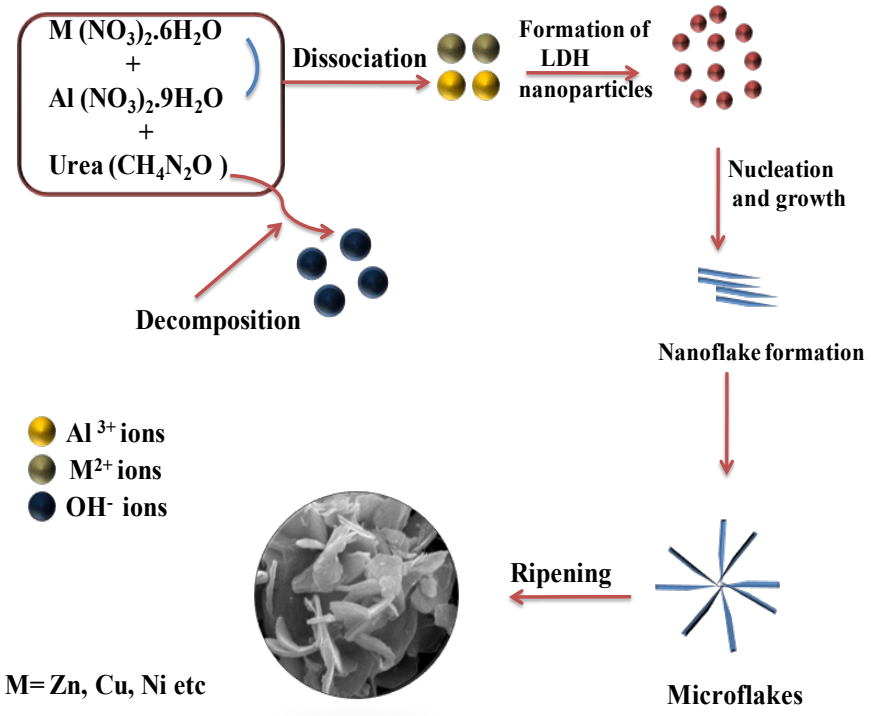

Scheme 2: Schematic Representation for the synthesis of different LDHs

1.4.3 Cu-Al/Ni-Al LDH-Bi_2O_3 nanocomposites: Anion impregnated Cu-Al LDH-Bi_2O_3 were synthesized by simple method and the detailed procedure is discussed in chapter 4, and under heading (4.2.2 Preparation of Carbonate and Sulphate Impregnated Hybrids Cu-Al LDH·Bi_2O_3-CO_3^{2-} and Cu-Al LDH·Bi_2O_3-SO_4^{2-})

1.5 Characterization Techniques: Phase and crystal properties were investigated by X-ray diffraction (XRD**,** analytical xpert pro) using Cu-Kα (1.54 Å) with diffraction angle 2θ (20°-80°) operating at 45 kV. The morphology and the structure of prepared samples were investigated by scanning electron microscopy (SEM) and high-resolution transmission electron microscopy (HRTEM, FEI Tecnai G2 F20, Netherlands operating at 200 kV). Besides, the oxidation state of the catalyst was examined using X-ray photoelectron spectroscopy (XPS, KRATOS axis 165 Shimadzu) with Mg-Kα radiations at 75 W. The elemental composition ratio was investigated by energy dispersive spectroscopy (SEM-EDS, JEOL JSM-7600 F) operated at 30 kV. Besides, the optical absorbance spectra was carried out on diffuse reflectance spectroscopy (DRS, Avantes) using $BaSO_4$ as an internal standard. Moreover, the emission spectrum was analyzed by spectro-fluorimeter (Perkin-Elmer LS55) at room temperature.

1.6 Adsorption and photocatalytic activity:

Adsorption isotherm for different toxic pollutants by different as prepared nanocomposites has been demonstrated by Langmuir and Freundlich adsorption isotherm models. A relationship between the amount of toxic pollutants adsorbed and the equilibrium concentration is given by the following equations:

$$\frac{C_e}{q_e} = \frac{C_e}{q_{max}} + \frac{1}{K_L q_{max}}$$

$$\log q_e = \log K_F + \log C_e$$

Where, q_e is the adsorption quantity at equilibrium, q_{max} is the adsorption at maximum corresponding to Langmuir model, C_e is the adsorbate concentration at equilibrium, K_L and K_F are the constants of Langmuir and Freundlich models, and n is the adsorption intensity factor. Thus, a plot of C_e/q_e versus C_e will be a straight line with slope equal to $1/q_{max}$ and intercept equal to $1/K_Lq_{max}$ and similarly in Freundlich model the plot of log q_e versus C_e will have slope 1/n and intercept equal to log K_F. Detailed method is discussed in chapter 3 under section (3.2.5 adsorption studies)

Photocatalytic oxidations of different type of pharmaceutical and waste water dyes were done in a test tube containing 5 mL of the varying concentrations of substrate molecules using different amounts of the catalyst in the presence of light irradiation with continuous stirrings. Kinetics studies viz. adsorption isotherms and degradations, order of the reaction (n) and rate constants (k) were studied systematically. From the plot of A_0/ A_t versus time rate constant values has been calculated. Detailed procedure is discussed in chapter 2 and 4 under section (2.2.5 and 4.2.5 Photo catalytic activity)

$$\mathbf{Rate = (A_o - A_t) / A_o}$$

A_o is the initial absorbance at t_o

A_t is the absorbance at time t

Several hazardous dyes and pharmaceutical wastes which will be adsorbed and

S.No	Name of compound	Structure	Source	Hazardous effects
1.	Naproxen	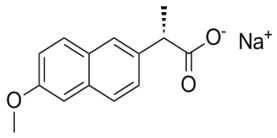	Pharmaceuticals product	tiredness, drowsiness, dizziness and rashes
2.	Basic dye Fuchsin Blue	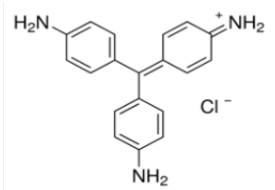	Waste water of dying industries	Bladder cancer, tuberculosis and leprosy
3.	Diclofenac Sodium	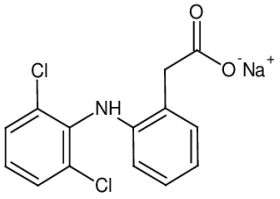	Pharmaceuticals product	osteoarthritis and rheumatoid arthritis.

photocatalytically degraded using the prepared nanostrucutres. Some of the examples are given in the table.

References

1. D. Majhi, PK. Samal, K. Das, SK. Gouda, YP. Bhoi, BG. Mishra, α-NiS/Bi_2O_3 nanocomposites for enhanced photocatalytic degradation of tramadol, ACS Appl. Nano Mater. 2 (2018) 395-407.
2. A. Hameed, V. Gombac, T. Montini, L. Felisari, P. Fornasiero, Photocatalytic activity of zinc modified Bi_2O_3, Chem. Phys. Lett. 483(2009) 254-61.
3. V. Ramakrishnan, KG. Nair, J. Dhakshinamoorthy, KR. Ravi, B. Pullithadathi, Porous, n–p type ultra-long, ZnO@Bi_2O_3heterojunction nanorods-based NO_2 gas sensor: new insights towards charge transport characteristics. 22 (2020) 7524-36.
4. NK. Eswar, S. Adhikari, PC. Ramamurthy, G. Madras, Efficient interfacial charge transfer through plasmon sensitized Ag@Bi_2O_3 hierarchical photoanodes for

photoelectrocatalytic degradation of chlorinated phenols, Phys. Chem. Chem. Phys. 20 (2018) 3710-23.

5. S. Martha, PC. Sahoo, KM. Parida, An overview on visible light responsive metal oxide based photocatalysts for hydrogen energy production, RSC Adv. 5 (2015) 61535-53.

6. P. Riente, T. Noël, Application of metal oxide semiconductors in light-driven organic transformations, Catal. Sci. 9 (2019) 5186-232.

7. A. Hezam, K. Namratha, D. Ponnamma, QA. Drmosh, AM. Saeed, KK. Sadasivuni, K. Byrappa, Sunlight-Driven Combustion Synthesis of Defective Metal Oxide Nanostructures with Enhanced Photocatalytic Activity, ACS omega. 4 (2019) 20595-605.

8. Z. Zhang, JT. Yates, Band bending in semiconductors: chemical and physical consequences at surfaces and interfaces, Chem. Rev. 112 (2012) 5520-51.

9. A. Zaleska Doped-TiO_2: a review. Recent patents on engineering, 2 (2008) 157-64**.**

10. SC. Chan, MA. Barteau, Preparation of highly uniform Ag/TiO_2 and Au/TiO_2 supported nanoparticle catalysts by photodeposition, Langmuir 21 (2005) 5588-95.

11. L.Wang, T. Egerton, The effect of transition metal on the optical properties and photoactivity of nano-particulate titanium dioxide, J. Mater. Sci. 1 (2012) 19.

12. MI. Litter, Heterogeneous photocatalysis: transition metal ions in photocatalytic systems, Appl. Catal., B. 23 (1999) 89-114.

13. A. Roguska, A. Kudelski, M. Pisarek, M. Opara, M. Janik-Czachor, Surface-enhanced Raman scattering (SERS) activity of Ag, Au and Cu nanoclusters on TiO_2-nanotubes/Ti substrate, Appl. Surf. Sci. 257 (2011) 8182-9.

14. MT. Greiner, L. Chai, MG. Helander, WM. Tang, ZH. Lu, Transition metal oxide work functions: the influence of cation oxidation state and oxygen vacancies, Adv. Funct. Mater. 22 (2012) 4557-68.

15. C. Karuppiah, M. Velmurugan, SM. Chen, SH. Tsai, BS. Lou, MA. Ali, FM. Al-Hemaid, A simple hydrothermal synthesis and fabrication of zinc oxide–copper oxide heterostructure for the sensitive determination of non-enzymatic glucose biosensor, Sensor Actuat B-Chem 221 (2015) 1299-306.

16. NA. Aziz, P. Palaniandy, HA. Aziz, I. Dahlan, Review of the mechanism and operational factors influencing the degradation process of contaminants in heterogenous photocatalysis, J. Chem. Res. 40 (2016) 704-12.

17. X. Li, J. Ye, Photocatalytic degradation of rhodamine B over $Pb_3Nb_4O_{13}$/fumed SiO_2 composite under visible light irradiation, J. Phys. Chem. 111 13109-16.
18. SJ. Moniz, SA. Shevlin, DJ. Martin, ZX Guo, J. Tang, Visible-light driven heterojunctionphotocatalysts for water splitting- a critical review, Energy Environ. Sci. 8 (2015) 731-59.
19. H. Zhou, W. Cai, J. Li, X. Liu, W. Xiong, Y. Zhou, Z. Xu, B.Wang, C. Ye, C $_2$N/ BluePvander Waals hetero-structure: an efficient photocatalytic water splitting 2D material, Phys. Chem. Chem. Phys 22 (2020) 1485-92.
20. WH. Yang, WC. Lu, KM. Ho, CZ. Wang, Hybrid silicon–carbon nanostructures for broadband optical absorption, RSC Adv. 7 (2017) 8070-6.
21. HM. Liu, XJ. Zhao, YQ. Zhu, H. Yan, DFT study on Mg Al-layered double hydroxides with different interlayer anions: structure, anion exchange, host–guest interaction and basic sites, Phys. Chem. Chem. Phys 22 (2020) 2521-9.
22. M. Laipan, J. Yu, R. Zhu, J. Zhu, AT. Smith, H. He, D. O'Hare, L. Sun, Functionalized layered double hydroxides for innovative applications. Mater. Horiz. 7 (2020) 715-45.
23. Q. Zhang, Q. Gu, F. Leroux, P. Tang, D. Li, Y. Feng, Co-intercalated layered double hydroxides as thermal and photo-oxidation stabilizers for polypropylene Beilstein, J. Nanotechnol. 9 (2018) 2980-8.
24. AE. Stamate, OD. Pavel, R. Zavoianu, IC. Marcu, Highlights on the Catalytic Properties of Polyoxometalate-Intercalated Layered Double Hydroxides: A Review. Catalysts.10 (2020) 57.
25. G. Starukh, O. Rozovik, O. Oranska, Organo/Zn-Al LDH nanocomposites for cationic dye removal from aqueous media. Nanoscale Res. Lett. 11 (2016) 228.
26. JC. Contreras-Ruiz, S. Martínez-Gallegos, JL. García-Rivas, JC. González-Juárez, E. Ordoñez, Influence of the synthesis method on the preparation composites derived from TiO_2-LDH for phenol photodegradation, Sustain. Environ. Res. 2 (2018) 27.
27. MG. Peleyeju, OA. Arotiba, Recent trend in visible-light photoelectrocatalytic systems for degradation of organic contaminants in water/wastewater, Environ. Sci. Water Res. 4 (2018) 1389-411.
28. M. Mercuri, R. Gimenez, CL. Berli, MG. Bellino, Configurable 2D nano-flows in mesoporous films using paper patches. RSC Adv. 8 (2018) 6414-8.

29. H. Tang, S. Chang, G. Tang, W. Liang, AgBr and g-C_3N_4 co-modified Ag_2CO_3 photocatalyst: a novel multi-heterostructured photocatalyst with enhanced photocatalytic activity. Appl. Surf. Sci. 391 (2017) 440-8.
30. J. Ma, J. Ding, L. Yu, L. Li, Y. Kong, S. Komarneni, BiOCl dispersed on Ni Fe–LDH leads to enhanced photo-degradation of Rhodamine B dye, Appl. Clay Sci. 109 (2015) 76-82.
31. H. Fan, J. Zhu, J. Sun, S. Zhang, S. Ai, Ag/AgBr/Co–Ni–NO_3 layered double hydroxide nanocomposites with highly adsorptive and photocatalytic properties, Chem. Eur. J. 19 (2013) 2523-30.
32. M. Alqathami, A. Blencowe, M. Geso, G. Ibbott, Quantitative 3D determination of radiosensitization by bismuth-based nanoparticles, J. Biomed. Nanotechnol. 12(3) 2016 464-71.
33. L. Mohapatra, K. Parida, A review on the recent progress, challenges and perspective of layered double hydroxides as promising photocatalysts, J. Mater. Chem. 4 (2016) 10744-66.
34. H. Kunioku, M. Higashi, O. Tomita, M. Yabuuchi, D. Kato, H. Fujito, H. Kageyama, R. Abe,Strong hybridization between Bi-6s and O-2p orbitals in Sillén–Aurivilliusperovskite Bi_4MO_8X (M= Nb, Ta; X= Cl, Br), visible light photocatalysts enabling stable water oxidation, J. Mater. Chem. 6 (2018) 3100-7.
35. VP. Zhukov, VM. Zhukovskii, VM. Zainullina, NI. Medvedeva, Electronic structure and chemical bonding in bismuth sesquioxide polymorphs. J. Struct. Chem. 40 (1999) 831-7.
36. RP. Wijitwongwan, SG. Intasa-ard, M. Ogawa, Preparation of Layered Double Hydroxides toward Precisely Designed Hierarchical Organization, *Chem. Eng. 3* (2019) 68.
37. IA. Ahmed, NS. Al-Radadi, HS, Hussein, AH. Ragab, Environmentally Friendly Mesoporous Nanocomposite Prepared from Al-Dross Waste with Remarkable Adsorption Ability for Toxic Anionic Dye, New J. Chem. 302019 (2019).
38. N. Kumar, H. Mittal, SM. Alhassan SS. Ray, Bio nanocomposite hydrogel for the adsorption of dye and reusability of generated waste for the photodegradation of ciprofloxacin: a demonstration of the circularity concept for water purification. ACS Sustain Chem Eng. 6 (2018) 17011-25.

39. BD. Viezbicke, S. Patel, B E Davis and DP. Birnie, III, Evaluation of the Tauc Method for Optical Absorption Edge Determination: ZnO Thin Films as a Model System, Physica Status Solidi, B. 252 (2015) 1700-1710
40. A. Misra , P. Kumar, R. Srivastava, S. Dhawan, K. Kamalasanan, MN. Chandra, Subhas, Electrochemical and optical studies of conjugated polymers for three primary colours, Ind. J. Appl. Phys. 43(2005) 921-925.

Chapter-2

Preparation and characterization of phase pure monoclinic α-Bi_2O_3 nanoparticles and influence of Ni^{2+} and Cu^{2+} impregnation on their photocatalytic properties

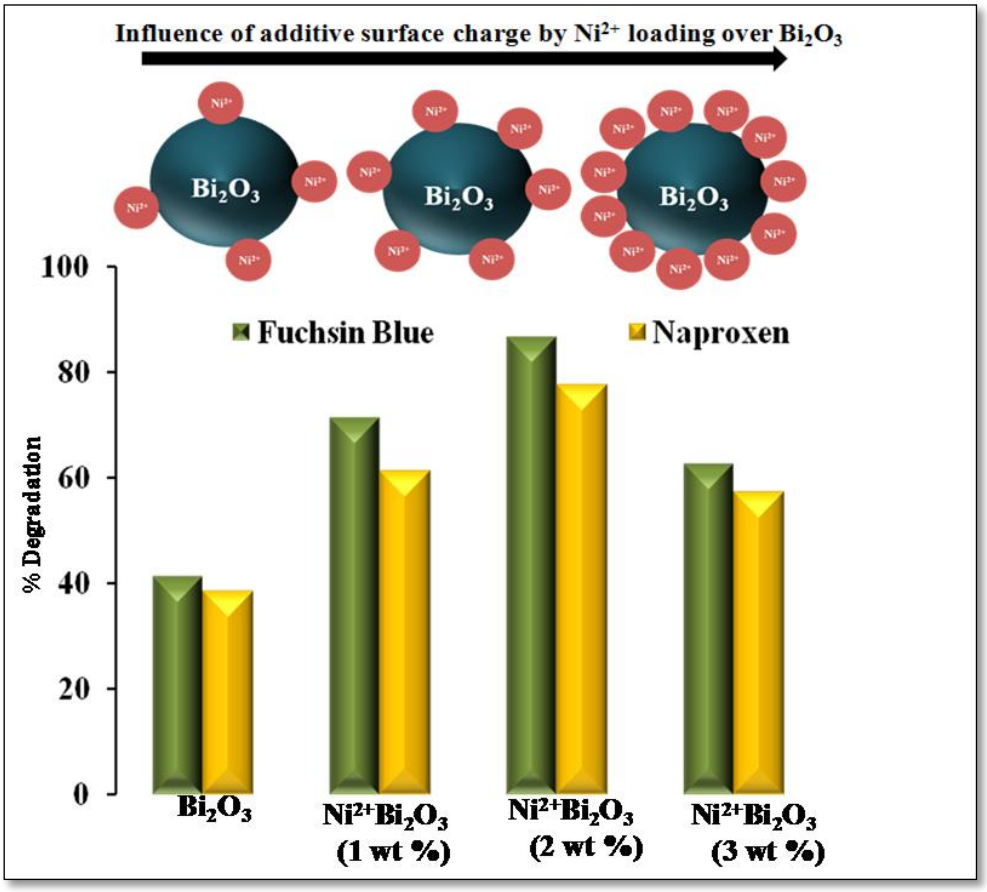

Summary:

In this chapter, metal ions impregnated (Ni^{2+} and Cu^{2+}) Bi_2O_3 hetero-structures have been prepared by simple wet-impregnation method exhibits high photocatalytic performance towards drug naproxen and dye fuschian blue.

2.1 Introduction

In recent years, environmental pollution which has begun by the excessive use of antibiotics and dyes that are used in almost 80% of the industries has become a huge concern. Large quantities of contaminants have entered into the aquatic life directly or indirectly at distinct concentrations between μgL^{-1} and ngL^{-1} due to the worldwide increased demand for drugs and dyes [1] Antibiotics have been observed in surface water, groundwater and drinking water. Among these drugs, naproxen (NPX), as one of the non-steroidal anti-inflammatory drug (NSAID), has a good activity by reducing the formation of inflammatory mediators called prostaglandins.[2]However, there are also several adverse side effects such as ulcers, heartburn, and drowsiness associated with naproxen.[3] Besides, dyes are used in various industries like silk paints, paper, leather and printing ink, etc. fuchsin blue (FB), when discharged into water, will affect aquatic life and human health. The waste of dyes and pharmaceutical wastewater without sufficient treatment can enter the human body through drinking water or even food chain. [4] Therefore, the removal of pharmaceutical/dye stuff has considerable environmental significance. Among various physicochemical approaches, semiconductor-based photocatalysts are considered to be of great interest for the removal of the water pollutants. Several techniques have been used to remove the unremitting toxins released into the water for example solvent extraction, adsorption, and chemical precipitation. [5-8]Therefore, photocatalytic methods based on these materials have shown potential in energy conversions and environmental remediation. Recently, Bi_2O_3 (band gap = 2.8 eV) has been seen as a promising photocatalyst in many practical applications such as superconductors, electrical ceramics, optical coating, solid oxide fuel cells and gas sensors.[9-14] It has been seen that hydrodynamic size, optical properties and structural changes of M-Bi_2O_3 (M=Pd, Pt etc) nanomaterial are dependent on the nature of metals and different metal deposition

techniques (photo-deposition and wet impregnation).[15-17] Among these preparation methods, metal ions are reduced to a lower or zero oxidation state. But loading the metal ion with zero oxidation state only cause change in band gap. These cations can interact with the pollutant much strongly compare to zero oxidation state. The metal loading prompt different electron transfer mechanism compared to bare Bi_2O_3, therefore improves photogenerated electron/hole pair separation and efficiency of photocatalytic performance. Due to the work function difference between Bi_2O_3 and metal, there is a formation of a Helmholtz double layer at the M- Bi_2O_3 nanocatalyst interfacial region.[18] When energy of the incident photon matches with the band gap of the material at the interface, a maximum separation between the photogenerated charge carriers take place leading to enhanced photocatalytic performance.

Recently, Sedigheh *et. al.* investigated the removal efficiency of Methyl Orange using different weight fractions of TiO_2- SnO_2 nano-composite.[19] The use of Ag loaded Bi_2WO_6 nanoparticles for visible light degradation of organic pollutants have shown the SPR effect that has been observed by changing the ratios of Ag:Bi_2WO_6.[20-21] Microspheres of Ni-doped Bi_2O_3 have been successfully synthesized by the facile route to study the morphological changes and geometrical changes.[22-23] The C/Bi/Bi_2O_3photocatalyst has been prepared by one-pot synthesis using EDTA as a starting material. Moreover, the synthesized composite has shown maximum mineralization of 2,4-DCP (dichloro phenol) under sunlight and visible light in comparison to Bi_2O_3.[24] The Pd, Y co-doped monoclinic α-Bi_2O_3 displayed higher decolorization of dye (methyl orange) by varying the molar ratio of Pd,Y:Bi_2O_3 nanoparticles.[25] Hemishama *et. al.* reported an effective method to make visible-light-driven photocatalyst by depositing of Cu-cluster on the surface of Bi_2O_3 for the decomposition of propanol to CO_2.[26]It has been reported that titania nanoparticles with anatase and rutile

crystalline structure coated titania were prepared by hydrolysis method showed the decomposition of methylene blue.[27] Cao *et. al.* prepared Au-$BiVO_4$ nanoparticles for improving the photocatalytic degradation and wastewater treatment for H_2 and O_2 production under visible light illumination.[28] Plasmonic photocatalyst Ag/AgCl /$BiPO_4$ with high stability has been modified with Ag nanoparticles for improvement in the photocatalytic response.[29] Sonaland co-workers reported modification of Bi_2O_3 with nickel deposited nanoparticles by precipitation method for analyzing the electron-hole separation for efficient dye (methylene blue) degradation.[30] Furthermore, the nanocomposites of Fe_3O_4@ZnO-graphene oxide have also synthesized to carry out photocatalytic activities.[31] Sasaki et. al. synthesized Z-scheme photocatalysts between $BiVO_4$ and Ru/$SrTiO_3$ to enhance H_2 evolution under visible light.[32] Phase controlled synthesis of α-Bi_2O_3 by post calcinations method has been reported for the degradation of several organic pollutants (methyl orange, methylene blue).[33] Malathy *et. al.* reported doping with 3d-transition metals (Ni, Zn) on the surface of Bi_2O_3 improved efficiency by 27.5 % in 180 min.[34] Various researchers have demonstrated that doping with Ni^{2+} over TiO_2, ZnS, Cds, and ZnO significantly improved the removal of dye and organic pollutants under visible light illumination.[35-39]So it is observed that when the ions of different metals are impregnated/loaded on the surface of Bi_2O_3 there occur changes in the optical and photocatalytic properties.

Inspired by these reports, transition metal (Ni^{2+} and Cu^{2+}) impregnated Bi_2O_3 nanoparticles were prepared using a simple wet impregnation method. Presence of transition metal ions can enhance the photocatalytic activity by different ways.1) the absorbance of the materials in the visible region will be higher 2) Due to photo induced electron transfer mechanism [40] the electron-hole recombination can be suppressed. Meanwhile, naproxen (NPX) and fuchsin blue (FB) were

chosen as target pollutants. The main objectives were to: (1) To prepare highly pure alpha phase Bi_2O_3 nanoparticles; (2) Impregnation of transition metal ion Ni^{2+} and Cu^{2+} onto monoclinic Bi_2O_3 ;(3)To evaluate the feasibility of NPX and FB degradation by bare Bi_2O_3, Cu^{2+}-Bi_2O_3 and Ni^{2+}-Bi_2O_3 nanomaterial under visible light irradiation;

2.2 Experimental Sections

2.2.1 Chemicals and reagents

Bismuth nitrate penta-hydrate (Bi $(NO_3)_3.5H_2O$, 98%),sodium hydroxide (NaOH ,>97%), cupric sulphate pentahydrate ($CuSO_4.5H_2O$, >97%) and nickel chloride anhydrous ($NiCl_2$,>97%) all were purchased from Lobachemie, India. Fuchsin blue dye (Pulver) we purchased from MERCK DARMSTADT, Germany. Tablets of Naproxen (200 mg) were purchased from CIPLA pharmaceuticals. All the chemicals were used without any further purification. Notably, distilled water was used during the whole experiment that was obtained from Milli-Q (Millipore), with an ultra-filtration system (40 mho cm^{-1} at 25^0C).

2.2.2 Synthesis of Bi_2O_3 nanoparticles

Firstly, 50 ml 1M Bi $(NO_3)_3.5H_2O$ solution was prepared. Subsequently, 50 ml 0.1M NaOH in was added drop-wise to the above solution. After this, the solution was continuously stirred for5 h at 80^0C until a yellow precipitate was formed. The solid product washed with deionized water and ethanol for five times and the final product dried at 55^0C for 12h.

2.2.3 Synthesis of M^{n+}-Bi_2O_3nanocomposites (M^{n+}= Ni, Cu)

Metal ion loaded bismuth nanoparticles were synthesized by a simple wet impregnation method. [41] In a typical procedure, a clear suspension of 100 mg of Bi_2O_3 in10 ml of deionized water

was prepared upon sonication for 20 min, then the requisite amount of $CuSO_4$ (0.01M) or $NiCl_2$ (0.01M) corresponding to different weight% (1,2 and 3) was added to this solution and stirred continuously for 48 h. Finally, the precipitate was washed several times with water and ethanol and dried at 55^0C to obtain the final catalysts.

2.2.4 Characterization techniques

Phase and crystal properties were investigated by X-ray diffraction (XRD**,** analytical xpert pro) using Cu-Kα (1.54 Å) with diffraction angle 2θ (20°-80°) operating at 45 kV. The morphology and the structure of prepared samples were investigated by scanning electron microscopy (SEM) and high-resolution transmission electron microscopy (HRTEM, FEI Tecnai G2 F20, Netherlands operating at 200 kV). Besides, the oxidation state of the catalyst was examined using X-ray photoelectron spectroscopy (XPS, KRATOS axis 165 Shimadzu) with Mg-Kα radiations at 75 W. The elemental composition ratio was investigated by energy dispersive spectroscopy (SEM-EDS, JEOL JSM-7600 F) operated at 30 kV. Besides, the optical absorbance spectra was carried out on diffuse reflectance spectroscopy (DRS, Avantes) using $BaSO_4$ as an internal standard. Moreover, the emission spectrum was analyzed by spectro-fluorimeter (Perkin-Elmer LS55) at room temperature.

2.2.5 Photocatalytic activity

The photocatalytic performance of various M^{2+}- Bi_2O_3 (20 mg) samples were carried out in by taking 5 mL of cationic dye (FB; 0.02 mM) and pharmaceutical waste (NPX; 0.01 mM) at room temperature for different time duration under visible light irradiation (50 mW/cm^2). The nano-catalyst containing reaction mixtures were kept under photocatalytic conditions with constant stirring. Then the aliquots were collected at regular intervals and the catalysts were removed by

centrifugation (at 5000 rpm for 10min).After that, the absorbance of residual solutions was analyzed by UV-Vis spectrophotometer (λ_{max}= 230 nm) for NPX and (λ_{max}=548 nm) for FB for further kinetic studies. The percentage of degradation (% D) has been calculated by equation 1[42-43].

$$\% D = \frac{A_0 - A}{A_0} \times 100 \text{----------(1)}$$

2.3 Results and discussions

2.3.1. Morphological and structural properties

The XRD patterns of pure Bi_2O_3, Cu^{2+}-Bi_2O_3 and Ni^{2+}-Bi_2O_3 are displayed in (Fig.2.1).The monoclinic phase of α-Bi_2O_3can be assigned by the JCPDS card No. 00-041-1449. The main diffraction peaks are located at 27.94°, 32.70°and 46.20° (2θ) that are consistent respectively with (1 2 1), (2 0 2) and (0 4 1) crystal planes of α -Bi_2O_3. Moreover, for the M^{2+}-Bi_2O_3sample, all of the characteristics peaks assigning to Bi_2O_3 could be observed and did not shift which might be due to either its low loading (5 wt %) or metal ion goes to the interstitial sites on the lattice of Bi_2O_3. As smaller ionic radii of Ni^{2+} (0.069 nm) and Cu^{2+} (0.073 nm) as compared to Bi^{3+}(0.103 nm), impregnated metal ions can easily be incorporated into Bi_2O_3 lattice [44]. Upon Ni^{2+} impregnation, crystallinity is slightly reduced as confirmed by FWHM values for a plane (121) which increased from 0.346 radian to 0.355 radian after impregnation. The crystallite sizes as calculated by Scherrer Formula [45] are 51, 50 and 47 nm for bare Bi_2O_3, Cu^{2+}-Bi_2O_3 and Ni^{2+}-Bi_2O_3 respectively.

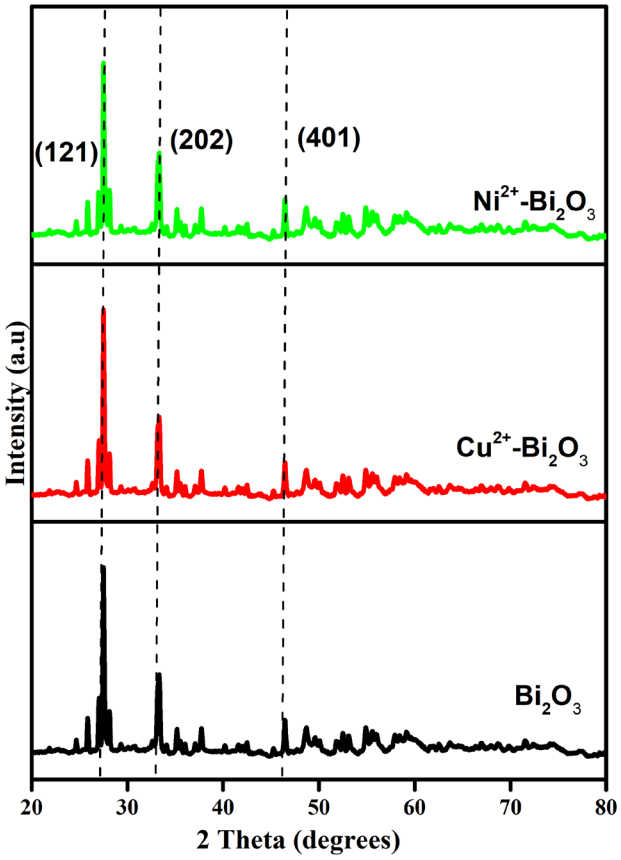

Fig .2.1: XRD patterns of bare Bi_2O_3, Cu^{2+}- Bi_2O_3 (2 wt %) and Ni^{2+}-Bi_2O_3 (2 wt %) catalyst

For the deeper understanding of the morphology of Ni^{2+}- Bi_2O_3 HRTEM was performed and the results were showed in (Figs. 2.2 a and 2.2 b). Ni^{2+} nanoparticles were dispersed on the surface of Bi_2O_3 and the morphology of Ni^{2+}-Bi_2O_3 was a layered structure. Moreover, the lattice fringes of 0.329 nm were assigned to the (1 2 1) plane of α-Bi_2O_3. In selected area electron diffraction (SAED) pattern (Fig. 2c) planes of Bi_2O_3 (121), (202), and (223) confirmed the formation of pure α-phase.

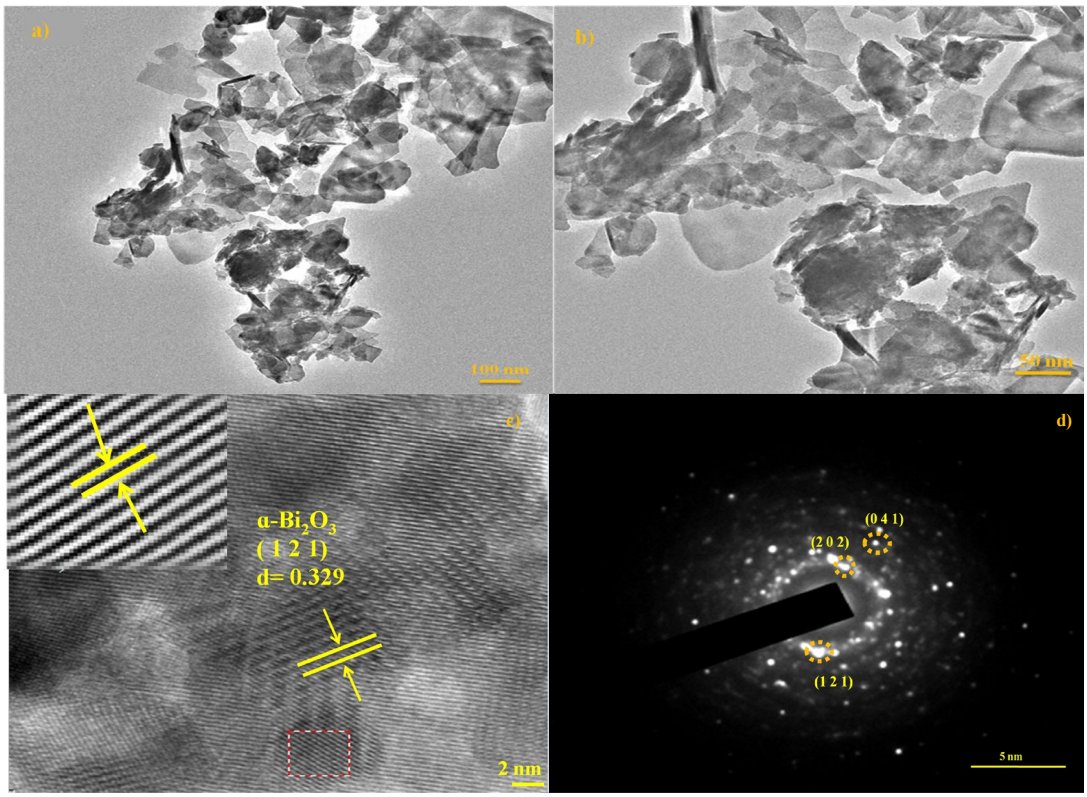

Fig. 2.2: (a-b) HR-TEM images, (c) SAED pattern, and the corresponding (d) lattice fringes of Ni^{2+}-Bi_2O_3 (2 wt %) nanocatalyst

The SEM images in (Fig.2.3) displayed that all the samples show the same morphology and irregular clusters consisting of the agglomerated particles having a size range in micrometers. It can be seen in (Fig. 2.3 b and 2.3 c) that there is no change in the surface structure of Bi_2O_3 after Cu^{2+} and Ni^{2+} impregnation. The loaded Cu, Ni ion and the bare Bi_2O_3 could not be differentiated by SEM due to the poor resolution by the instrument. However, the energy-dispersive of Cu^{2+}-Bi_2O_3 and Ni^{2+}-Bi_2O_3 confirms the presence of Ni and Cu ions in the synthesized samples and weight percent was found to be (0.80 wt%) for Ni^{2+} and(1.02 wt%) for Cu^{2+}as shown in fig. 2.3.The EDX spectrum also revealed that no extra peak was observed other than constituents. The mechanism of Ni^{2+} and Cu^{2+} impregnation in Bi_2O_3 surfaces has been demonstrated in Scheme 2.1 and 2.2. The Bi_2O_3 nanoparticles contains negatively charged oxide group in its surface, such assumption has been supported by negative zeta potential (-25 mV) of

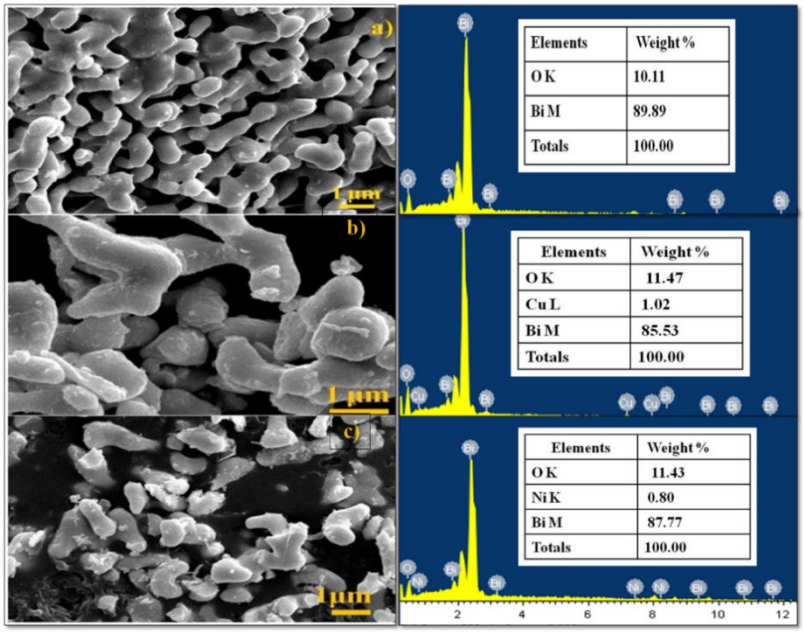

Fig. 2.3: SEM images of (a) bare(b) Cu^{2+}-Bi_2O_3 (2 wt %) and c) Ni^{2+}-Bi_2O_3 (2 wt %) catalyst and their corrosponding EDX profiles

Bi_2O_3 (Fig.2.4). These oxides groups can act as excellent anchors for cations. These cations will be first attracted by negatively charged oxide groups and move closer to the surface then finally get covalently bonded with these groups. Interestingly, the zeta potential values of impregnated Bi_2O_3 are less negative (Cu^{2+}-Bi_2O_3 = -17 mV & Ni^{2+}-Bi_2O_3 = -15 mV) (Fig.2.4) in comparison to bare analogue suggesting partial neutralization of negative charges upon impregnation.

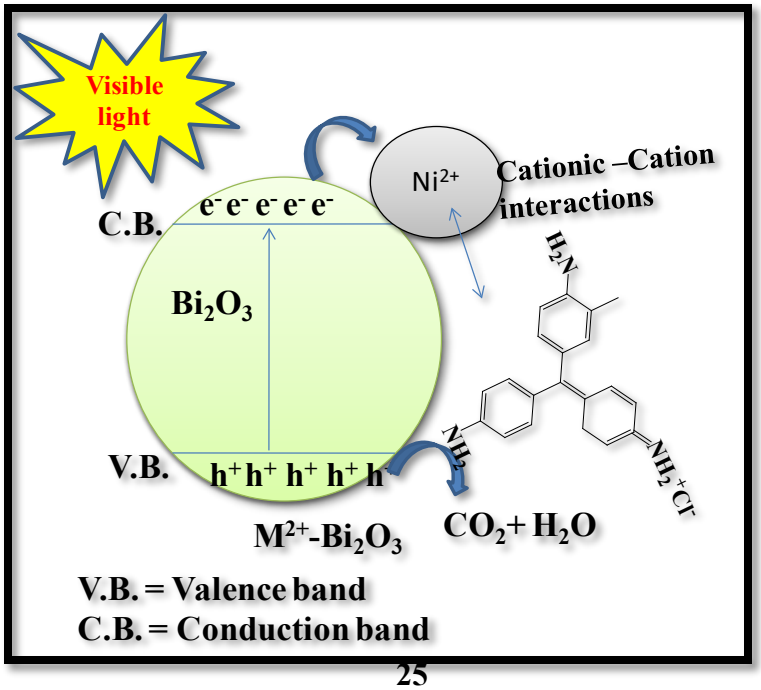

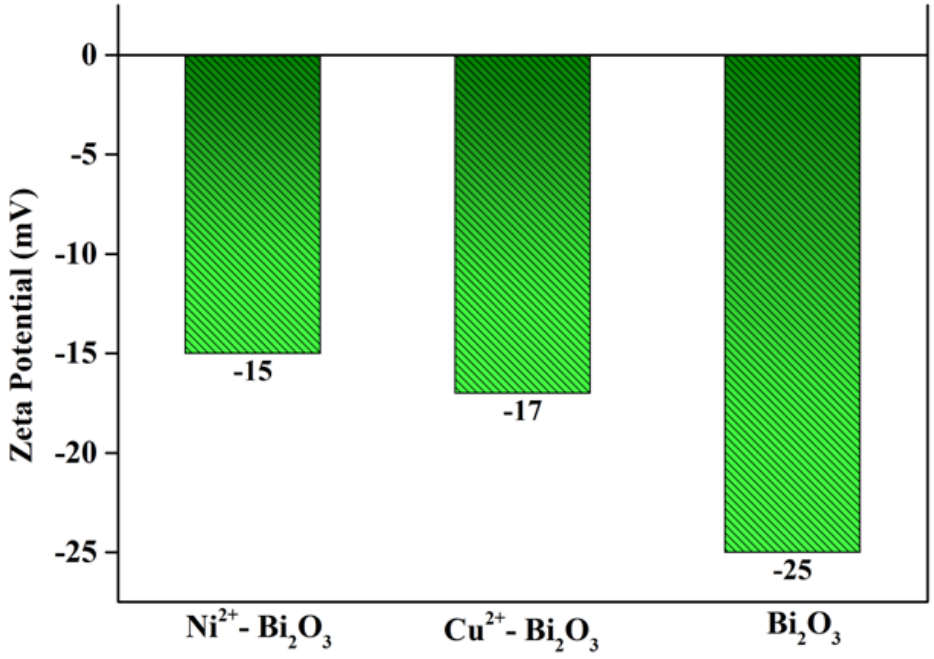

Fig. 2.4: Zeta potential values of bare and impregnated Bi_2O_3 nanoparticles

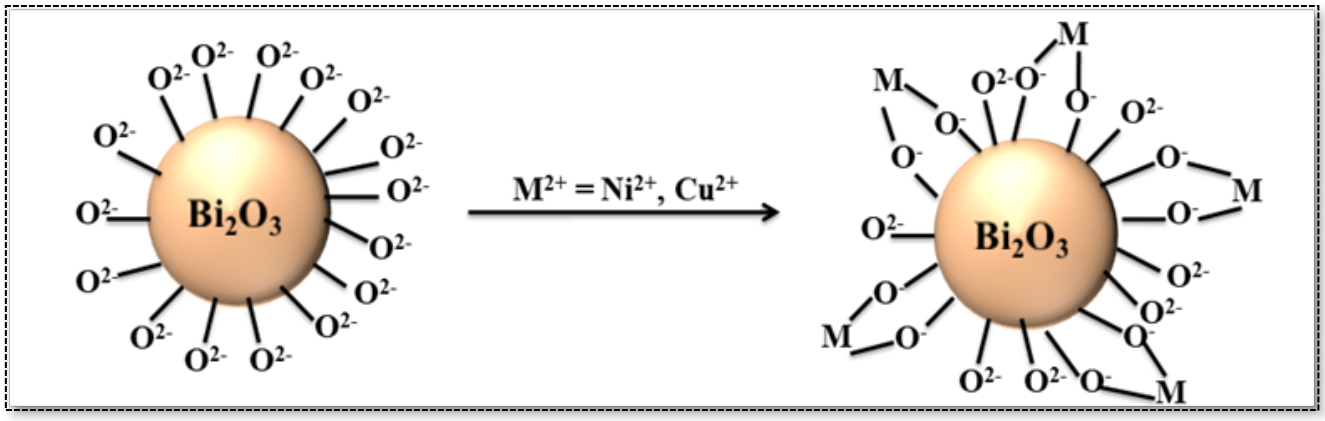

Scheme 2.1: Schematic representation of Ni^{2+} and Cu^{2+} impregnation of the surface of Bi_2O_3

XPS measurements were further carried out to study the chemical composition and bonding characteristics of the highest active Ni^{2+}-Bi_2O_3 (2 wt %) sample. The peaks of Ni 2p, Bi 4f, C 1s, and O 1s are seen in the survey spectrum (Fig. 2.5 a) indicating the presence of Ni, Bi, and O in the sample. The C 1s peak with binding energy (284.6 e V) is used as an internal reference [46].

The two peaks with binding energy occurring at 164.3 e V and 159.0 e V correspond to Bi 4f $_{5/2}$ and Bi 4f $_{7/2}$ respectively, which can be referred to Bi^{3+} [46]. Additionally, the XPS spectra of Ni 2p was fitted by assigning four peaks at 879.31 e V, 873.32 e V, 861.20 e V, and 855.24 e V.The

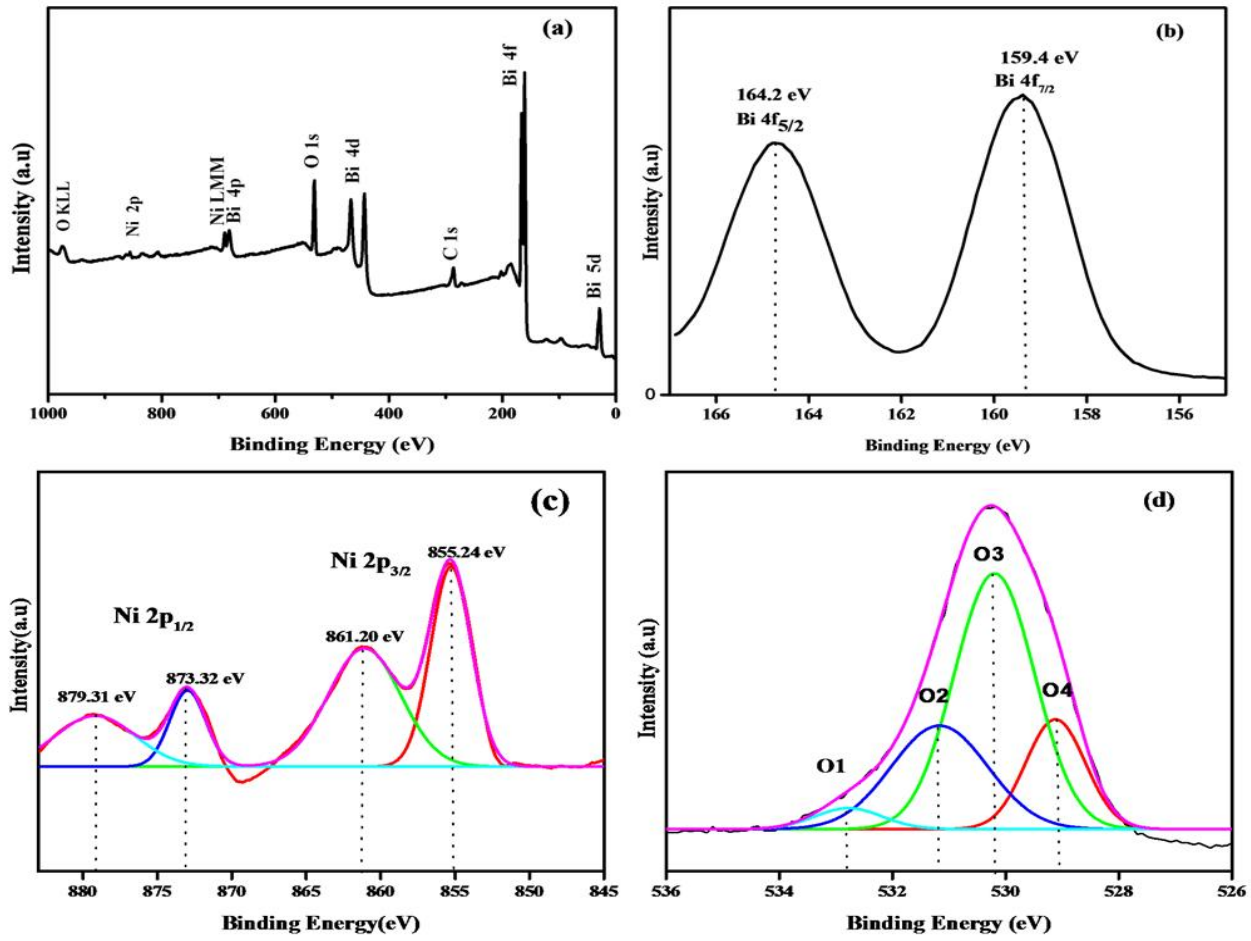

Fig.2.5:(a) XPS full survey spectra of Ni^{2+}-Bi_2O_3 (2 wt %) sample; their corresponding high resolution spectra of (b) Bi 4f (c) Ni 2p and (d) O 1s

binding energy at 855.24 eV and 861.20 eV can refer to Ni 2p $_{1/2}$ and binding energy at 873.32 eV and 879.31 eV can be attributed to Ni 2p$_{3/2}$ by the presence of Ni-O bond [47-48**].** Furthermore, XPS spectra for O 1s (Fig.2.5d) can be divided into four peaks O 1, O 2,O 3, and O 4. The peak of O4 with binding energy 529.7 e V could be assigned to Bi/Ni-O [49] and the peak of O3 with binding energy 530.4 e V was ascribed with O in OH^- groups. The peak located as

O2 with binding energy 531.4 eV correlates to low coordination of oxygen with defect sites that can be usually seen in catalysts having small particles. Additionally, peak O1 having binding energy at 532.4 eV referred to as a multiplicity of physically and chemically bonded H_2O near the surface [50].Thus it can be seen that the prepared Ni ion impregnated Bi_2O_3 nanostructures showed a polybasic nature with Ni^{2+}-Bi_2O_3 catalyst.

2.3.2 Optical properties

The absorption spectra of pure Bi_2O_3, Cu^{2+}-Bi_2O_3, and Ni^{2+}-Bi_2O_3 samples were exhibited in Fig. 2.6.Absorption spectrum of Bi_2O_3 was about 400 nm, which could be due to the transition of an electron from the valence band to the conduction band. After Cu^{2+} and Ni^{2+} loading over Bi_2O_3, the absorption spectra show appearance of broad bands above 400 nm due to the excitation of electrons of metal ions to the conduction band of Bi_2O_3 by their respective energy levels [51].The absorption in the range of 600-800 nm may be due to the d-d transition (inter-band transition) in Cu^{2+} species [52]. Cu^{2+} has d^9 configuration and its ^2D state is split into the ground state ($^2T_{2g}$) and excited state (^2E_g) energy levels with one electronic transition. The ground level and the excited levels are further split and transitions take place from $^2B_{1g}$ to ^2A_g, $^2B_{1g}$ to $^2B_{2g}$,and $^2B_{1g}$ to ^2E_gthat correspond to appearance of absorption bands (550-800 nm). However, Ni^{2+}-Bi_2O_3nanoparticlesshowed a small absorption peak between 400-500 nm which can be attributed to ($^3A_{2g}$ to $^3T_{1g}$) transition[53].As calculated from Tauc plot [54], the band gaps of Cu^{2+}(2.69 eV) and Ni^{2+}(2.75 eV) loaded hybrids are slightly reduced upon than bare Bi_2O_3 (2.79 eV) (Fig.2.7).

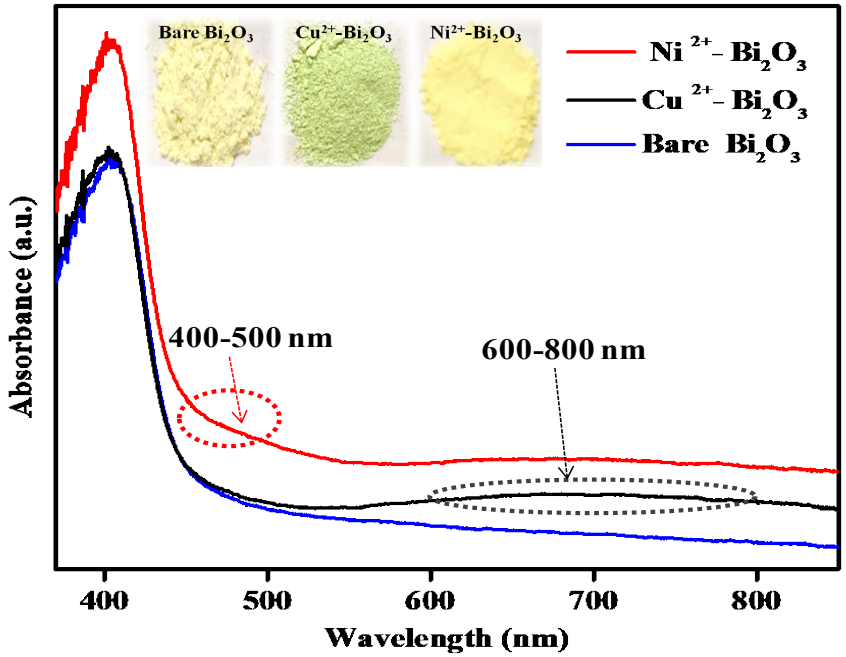

Fig.2.6: Diffuse reflectance spectra of bare, Cu^{2+}-Bi_2O_3 (2 wt %) and Ni^{2+}-Bi_2O_3 (2 wt %) photocatalysts with their corresponding photographs (inset)

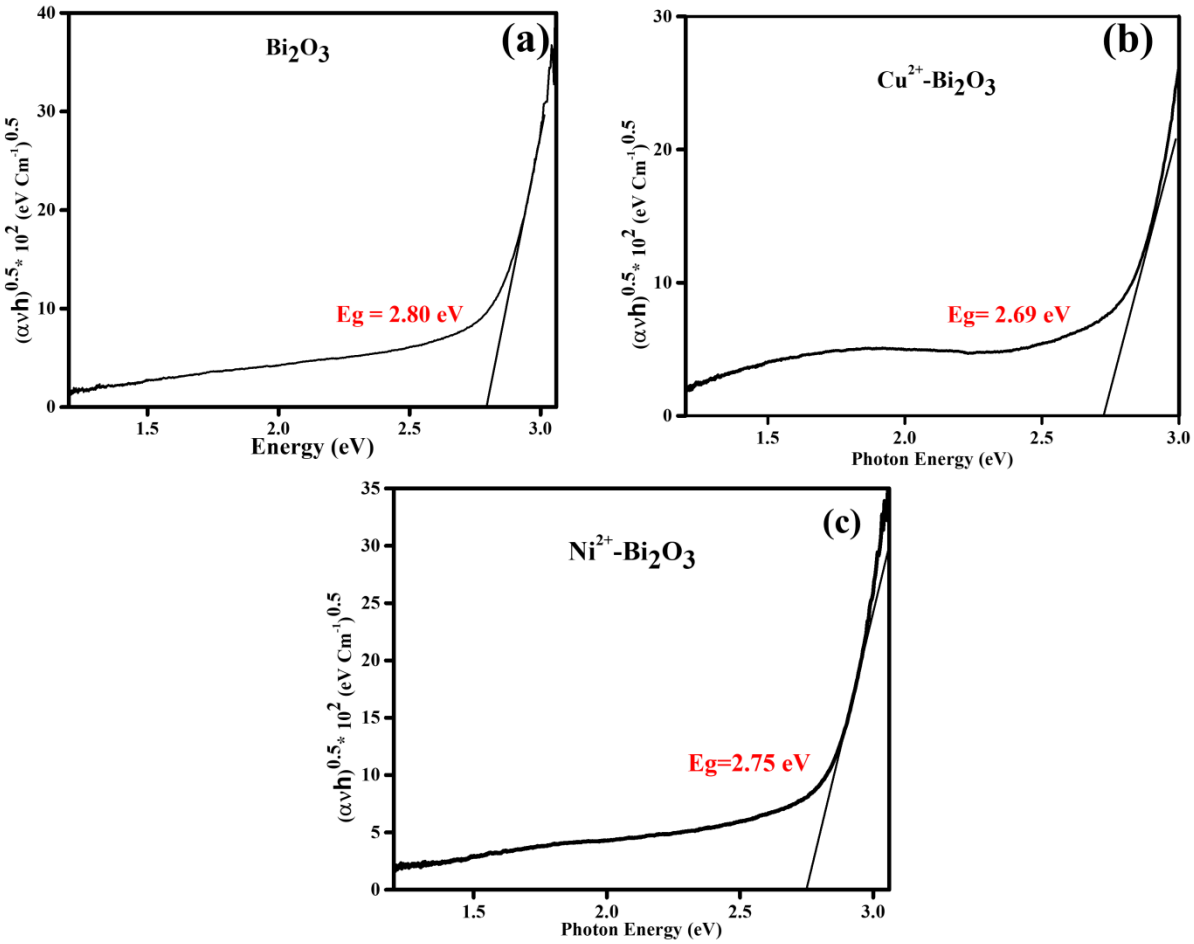

Fig.2.7: Tauc Plots of (a) bare Bi_2O_3(b) Cu^{2+}- Bi_2O_3 and (c) Ni^{2+}- Bi_2O_3 nanoparticles

To determine the efficiency of prepared catalysts in terms of the lifetime of charge carrier and recombination rate, PL was analyzed by exciting the photocatalysts at a wavelength of a 329 nm. Fig.2.8 showed emission peaks are mainly centered in UV (350-420 nm) and visible region (430-530 nm). As the charge transfer transition was expected to occur from the valence band of (Bi 6s) to the conduction band of (O_2 2p). The intensity of Cu^{2+}-Bi_2O_3 (2 wt%) and Ni^{2+}-Bi_2O_3 (2 wt %) nanoparticles are lower in the UV range as well as in visible range demonstrating further decreasing of recombination rate of holes and electrons. Interestingly, Ni^{2+}-Bi_2O_3catalyst showed greater quenching of emission peak intensities as compared to bare. On this basis, it has been concluded that Ni^{2+}on Bi_2O_3 surface generates more defective sites and greater charge carrier trapping suppressing the recombination rate which might lead to higher photocatalytic activity.

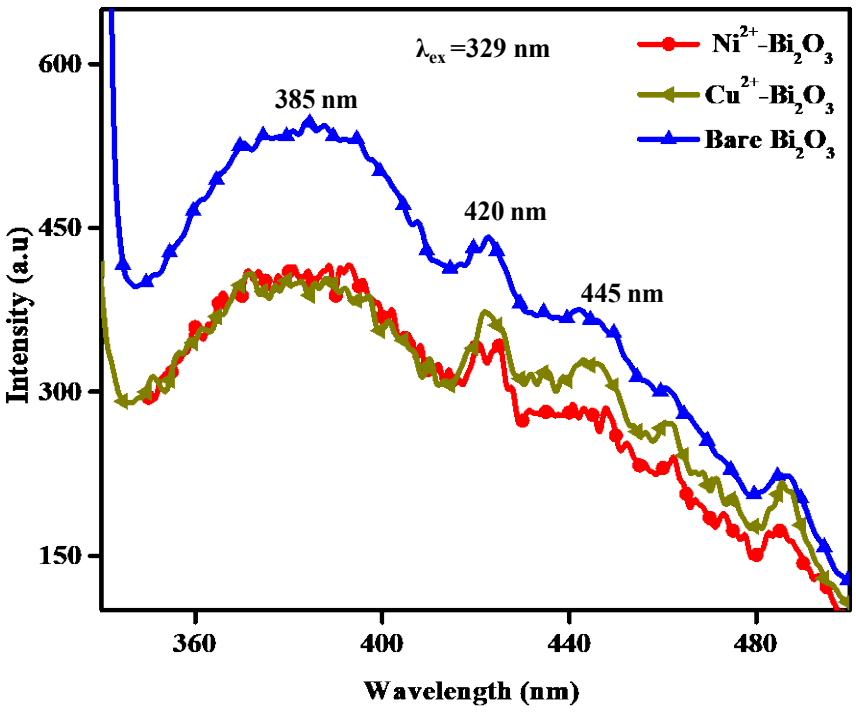

Fig. 2.8 : Comparative photoluminescence spectra of different photocatalysts with excitation wavelength of 329 nm

2.4 Photocatalytic activity

The photocatalytic performance of prepared M^{2+}-Bi_2O_3 catalysts occurred by their interactions with the substrate molecule. During photocatalytic degradation, the impregnated metal ions are excited and shift the excited electrons to the conduction band of Bi_2O_3 for reduction purposes while the holes left behind within metal ions are used for various oxidation processes. The maximum decrease in peak intensities of the substrate molecule is due to complete oxidation after treatment with different M^{2+}-Bi_2O_3 catalysts under visible light irradiation have been shown in Fig.2.9. The complete degradation of a cationic substrate (F.B) was achieved in 45 minutes while for pharmaceutical waste (NPX), it occurred within 120 min. As naproxen is a reduced form of propionic acid, its complete photo-oxidation will require more time in comparison to fuchsin blue. The low degradation efficiency of pristine Bi_2O_3 (43% for FB and 40% for NPX) is due to its low conduction band potential [55].

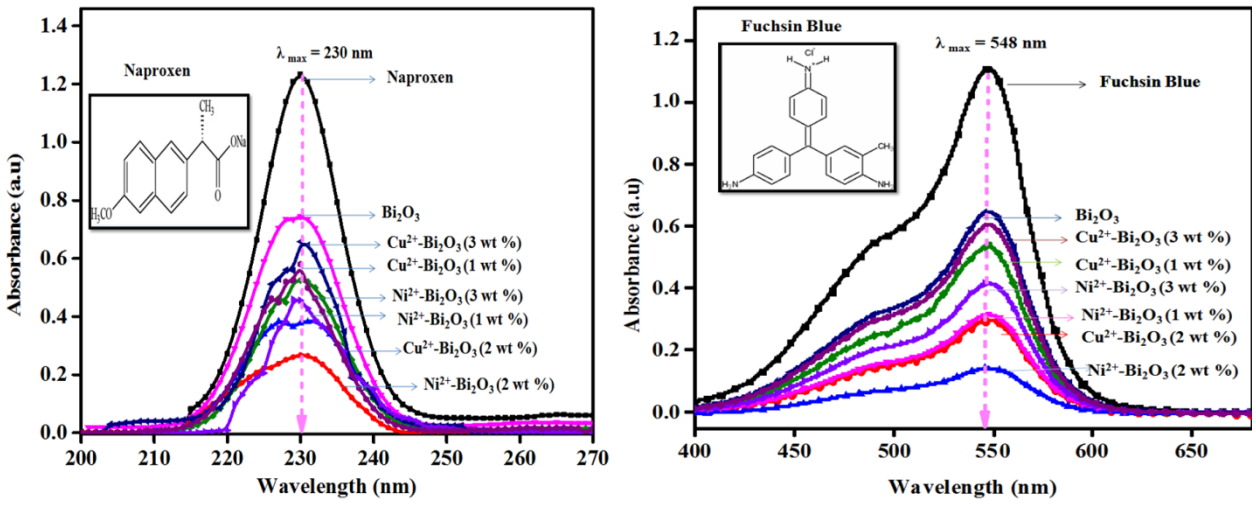

Fig. 2.9: Change in absorption spectra of Fuchsin Blue (FB) and Naproxen (NPX) during its degradation by different (1, 2 and 3 wt%) Ni^{2+}-Bi_2O_3 and Cu^{2+}-Bi_2O_3 samples under visible light irradiation

Therefore, the one-electron transfer process through the reduction of O_2 to O_2^- cannot proceed which leads to a high recombination rate, and the photogenerated electrons are not consumed. There was a significant change in the band gap of semiconductor after Ni and Cu ion impregnation which could be responsible for the variation in the photocatalytic properties of the photocatalyst. Another reason for variation in photocatalytic properties is due to its dependency on the substrate molecule. In literature, it is reported that addition or impregnation of metal ion on the semiconductor surface can improve efficiency due to the charge trapping phenomenon. As the energy level of the metal ion (M^{n+}) lie below the conduction band. So, the energy level of metal ion affects the trapping efficiency. The trapping e^- make it easy for h^+ to shift onto the surface of Bi_2O_3 and further react with OH^-in the solution and form $OH^{\cdot}$. These radicals participate in the degradation process. For constructive degradation reaction, the lifetime of electrons and holes is important. As a lifetime of holes and electrons can be increased by trapping electrons, thereby reducing the recombination and thus allowing holes to diffuse to the surface of particles and take part in an oxidation reaction. Moreover, the results indicated that the degradation of dye and drug increased with metal ion loading up to 2.0 %. It may be because the impregnated metal ion acts as an electron sink by capturing the more number of photogenerated electrons that increase the lifetime of charge carriers and leading to decreases in the recombination of e-/h^+ pairs which is also evident by photoluminescence spectra. Further, on increasing the metal ion concentration above 2.0 wt%, photocatalytic efficiency decreases. It may depend upon several factors that is screening or covering effect by the Ni^{2+} and Cu^{2+} species leading to blockage of light particles by covering the surface of Bi_2O_3. Another reason was multiple trapping of charge carriers due to which active sites were decreased leading to increases in the possibility of e^-/ h^+ recombination and resulting in a lesser number of charge carriers

reaching the surface for photocatalytic degradation. It may be concluded that considerably higher degradation for both drug and dye was found in the case of Cu^{2+}-Bi_2O_3 (73% for FB and 70% for NPX) and Ni^{2+}-Bi_2O_3(87% for FB and 79% for NPX) catalysts as compared to Bi_2O_3 (43% for FB and 40% for NPX). The kinetics of log C_0/C versus time (minutes) for FB and NPX has been plotted where C_t is the concentration at time t and C_0 at time t_0.In both cases, reaction rates follow pseudo-first-order kinetics as described by using simple Langmuir-Hansel-wood equation (2):

$$2.303 \log \frac{C_0}{C_t} = kt \text{----------(2)}$$

The rate constant (k) (min^{-1}) values for Cu^{2+} and Ni^{2+}-Bi_2O_3 samples after NPX and FB have been determined and shown in Fig. 2.10. The rate constant values calculated for FB; (0.0154,0.0324 and 0.0518min^{-1}) and NPX (0.004,0.009 and 0.0154min^{-1}) were observed with Bi_2O_3,Cu^{2+}-Bi_2O_3 and Ni^{2+}-Bi_2O_3photocatalysts respectively. The kinetics study confirms that

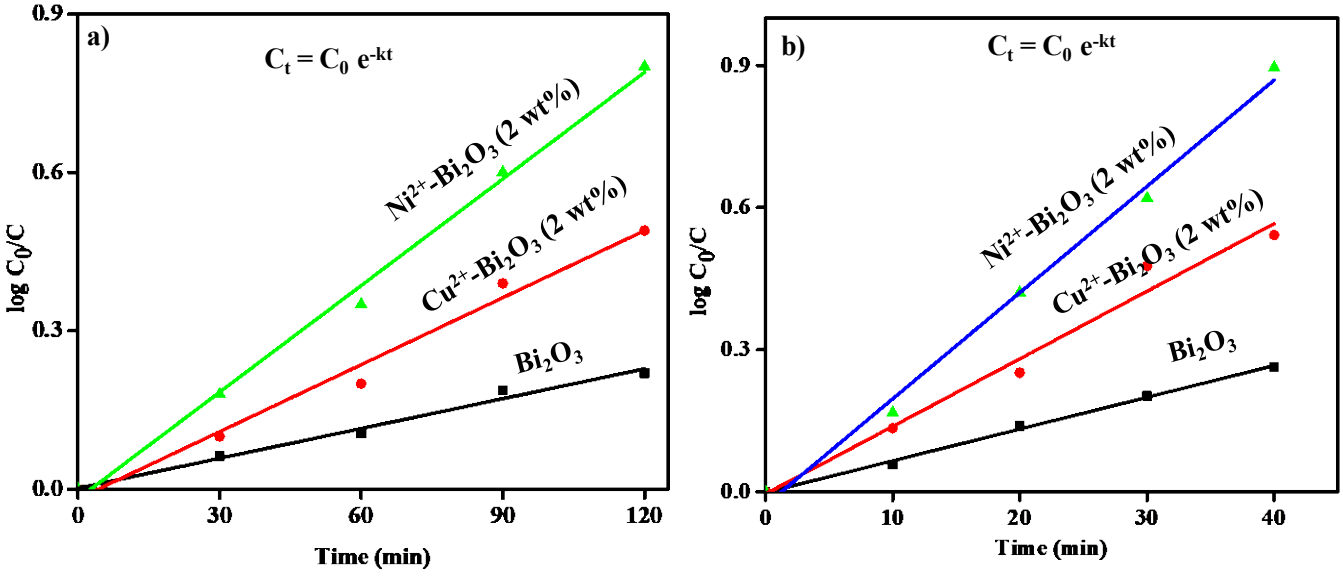

Fig. 2.10. Reaction kinetics for a) NPXand b) FBdegradation by bare , Cu^{2+}-Bi_2O_3 (2 wt %) and Ni^{2+}- Bi_2O_3 (2 wt %) samples

the optimum amount of Cu and Ni ion concentration increases the number of photogenerated holes and electrons in comparison to the bare Bi_2O_3 photocatalyst resulting in increased photocatalytic activity.

The rate constant values show that the highest photocatalytic performance is obtained for nickel impregnated catalysts in both cases. This is due to the efficient charge separation and less recombination rate. The work function of the metal is higher than that of Bi_2O_3, then e^-s are removed from Bi_2O_3 in the vicinity of the metal particle. As nickel deposits generate large no. of holes by acting as an electron sink. These results in the formation of Schottky barriers at each of the metal-semiconductor regions and results in less recombination and greater photocatalytic performance. Remarkably, our catalyst is having shorter reaction time as well as either comparable or higher degradation compare to TiO_2 derived catalysts towards photocatalytic degradation of Naproxen (Table 1). [56,57]

Sample	**Substrate**	**Irradiation time**	**% degradation**	**References**
Ni^{2+}-Bi_2O_3	Naproxen	120 min	79%	This work
SiO_2@Au@TiO_2	Naproxen	360 min	29.7%	[55]
TiO_2	Naproxen	210 min	83%	[56]

Table 1: Comparative photocatalytic activity of Ni^{2+}-Bi_2O_3 towards Naproxen degradation with the recent reported litterature.

2.4.1. Effect of Catalyst loading

Further, we optimize the catalyst amount for the degradation of FB to avoid the excess of catalyst loading. Fig 2.11 shows the degradation rate of FB as a function of the catalyst amount (Ni^{2+}-Bi_2O_3) under visible light irradiations. The degradation efficiency increases with the increase in the catalyst amount from 0.01 to 0.02 g L^{-1}. As more active sites are available for the dye adsorption, the % of degradation increases with the increase in the catalyst amount. Further increase in the catalyst amount decreases the degradation efficiency. This may be due to the agglomeration of nanoparticles which decreases the availability of the active sites leading to a decrease in the efficiency of the photocatalyst. Therefore, all activities were done under the optimum catalyst amount.

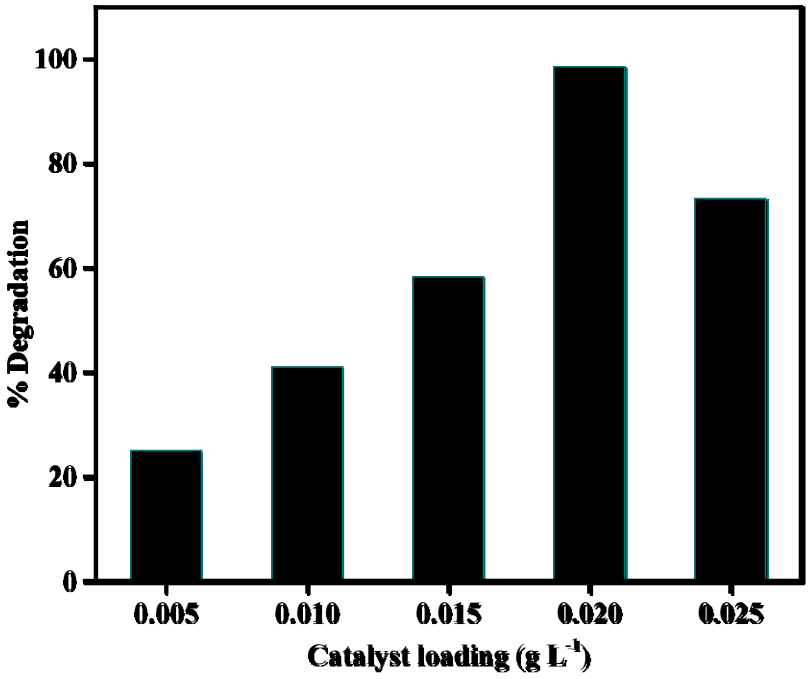

Fig.2.11. Effect of catalyst loading on % degradation of fuchsin blue in the presence of (Ni^{2+}-Bi_2O_3) photocatalyst under visible light irradiation

FTIR-spectra of Bi_2O_3 and pure naproxen before and after photocatalytic degradation with Bi_2O_3 are given in (Fig 2.12). Before degradation, the NPX exhibited the characteristic peaks at –CH (1465 cm^{-1}),-OCH_3 (3002 cm^{-1}). The peak showed by Bi_2O_3 at 837cm^{-1}correspond to stretching vibration mode of Bi-O in the Bi_2O_3 [58] and the peak at 1375 cm^{-1} corresponds to the bending vibration of OH bonds of the absorbed water [59]. After the photocatalytic degradation with

Bi_2O_3 catalyst, the FTIR spectra display a new peak at 1085-1050 cm^{-1} indicating the dissociation of respective functional groups and possibly the formation of primary alcohol. In addition to it, the FTIR peak at 3002 cm^{-1} has disappeared indicating the cleavage of carbon-hydrogen bond in NPX molecule.

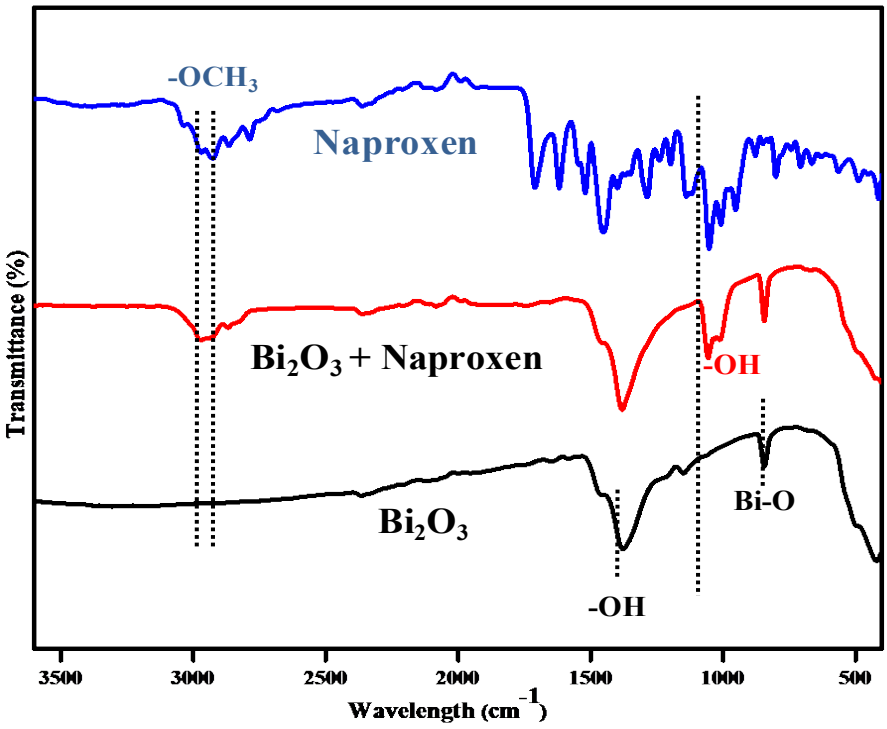

Fig.2.12. FTIR spectra of Bi_2O_3 and pure naproxen before and after photocatalytic degradation

2.4.2. Reusability of Ni^{2+}- Bi_2O_3photocatalyst

Additionally, reusability and stability is the key to investigating the potential application of catalyst. The recyclability of Ni^{2+}-Bi_2O_3 was monitored after recovering from the reaction system and reused in the next experiment under the same conditions. As showed in Fig 2.13, the reusability efficiency of Ni^{2+}-$Bi_2O_3$from the first run to the fourth run was 92 %, 90%, 85%, and

80% respectively. Only a 12% decrease in FB degradation efficiency was shown compared with the initial cycle.

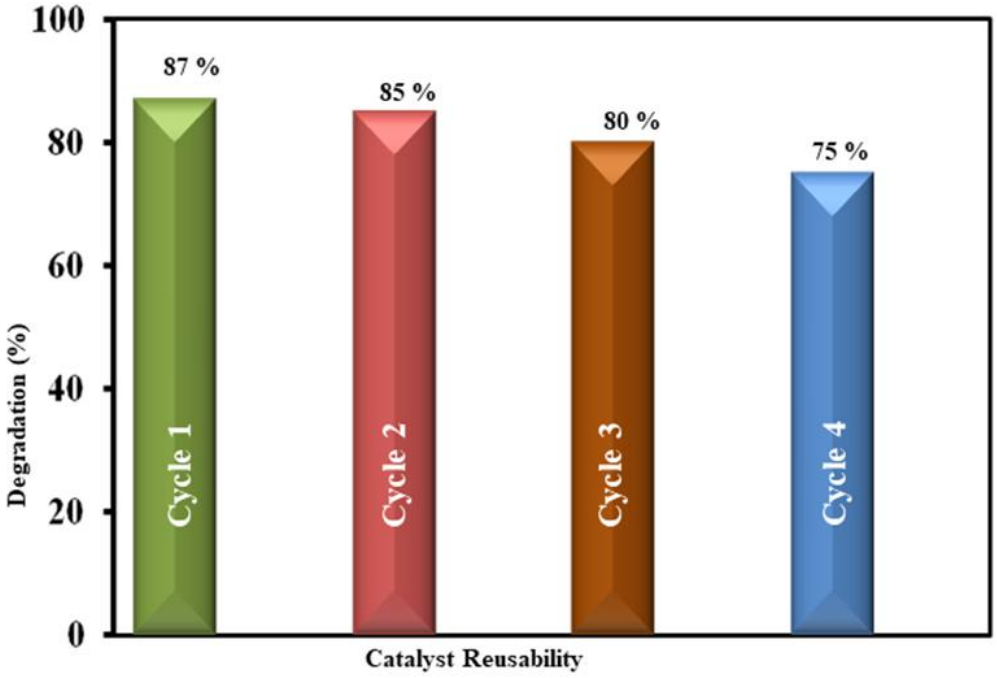

Fig. 2.13. Reusability of the Ni^{2+}-Bi_2O_3 photocatalyst in four successive experimental runs for the photocatalytic degradation of FB in aqueous solution under visible light irradiation

In this perspective, metal ions impregnated (Ni^{2+} and Cu^{2+}) Bi_2O_3 hetero-structures have been investigated as a potential material for photocatalytic degradation of NPX and FB. The impregnated hybrids shows considerably smaller zeta potential values (−15 and −17 mV for Ni^{2+} -Bi_2O_3 and Cu^{2+}-Bi_2O_3 respectively). The adsorption edge of Ni^{2+}-Bi_2O_3 and Cu^{2+}-Bi_2O_3 nanostructures were shifted slightly towards lower frequency. The photoluminescence spectrum impregnated materials shows significant quenching compare to pristine Bi_2O_3 .suggesting lesser degree electron-hole recombination upon metal loading. Due to the photocatalytic degradation efficiencies of both Ni^{2+}-Bi_2O_3 (87% for FB and 79% for NPX) and Cu^{2+}-Bi_2O_3 (73% for FB and 70% for NPX) hetero-structures are significantly higher compare to the pristine one (43% for FB and 40% for NPX). The photo-degradation process obeys the pseudo first order kinetics. Due to

simpler synthesis and enhanced activity metal ion loaded Bi_2O_3 photocatalysts can be potential photo-catalysts for removing NPX and FB from wastewater.

References

[1] E. Hapeshi, A. Achilleos, MI. Vasquez, C. Michael, NP. Xekoukoulotakis, D. Mantzavinos, D. Kassinos, and Drugs degrading photocatalytically: kinetics and mechanisms of ofloxacin and a tenolol removal on titania suspensions, water.res. 44(6) (2010) 1737-46, https://doi.org/10.1016/j.watres .2009.11 .044 .

[2] D. Štrbac, CA. Aggelopoulos, G. Štrbac, M. Dimitropoulos, M. Novaković T. Ivetić, SN. Yannopoulos, Photocatalytic degradation of Naproxen and methylene blue: comparison between ZnO, TiO_2 and their mixture,Process. Saf. Environ. Prot. 113 (2018) 174-83, https://doi.org/10.1016/j.psep.2017.10.007 .

[3] S. Harirforoosh, W. Asghar, F. Jamali, Adverse Effects of Nonsteroidal Antiinflammatory Drugs: An Update of Gastrointestinal, Cardiovascular and Renal Complications, J. Pharm. Pharm. Sci. 16(2013), 821-847, https://doi.org/10.18433/J3VW2F.

[4] J. Shah, MR. Jan, F. Khitab, Sonophotocatalytic degradation of textile dyes over Cu impregnated ZnO catalyst in aqueous solution, Process.Saf. Environ. Prot. 116 (2018) 149-58, https://doi.org/10.1016/j.psep.2018.01.008 .

[5] S. Abbasi, MS. Ekrami-Kakhki, M. Tahari, Modeling and predicting the photodecomposition of methylene blue via ZnO–SnO_2 hybrids using design of experiments (DOE). J. Mater. Sci.: Mater. Electron. 28(20) (2017)15306-12.https://doi.org/10.1007/s10854-017-7414-4.

[6] T. Kida, G. Guan, N. Yamada T. Ma, K. Kimura, A.Yoshida, Hydrogen production from sewage sludge solubilized in hot-compressed water using photocatalyst under light irradiation. Int. J. Hydrog. Energy.29(3) (2004) 269-74.10.1007/s10854-017-6745-5.

[7] S. Abbasi, Investigation of the enhancement and optimization of the photocatalytic activity of modified TiO_2nanoparticles with SnO_2 nanoparticles using statistical method, Mater. Res. Express. 5(6) 2018066302.10.1088/2053-1591/aac7f4.

[8] G. K. Ramesha, A. V. Kumara, H. B. Muralidhara, S.Sampath,Graphene and graphene oxide as effective adsorbents toward anionic and cationic dyes,J. Colloid. Interface. Sci.361(1) (2011) 270-277, https://doi.org/10.1016/j.jcis.2011.05.050.

[9] WF. Yao, H. Wang, XH. Xu, JT. Zhou, XN. Yang, Y. Zhang, SX. Shang, M.Wang,Sillenites materials as novel photocatalystsfor methyl orange decomposition,Chem. Phys. Lett. 377(5-6) (2003) 501-506, https://doi.org/10.1016/S0009-2614(03)01209-0 .

[10] T. Iwasaki, M. Satoh, T. Masuda, T. Fujita, Powder design for UV-attenuating agent with high transparency for visible light,J. Mater. Sci. 35(16) (2000) 4025-4029, https://doi.org/10.1023/A:1004826002503 .

[11] K.Brezesinski, R.Ostermann, P.Hartmann, J. Perlich, T. Brezesinski, Exceptional photocatalytic activity of ordered mesoporous β-Bi_2O_3 thin films and electrospunnanofiber mats Chem. Mater. 22(10) (2010) 3079-3085.https://doi.org/10.1021/cm903780m.

[12] H. Zhang, P. Wu, Y. Li, L. Liao, Z. Fang, X. Zhong, Preparation of bismuth oxide quantum dots and their photocatalytic activity in a homogeneous system, ChemCatChem. 2(2010) 1115-1121, https://doi.org/10.1002/cctc.201000090.

[13] J. Krishna Reddy, B. Srinivas, V. DurgaKumari, M. Subrahmanyam, Sm^{3+}doped Bi_2O_3photocatalyst prepared by hydrothermal synthesis, ChemCatChem.1(2009) 492-496, https://doi.org/10.1002/cctc.200900189 .

[14] A. Hameed, T. Montini, V. Gombac, P. Fornasiero, Surface phases and photocatalytic activity correlation of Bi_2O_3/Bi_2O_{4-x}nanocomposite, J. Amer. Chem. Soc.,130(2008) 9658-9659, https://doi.org/10.1021/ja803603y.

[15] S. Bhardwaj, B. Pal, Effect of variable oxidation states of Mn^{+n} ion impregnated TiO_2nanocomposites for superior adsorption and photoactivity under visible light, J. Alloys Compd. 816 (2020) 152639, https://doi.org/10.1016/j.jallcom.2019.152639.

[16] A. Zaleska, Doped-TiO_2: a review. Recent Pat. Eng.,2(2008) 157-164, https://doi.org/10.2174/187221208786306289.

[17] Z. Zhang, JT. Yates Jr, Band bending in semiconductors: chemical and physical consequences at surfaces and interfaces,Chem. Rev.112(10) (2012) 5520-5551, https://doi.org/10.1021/cr3000626 .

[18] NK. Eswar, S. Adhikari, PC. Ramamurthy, G. Madras, Efficient interfacial charge transfer through plasmon sensitized Ag@ Bi_2O_3hierarchical photoanodes for photoelectrocatalytic degradation of chlorinated phenols, Phys. Chem. Chem. Phys. 20(5) (2018) 3710-3723, https://doi.org/10.1039/C7CP04888B.

[19] S. Abbasi, M. Hasanpour, F. Ahmadpoor, M. Sillanpää, D. Dastan, A. Achour, Application of the statistical analysis methodology for photodegradation of methyl orange using a new nanocomposite containing modified TiO_2 semiconductor with SnO_2, Int. J. Environ. Anal. Chem. (2019) 1-7. https://doi.org/10.1080/03067319.2019.1662414.

[20] Y. Guo, J. Wei, T. Yang, Z. Lv, Z. Xu, Manipulation of surface plasmon resonance for high photocatalytic activity of Ag-Bi_2WO_6 hetero-architecture,Optik 180(2019) 285-29, https://doi.org/10.1016/j.ijleo.2018.11.094.

[21] CJ. Chang, JK. Chen, KS. Lin, YH. Wei, PY. Chao, CY. Huang, Enhanced visible-light-driven photocatalytic degradation by metal wire-mesh supported Ag/flower-like Bi_2WO_6photo catalyst, J. Alloys. Compd. 813(2020) 152186, https://doi.org/10.1016/j.jallcom.2019.152186 .

[22] D. Paraschiv, C. Tudor, R. Petrariu, The textile industry and sustainable development: a Holt- Winters forecasting investigation for the Eastern European area, Sustainability, 7(2015)1280-1291, https://doi.org/10.3390/su7021280 .

[23] S. Zhu, L. Lu, Z. Zhao, T. Wang, X. Liu, H. Zhang, F. Dong, Y. Zhang,Mesoporous Ni-doped δ-Bi_2O_3 microspheres for enhanced solar-driven photocatalysis: a combined experimental and theoretical investigation,J. Phys. Chem.121(17)(2017) 9394-401,https://doi.org/10.1021/acs.jpcc.7b01608 .

[24] Q. Hao, R. Wang, H. Lu, W. Ao, D. Chen, C. Ma, W. Yao, Y. Zhu. One-pot synthesis of C/Bi/Bi_2O_3composite with enhanced photocatalytic activity,Appl. Catal. B-Environ.219 (2017) 63-72, https://doi.org/10.1016/j.apcatb.2017.07.030 .

[25] A. Lebedev, F. Anariba, Li X. Leng DS, P. Wu. Rational design of visible-light-driven Pd-loaded α/β-Bi_2O_3 nanorods with exceptional cationic and anionic dye degradation properties, Sol. Energy,190 (2019) 531-42,https://doi.org/10.1016/j.solener.2019.08.015.

[26] J. Hu, H. Li, C. Huang, M. Liu, X. Qiu, Enhanced photocatalytic activity of Bi_2O_3 under visible light irradiation by Cu (II) clusters modification, Appl. Catal. B-Environ.142 (2013) 598-603,https://doi.org/10.1016/j.apcatb.2013.05.079.

[27] S. Abbasi, Photocatalytic activity study of coated anatase- rutile titania nanoparticles with nanocrystalline tin dioxide based on the statistical analysis, Environ.Monit.Assess., 191(2019) 206.https://doi.org/10.1007/s10661-019-7352-0

[28] SW. Cao, Z. Yin, J. Barber, FY. Boey, SC. Loo, C. Xue, Preparation of Au-$BiVO_4$ heterogeneous nanostructures as highly efficient visible-light photocatalysts, ACS. Appl. Mater. Interfaces.. 4(1) (2011) 418-423, https://doi.org/10.1021/am201481b .

[29] P. Shan, C. Niu, D. Huang, G. Zeng, H. Zhang, Facile synthesis of Ag/AgCl/$BiPO_4$plasmonicphotocatalyst with significantly enhanced visible photocatalytic activity and high stability, RSC. Adv. 5(108) (2015) 89105-89112, https://doi.org/10.1039/C5RA12479D.

[30] S. Singh, R. Sharma, Bi_2O_3/Ni-Bi_2O_3 system obtained via Ni-doping for enhanced PEC and photocatalytic activity supported by DFT and experimental study,SOL. ENERG. MAT. SOL. C.186 (2018) 208-216, https://doi.org/10.1016/j.solmat.2018.06.049.

[31] S. Abbasi, F. Ahmadpoor, M. Imani, M. S. Ekrami-Kakhki, Synthesis of magnetic Fe_3O_4@ ZnO@ graphene oxide nanocomposite for photodegradation of organic dye pollutant,Int J Envir Anal. Chem.100(2020) 225-40.https://doi.org/10.1080/03067319.2019.1636038.

[32] Y. Sasaki, H. Nemoto, K. Saito, A. Kudo, Solar water splitting using powdered photocatalysts driven by Z-schematic interparticle electron transfer without an electron mediator,J. Phys. Chem. C. 113(40) (2009)17536-17542, https://doi.org/10.1021/jp907128k.

[33] T. Selvamani, S. Anandan, Granone L, Bahnemann DW, M. Ashokkumar, Phase-controlled synthesis of bismuth oxide polymorphs for photocatalytic applications, Mater. Chem. Front. 2(9) (2018) 1664-1673, https://doi.org/10.1039/C8QM00221E .

[34] P. Malathy K.Vignesh, M. Rajarajan, A. Suganthi, Enhanced photocatalytic performance of transition metal doped Bi_2O_3 nanoparticles under visible light irradiation,Ceram. Int. 40(1) (2014) 101-107, https://doi.org/10.1016/j.ceramint.2013.11.042.

[35] Y. Huang, W. Ho, Z. Ai, X. Song, L. Zhang, S. Lee, Aerosol-assisted flow synthesis of B-doped, Ni-doped and B–Ni-codoped TiO_2 solid and hollow microspheres for photocatalytic removal of NO, Appl. Catal. B-Environ.89 (2009) 398-405, https://doi.org/10.1016/j.apcatb.2008.12.020.

[36] A. Kudo, M.Sekizawa,Photocatalytic H_2 evolution under visible light irradiation on Ni-doped ZnS photo catalyst, Chem. Commun.15 (2000) 1371-1372, https://doi.org/10.1039/B003297M.

[37] D. Jing, Y. Zhang, L. Guo, Study on the synthesis of Ni doped mesoporous TiO_2 and its photocatalytic activity for hydrogen evolution in aqueous methanol solution, Chem. Phys. Lett. 415(1-3) (2005) 74-78, https://doi.org/10.1016/j.cplett.2005.08.080.

[38] M. Luo Y. Liu, J. Hu, H. Liu, J. Li, One-pot synthesis of CdS and Ni-doped CdS hollow spheres with enhanced photocatalytic activity and durability,ACS. Appl. Mater. Interfaces. 4(3) (2012) 1813-1821, https://doi.org/10.1021/am3000903.

[39] J. Zhao, L. Wang, X. Yan, Y. Yang, Y. Lei, J. Zhou, Y. Huang, Y. Gu, Y. Zhang, Structure and photocatalytic activity of Ni-doped ZnOnanorods, Mater. Res. Bull. 46(8) (2011) 1207-1210, https://doi.org/10.1016/j.materresbull.2011.04.008.

[40] V. Ramamurthy, K. S. Schanze 1998 Organic and Inorganic Photochemistry (Volume 2) Marcel Dekker Inc., New York, 1998

[41] R. Kaur, B. Pal, Plasmonic coinage metal–TiO_2 hybrid nanocatalysts for highly efficient photocatalytic oxidation under sunlight irradiation.New. J. Chem. 39(8) (2015) 5966-5976, https://doi.org/10.1039/C5NJ00450K.

[42] A. Ghaderi, S. Abbasi, F. Farahbod, Synthesis, characterization and photocatalytic performance of modified ZnO nanoparticles with SnO_2 nanoparticles, Mater. Res. Express 5 (2018) 065908, https://doi.org/10.1088/2053-1591/aacd40.

[43] N. Roozban, S. Abbasi, M. Ghazizadeh, The experimental and statistical investigation of the photo degradation of methyl orange using modified MWCNTs with different amount of ZnO nanoparticles.J Mater Sci: Mater Electron 28(2017) 7343–7352, https://doi.org/10.1007/s10854-017-6421-9.

[44] X. Liu, H. Cao, J. Yin, Generation and photocatalytic activities of Bi@ Bi_2O_3 microspheres. Nano. Res. 4(5) (2011) 470-482,doi:10.1088/2053-1591/1/1/015012.

[45] A. L. Patterson, The Scherrer Formula for X-Ray Particle Size Determination,Phys. Rev. 56 (1939) 978-982, https://doi.org/10.1103/PhysRev.56.978

[46] L. Zhang, Y. Hashimoto, T. Taishi, I. Nakamura, QQ. Ni, Fabrication of flower-shaped Bi_2O_3 superstructure by a facile template-free process,Appl. Surf. Sci. 257(15) (2011) 6577-6582, https://doi.org/10.1016/j.apsusc.2011.02.081.

[47] V. Biju,Ni_{2p} X-ray photoelectron spectroscopy study of nanostructured nickel oxide,MATER. RES. BULL. 4 (2007) 791-796, https://doi.org/10.1016/j.materresbull.2006.10.009.

[48] B. Sasi, KG. Gopchandran, Nanostructured mesoporous nickel oxide thin films, Nanotechnology, 18(2007) 115613, doi:10.1088/0957-4484/18/11/11561.

[49] F. Dong, Y. Sun, M. Fu, WK. Ho, SC. Lee, Z. Wu, Novel in situ N-doped $(BiO)_2CO_3$ hierarchical microspheres self-assembled by nanosheets as efficient and durable visible light driven photo catalyst,Langmuir, 28(2011) 766-773, https://doi.org/10.1021/la202752q.

[50] LC. Sim, KW. Ng, S. Ibrahim, P. Saravanan, Preparation of improved p-n junction NiO/TiO_2 nanotubes for solar-energy-driven light photocatalysis. INT.J. PHOTOENERGY.(2013)2013, https://doi.org/10.1155/2013/659013.

[51] T. Suwannaruang, K. Kamonsuangkasem, P. Kidkhunthod, P. Chirawatkul, C. Saiyasombat, N. Chanlek, K. Wantala, Influence of nitrogen content levels on structural properties and photocatalytic activities of nanorice-like N-doped TiO_2 with various calcination temperatures. Mater. Res. Bull.105(2018) 265-276,https://doi.org/10.1016/j.materresbull.2018.05.010.

[52] B. Choudhury, M. Dey, A. Choudhury, Defect generation, d-d transition, and band gap reduction in Cu-doped TiO_2 nanoparticles,Int. Nano. Lett. 3(1) (2013) 25, https://doi.org/10.1186/2228-5326-3-25.

[53] X. Meng, Z. Zhang, Bismuth-based photocatalytic semiconductors: introduction, challenges and possible approaches,J. Mol. Catal. A-Chem.423(2016) 533-49, https://doi.org/10.1016/j.molcata.2016.07.030.

[54] J. Tauc, Optical properties and electronic structure of amorphous Ge and Si, Mater. Res. Bull. 3 (1968) 37-46; https://doi.org/10.1016/0025-5408(68)90023-8.

[55] W. Liu, J. Zhou, J. Zhou, Facile fabrication of multi-walled carbon nanotubes (MWCNTs)/α-Bi_2O_3nanosheets composite with enhanced photocatalytic activity for doxycycline degradation under visible light irradiation, J. Mater. Sci. 54(4) (2019) 3294-3308, https://doi.org/10.1007/s10853-018-3090-x.

[56] M.Ye, H.Zhou, T.Zhang, Y.Zhang, Y. Shao, Preparation of SiO_2@ Au@ TiO_2 core–shell nanostructures and their photocatalytic activities under visible light irradiation. Chemical engineering journal 226 (2013) 209-16.https://doi.org/10.1016/j.cej.2013.04.064.

[57] N.Jallouli, K.Elghniji, O.Hentati, AR.Ribeiro, AM.Silva, M.Ksibi, UV and solar photo-degradation of naproxen: TiO_2 catalyst effect, reaction kinetics, products identification and

toxicity assessment, Journal of hazardous materials.304(2016)329-36.https://doi.org/10.1016/j.jhazmat.2015.10.045.

[58] HY. Jiang, K. Cheng, J. Lin, Crystalline metallic Au nanoparticle-loaded α-Bi_2O_3microrods for improved photocatalysis, Phys. Chem. Chem. Phys. 14(35) (2012) 12114-12121, https://doi.org/10.1039/C2CP42165H.

[59] CK. Lo, D. Xiao, MM. Choi,Homocysteine-protected gold-coated magnetic nanoparticles: synthesis and characterization,J. Mater. Chem. 17(23) (2007) 2418-2427,https://doi.org/10.1039/B617500G.

Chapter-3

Superior adsorptive removal of eco-toxic drug diclofenac sodium by Zn-Al LDH.xBi_2O_3 layer double hydroxide composites

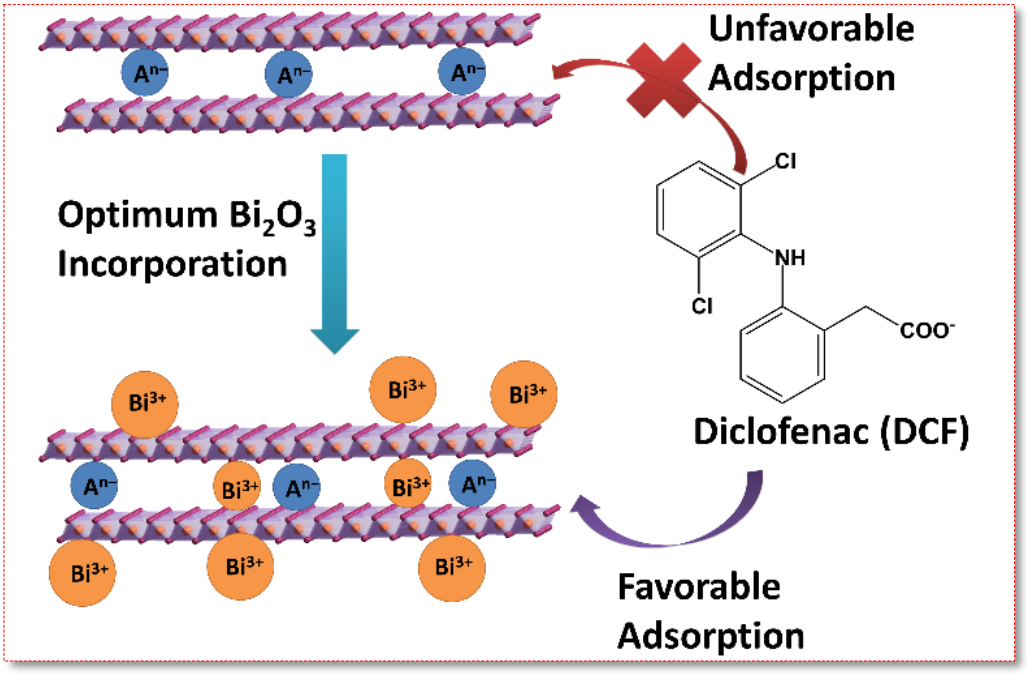

Summary

This chapter deals with the preparation and characterization of Bi_2O_3 loaded Zn-Al layer double hydroxides (Zn-Al LDH.xBi_2O_3) hetero-composites for superior adsorptive removal of diclophenac sodium, a pharmaceutical drug present in waste water. It found that absorption capacity of Zn-Al LDH.xBi_2O_3 displayed 10 fold higher relative to bare LDH material.

3.1 Introduction

Emerging pollutants are a class of fabricated compounds that have been detected in surface water at minute amounts [1-4]. They enter aquatic ecosystem through various pathways, for example, release of wastewater from medical clinics or pharmaceutical manufacturing zones, animal wastewater from poultry, aquaculture, etc [5-8]. Among several the pharmaceutical wastes are recently identified as a new class of contaminants those hare having significant eco-toxicity even at a very low concentration (ppb to ppm level) [9-10]. Due to such environmental significance, efficient removal of these pollutants has drawn substantial attention in recent years [11-14].The non-steroid anti-inflammatory drug Diclofenac sodium (DCF) has been used for the osteoarthritis treatment [15]. However, it established a significant concern as it is neither biodegradable nor simple to be expelled completely from water by conventional treatment method [16-17]. Among different methods, including ion exchange [18], precipitation [19], advanced oxidation and biological, adsorption is considered to an effective approach for treating emerging pollutants due to its high feasibility, effective efficiency and simplicity over a broad concentration range [20-22]. There has been rising amount of research on the preparation of suitable adsorbents for removing diclofenac sodium from water [15, 23-25]. However, slow adsorption capacity, high cost and low regeneration ability of these adsorbents are still challenges to wide scale operation. Therefore, an inexpensive and effective adsorbent catalyst with high diclofenac removal efficiency is urgent.

Layered double hydroxides (LDH) are a class of layered material having exchangeable anions intercalated between positive charged layers. These materials have been attracted significant attraction in the field of wastewater treatment because of the adsorption, catalytic and electrochemical properties [26-33].The surface charge of LDH materials can easily be controlled

by simply varying the stoichiometric ration of divalent and trivalent ions. Recently, wide varieties of LDH based materials with different composition, morphologies have been reported as superior candidate for pharmaceutical waste adsorption. Recently, Sun *et .al.*utilized Mg-Al LDH/Fe_3O_4 for adsorptive removal of Pb^{2+}, Cd^{2+} and Cu^{2+} from waste water [34].Sidra and co-workers utilized a`Zn-Al LDH to remove sulphate and phosphate anion in the water [35].Shamsayei *et al.*prepared nanosheets of LDH/ zwitter ionic histidiene [36] and confirmed their adsorption activity. Chen *et al.* reported[37] carbon/ hydrotalcite for chromium ion removal. Besides, inorganic adsorbents, such as carbon materials, biochar, bentonite, chitosan and bismuth based materials are used to adsorb diclofenac from water [15, 23-25]. However, these adsorbents show low adsorption efficiency, owing to their less ordered pore structure and less surface area. In detail, the disadvantages of these pharmaceutical waste adsorbents are associated to their more cost and less stability in environments [38]. As environmental matter, bismuth based adsorbents are showing a positive effect in water pollution control, that is extensively used for the degradation or removal of pollution from wastewater because of its high stability, low toxicity and simpler synthetic conditions [39-41].

However, Diclofenac adsorption on LDH based and bismuth based materials has been reported by few research groups,[15] but as per best of our knowledge there have been no reports on the adsorption of DCF from water using Zn-Al LDH/Bi_2O_3 composites till date.We had chosen the nitrate salts to synthesize the LDH materials. Because unlike other anions (e.g. chloride, acetate etc.) nitrate is a non-coordinating anion so it does not stick to the LDH layers and remains in the inter-layer space. As a result, the active sites will remain available for guest binding. Also, in the transition metal series Zn (II) has the lowest ionic radius. Moreover, Al (III) is the smallest stable trivalent ion. So, they will result formation of LDH with higher surface charge density. So,Zn-

Al/ LDH Bi_2O_3 hetero-structures can interact with the DCF molecules quite because of the higher surface charge resulting enhance extent of DCF uptake.

In this present study, the Zn-Al LDH.xBi_2O_3 composites were firstly prepared using hydrothermal followed by solvent evaporation method. The as-prepared Zn-Al LDH materials were soft and possess a porous structure. Meanwhile, Diclofenac sodium (DCF) was chosen as a target pollutant. The main objectives was to; fabricate Zn-AlLDH.xBi_2O_3 composites; to evaluate the feasibility of DCF adsorption by varying composition. Thus, Zn-Al-LDH.xBi_2O_3 composites showed an outstanding adsorption activity towards DCF, therefore demonstrating that it can act as capable material for superior adsorptive removal of emerging contaminants from waste water.

3.2 Materials and Methods

3.2.1 Chemicals

All the chemicals Zn $(NO_3)_2.6H_2O$ (98%), $Al(NO_3)_3.9H_2O$ (>96%) ethanol (>96)%, Urea (98%), NaOH(97%), Cyclohexanol (99%) and $Bi(NO_3)_3.5H_2O$ (97%) were purchased from Loba chemie and used without any additional purification.

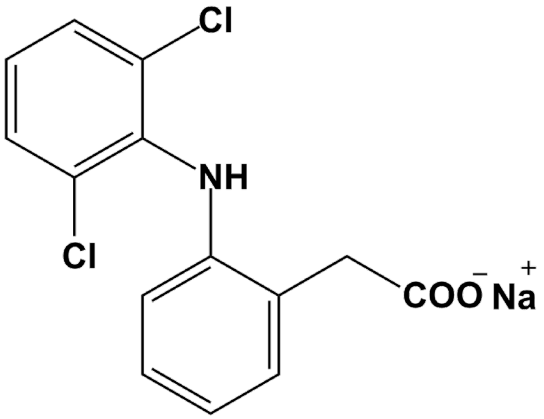

Scheme 3.1: Chemical strucutre of diclofenac sodium (DCF)

Diclofenac Sodium (50 mg) (Scheme 3.1) was purchased from the pharmaceutical company Cipla ltd. The deionized water obtained from (Millipore), an ultrafilteration system (conductivity = 35 mho cm^{-1} at 25ºC) was used in whole experiments.

3.2.2 Synthesis of Bi_2O_3 nanoparticles

50 ml 0.1 M NaOH solution in water was added drop-wise to the 1M of Bi $(NO_3)_3$ solution with vigorous stirring [42]. The resulting solution was heated at 80°C for 5 hours with continuous stirring. The precipitates thus formed were collected by centrifugation and were several times washed using water followed by ethyl alcohol and then dried at 55°C for 12 hours to obtain yellow colored solid.

3.2.3 Synthesis of Zn-Al layer double hydroxides (LDH)

Urea (0.4064 g), $Zn(NO_3)_2.6H_2O$ (1.1156 g) and $Al(NO_3)_3.9H_2O$ (0.4689 g) were dissolved in 25 ml of a water / Cyclohexanol (1:4) mixture. The resulting mixture was sonicated for 15 minutes and transferred to a 100 ml Teflon-lined autoclave that was heated at 150°C for 5 hours [43]. The product obtained upon cooling to room temperature is washed with ethanol and air-dried.

3.2.4 Synthesis of Zn-Al LDHx.Bi_2O_3 (x =0.33, 0.5, 1, 2, 3) composite

For the preparation of Zn-Al LDH.xBi_2O, (x=1) a uniform suspension of 0.2 g Bi_2O_3 in 20 ml ethanol was prepared by sonication (15 minutes). Then, the prepared 0.2 g of ZnAl LDH was to the above solution sonicated again for additional 2 hours. Finally, the solution was dried at 70º C until the ethanol was completely evaporated [44]. Similarly, other composites, Zn-Al LDH.xBi_2O_3(x =0.33, 0.5, 2, 3) were prepared by varying the amount of Bi_2O_3.

3.3 Characterization techniques

X-ray diffraction (XRD) patterns were recorded using the PANALYTICAL X'Pert PRO X-ray diffractometer with Cu Kα (λ=1.540Å) radiation in 2Θ range of 10–80° at a scanning rate of 10° min^{-1}. The surface morphology and elemental composition was recorded in JEOL JSM-7600 F operated at 30 kV. Transmission electron microscopy (TEM) patterns was recorded in Jeol jem 2100 plus microscope operated at 20 kV and HRTEM, FEI Tecnai G2 F20, Netherlands operating at 200 kV.DLS (dynamic light scattering) analysis was used to measure the average hydrodynamic size of prepared samples and zeta potentials of the samples were measured by Zetasizer (ZEN 3600, Malvern, U.K.). BET surface areas were measured using BELSORP MINI-II sorption instrument. X-ray photoelectron spectral (XPS) measurements were recorded by Kratos axis ultra with DLD system (Al (ka) source- 1486.7eV).The concentration of DCF in the solutions were determined by Shimadzu UV-2600 spectrophotometer**.**

3.4 Adsorption experiments

Adsorption measurements (Scheme 2) were carried out by adding 10 mg of prepared samples to the 100 ml of DCF solution (50 mg L^{-1}). The solutions were placed on magnetic stirrer (120 rpm). The aqueous solutions were taken out at pre-fixed intervals. The adsorption quantity of the composites at various time intervals was computed by the equation 1.

$$q_t = \frac{(C_0 - C_t)V}{W} - - - - - - - (1)$$

Where C_t is the concentration of the DCF at time t, C_0 is the initial concentration of the DCF, V is the total volume of the DCF solution, W is the mass of the adsorbent, and q_t is the adsorption capacity at different time t.

Then the above solution was then stirred for 3 hours at ambient temperature. Subsequently, the residual concentration of DCF was obtained. The adsorption quantity is determined using equation 2.

$$q_e = \frac{(C_0 - C_e)V}{W} - - - - - - - - (2)$$

Where C_e is the DCF concentration at equilibrium, C_0 is the initial concentration of the DCF, V is volume of DCF solution, W is the mass of the adsorbent and q_e is the adsorption quantity at equilibrium. In order to confirm the exact nature of the sorption process the uptake quantities after short (1 hour) and long (24 hours) time intervals are compared.

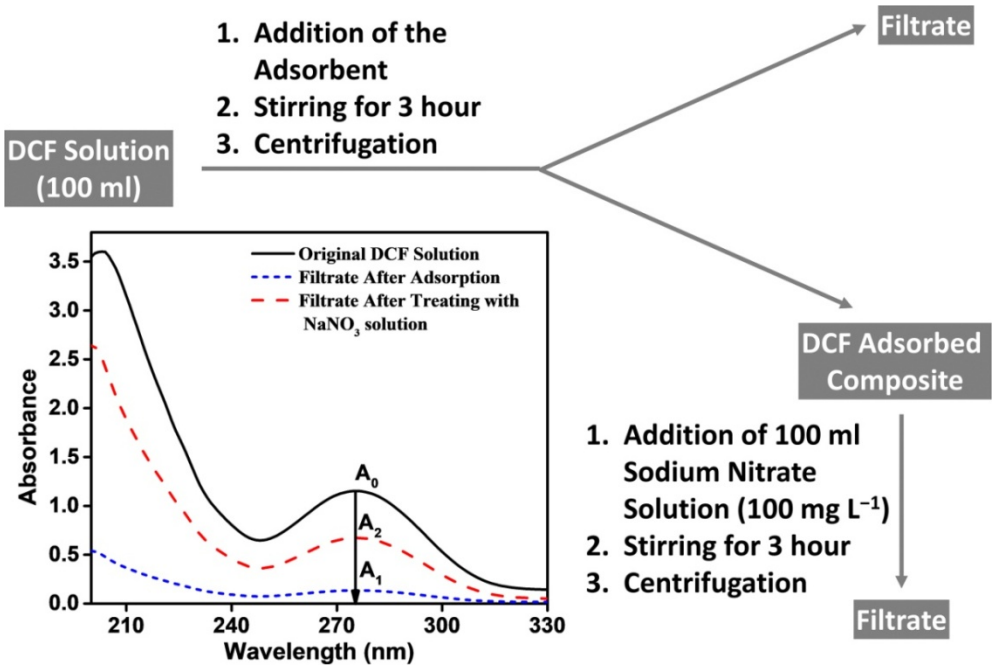

Scheme 3.2 Schematic representation of DCF sorption and adsorbent regeneration process.

In order to check the reversibility of the regeneration (Scheme 3.2) process the DCF adsorbed composite was first stirred with 100 ml $NaNO_3$ solution (100 mg L^{-1}) for 3 hours. Consequently,

the absorbance of the solution was measured to determine the concentration of DCF released. The percentage of DCF release was calculated by equation (3)

$$\%\ of\ DCF\ Released = \frac{A_2}{(A_0 - A_1)} - - - - - - - - (3)$$

Where A_0, A_1 and A_2 are the absorbance values for the original DCF solution, DCF solution after adsorption and the solution obtained after treating with $NaNO_3$ solution.

3.5 Results and discussions

3.5.1 XRD analysis

X-ray diffraction (XRD) patterns for the prepared hetero-structures (Zn-Al LDH.xBi_2O_3) with different composition (x=0 to 2) as well as the α-Bi_2O_3 were shown in Fig.3.1. The diffractions pattern of different samples matches perfectly with the monoclinic α-Bi_2O_3 phase (JCPDS: 00-041-1449) with main diffraction peaks consistent with (111) (041) and (241) lattice plane sand the Zn-Al LDH with major diffraction peaks consistent with (003), (006), (012) and (110)[45,46].No crystalline phase impurities were observed, showing the formation of phase pure α-Bi_2O_3. Moreover, the diffraction peak positions of prepared samples confirmed that there was no noticeable variation in the presence of Bi_2O_3 only a minor reduction in the relative intensities is observed. It confirms the formation of Zn-Al LDH.xBi_2O_3 mixed composites. It has been also confirmed that by varying the amount of Bi_2O_3 crystal structure does not gets affected. However, by increasing the stoichiometery of Bi_2O_3 the relative intensities of the peaks correspond to Bi_2O_3 starts increasing which was generally referred as “solid dilution effect”. The crystalline sizes for the Zn-Al LDH.xBi_2O_3 sample were determined by Scherrer formula from the characteristic peak related to Bi_2O_3(111) crystal plane were about 22 nm indicating the

formation of Bi_2O_3 nanoparticles, due to the presence of Zn-Al LDH to preclude the extent of aggregation.

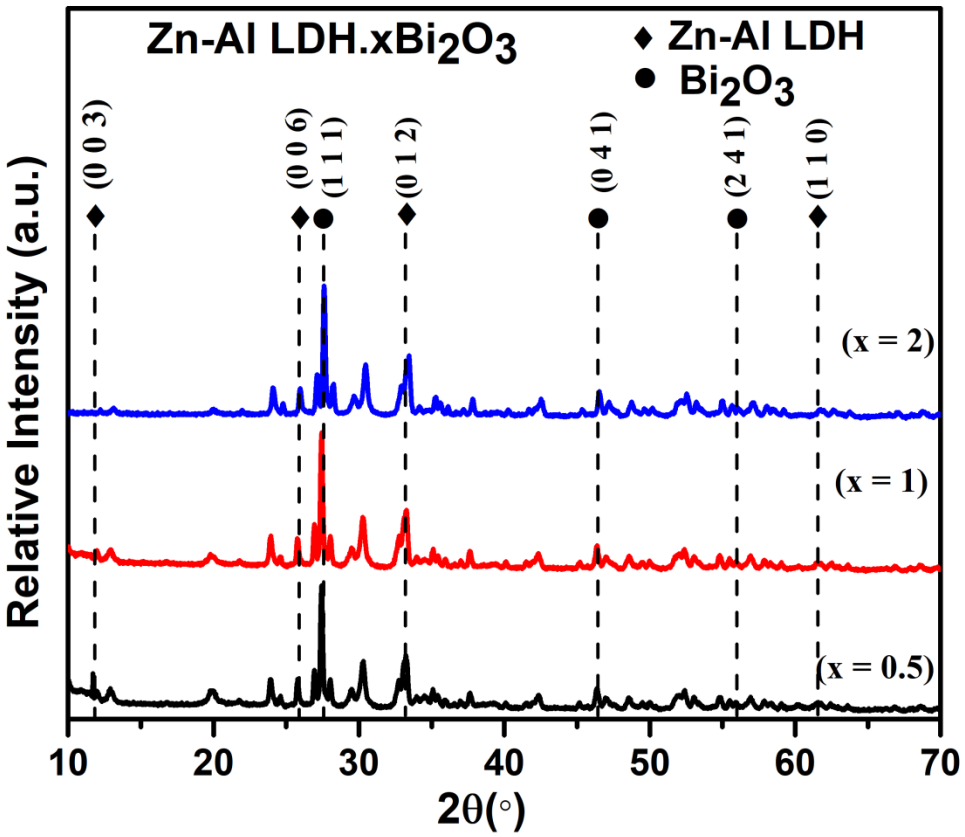

Figure 3.1: X-Ray diffraction patterns of as synthesized Zn-Al LDH.xBi_2O_3 heterostrctures

TEM images of Bi_2O_3-Zn-Al LDH (1:1) were shown in Fig 3.2.As shown in Fig (3.2: a-d) the structure was flower shaped morphology. The Fig 3.2-e showed lattice planes (041) and (012) for Bi_2O_3 and Zn-Al LDH respectively. It has been observed that the composite material was having very tiny thickness, and thin layer of Bi_2O_3 was homogeneously spread on the outer surface of the LDH (Fig 3.2-e). Furthermore, the lattice plane (012) was well matched with fringes (Fig. 3.2 f) of Zn-Al LDH.

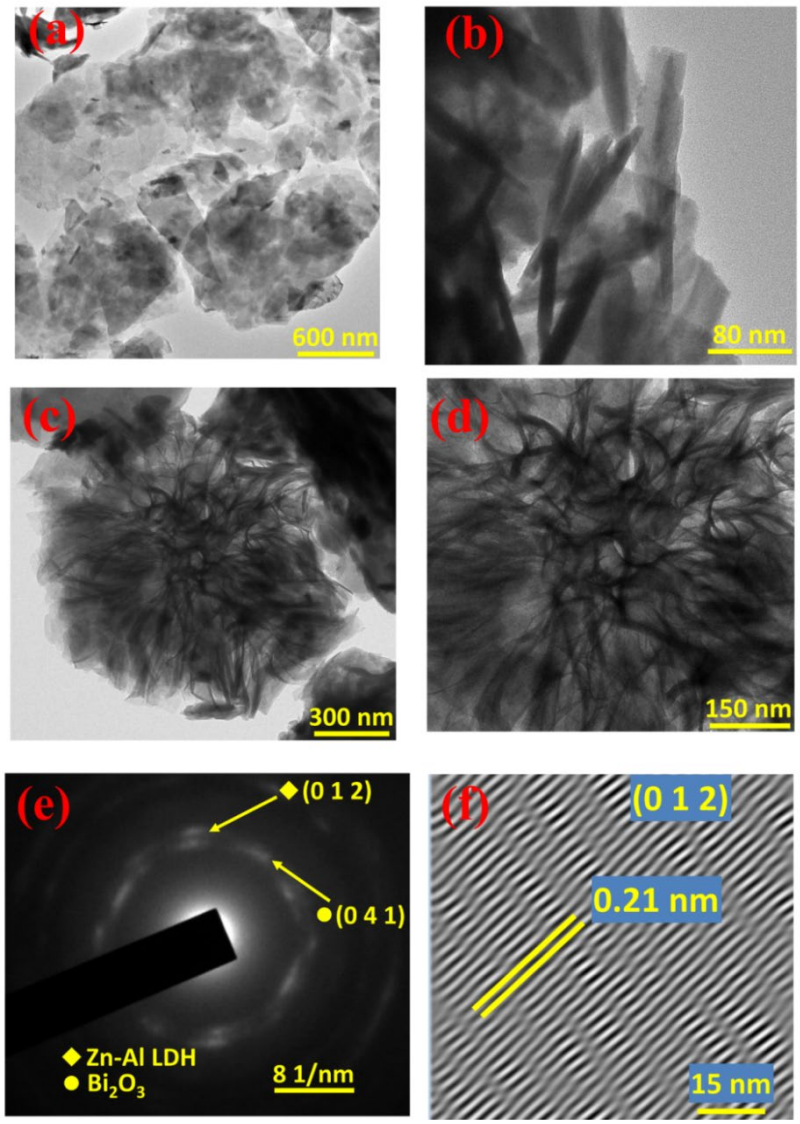

Figure 3.2: (a-d) TEM imgaes (e) SAED patterns and (f) HRTEM images of as synthesized Zn-Al LDH.xBi_2O_3 (x=1) composite particles

However, it has been observed that in the hetero-structure, the interlayer spacing was substantially greater and dispersed and more defect sites were formed and that can greatly improve its adsorption capacity.

3.5.2 XPS analysis

Elemental compositions and oxidation state of Zn-Al LDH.xBi_2O_3(x=1) composites were further determined by X-ray photoelectron spectroscopy (XPS).

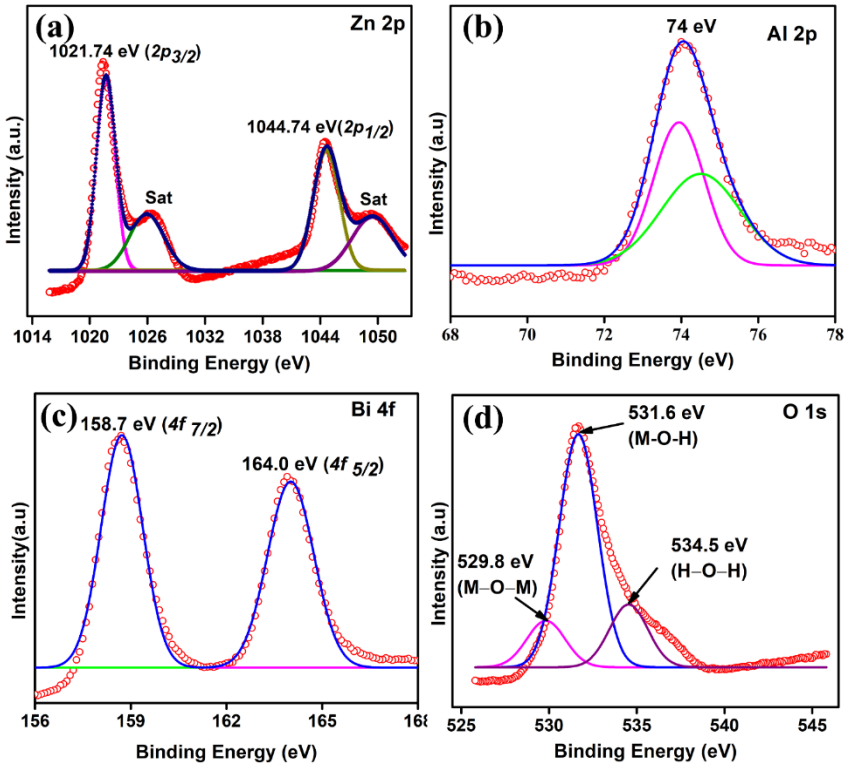

Figure 3.3: (a) Zn 2p, (b) Al 2p, (c) Bi 4f and (d) O 1s XPS spectra of Zn-Al LDH.xBi_2O_3 (x=1) heterostructures

The representative peaks for each element was all identified in individual XPS patterns (Fig. 3.3). The Zn $2p_{3/2}$ and $2p_{1/2}$ signals were located 1021.74 eV and 1044.74 eV [47] with a typical Russel-Saunders splitting of 23.0 eV that was consistent with the standard Zn^{2+} peaks of Zn-Al LDH. Such observation was consistent with alteration of that Zn-Al LDH structure due to formation of Zn-Al LDH.Bi_2O_3 binary composites. The Al 2p peak has been deconvoluted into two symmetric single peaks. The Al 2p peaks at around 74.0 eV suggested the presence of Al–O and Al–OH bonds. The O 1s spectrum (Fig. 3d) confirmed presence of three distinct oxygen

species. The characteristic peaks at about 529.8 eV, 531.8 eV and 534.5 eV were consistent with presence of oxide (M–O), hydroxide, hydroxide (M–OH) and hydrogen bonded adsorbed water (H–O–H) respectively [47, 48].The binding energies of Bi $4f_{7/2}$ (158.7eV) and $4f_{5/2}$ (164.0 eV) has been attributed to the Bi^{3+} species of α-Bi_2O_3phase [49].All the above observations led to the information about Zn-Al LDH.xBi_2O_3 (x=1) hybrid composite formation.

3.5.3 Morphology

The SEM images of original LDH and the hybrid composites were shown in Fig.3.4. As revealed by Fig. 3.4 a and b, the morphology of Zn-Al LDH assembled by sheets of LDH were oriented different directions to afford flower shaped morphology.

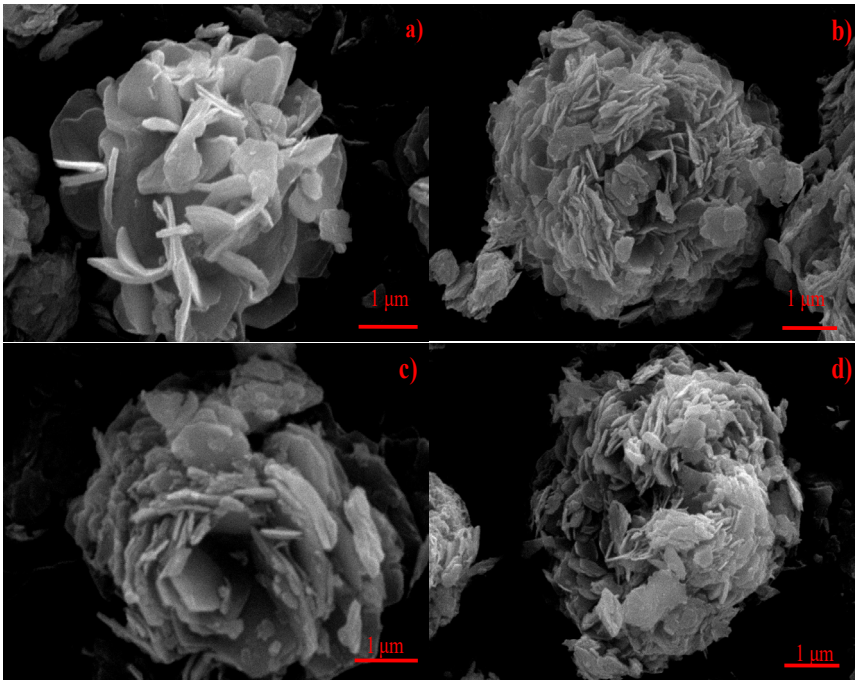

Figure 3.4: SEM images of Zn-Al LDH.xBi_2O_3 (x=1) heterocomposites

The whole arrangement has been extended from the origin of the core if different orientations. Fig. 3.4c and 3.4 d offered a direct observation of the Zn-Al LDH.xBi_2O_3 composite. It could be observed that small particles of Bi_2O_3 nanoparticles were dispersed on the exterior of LDH,

which indicated the formation of the Zn-Al LDH.xBi_2O_3.This appropriate structure of composite can result in a coupling of Bi_2O_3 and Zn-Al LDH; hence it was good for the adsorption performance. The possible mechanism for the formation of rose-like Zn-Al LDH has been presented in Scheme 3.3.

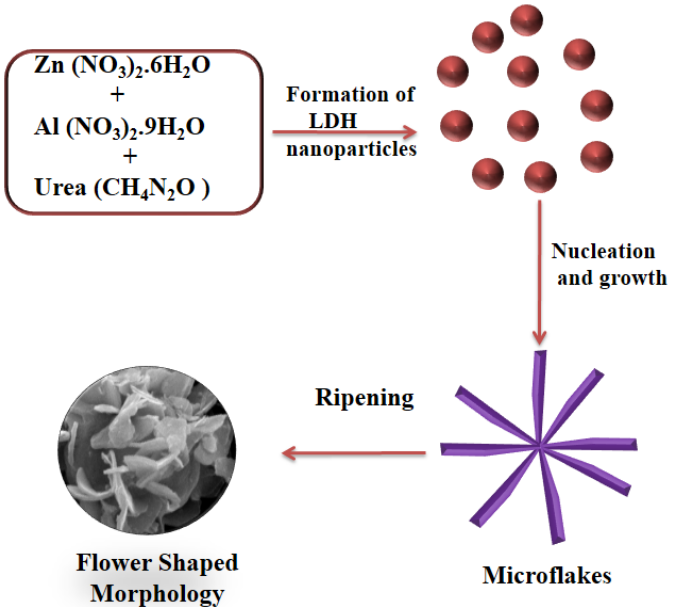

Scheme 3.3 Schematic interpretation of growth mechanism for Zn-Al LDH rose-like microstructure

When the volume ratio of water to cyclohexanol is 1:4, a large quantity of cyclohexanol and water to afford a microemulsion, which limits the growth of hydrotalcite, to yield droplets. At a suitable temperature, urea hydrolyzes to form CO_3^{2-} and OH^- and then reacts with Al^{3+}, Zn^{2+} to afford Zn-Al-LDH composite particles. According to Ripening phenomenon [50], as the reaction time precedes the concentration of reactants decreases and equilibrium was formed at the solid-liquid interface and the concentration around small particles of parent component was more than the larger particles. At this stage, transmission of the components to low concentration region takes place due to the concentration difference of the original component. Thus, the smaller

meta-stable particles were adsorbed at the surface of the larger particles and layers progressively start dissolving and then recrystallize to developed Zn-Al-LDH layers. Further, Zn-Al layers then spontaneously assemble under solvothermal conditions. Thermodynamically the nanosheets have a substantial surface energy. In order to reduce the surface energy sheets, aggregate to eventually form layered rose like formation. Fig.3.5 and 3.6 showed the EDS patterns of Zn-Al LDH and the Zn-Al LDH.xBi_2O_3 respectively. The elemental mapping suggested that the Bi_2O_3 particles were homogenously dispersed on the LDH surface. Moreover, EDS pattern confirmed formation of few larger Bi_2O_3 aggregates as well.

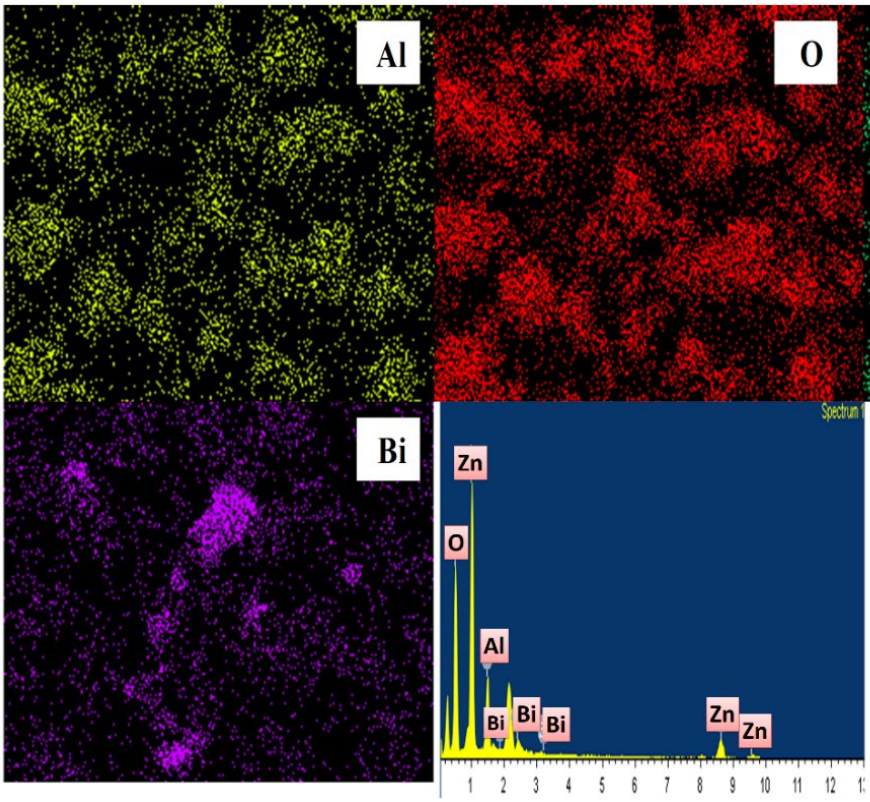

Elements	Weight %	Atomic %
O K	37.08	68.33
Al K	8.70	9.51
Zn L	46.80	21.16
Bi M	7.41	1.00
Total	100	

Figure 3.5: EDS spectra of Zn-Al LDH.xBi_2O_3 (x=1) heterostructures showing compositional uniformity

It has been recognized that the stoichiometric ratio for Zn to Al is (21.1: 7.51) which was very close to the amount taken in reactant i.e. (1:0.33).It confirmed that the ratio of cyclohexanol and water had played a key role for the formation of flower shaped structure

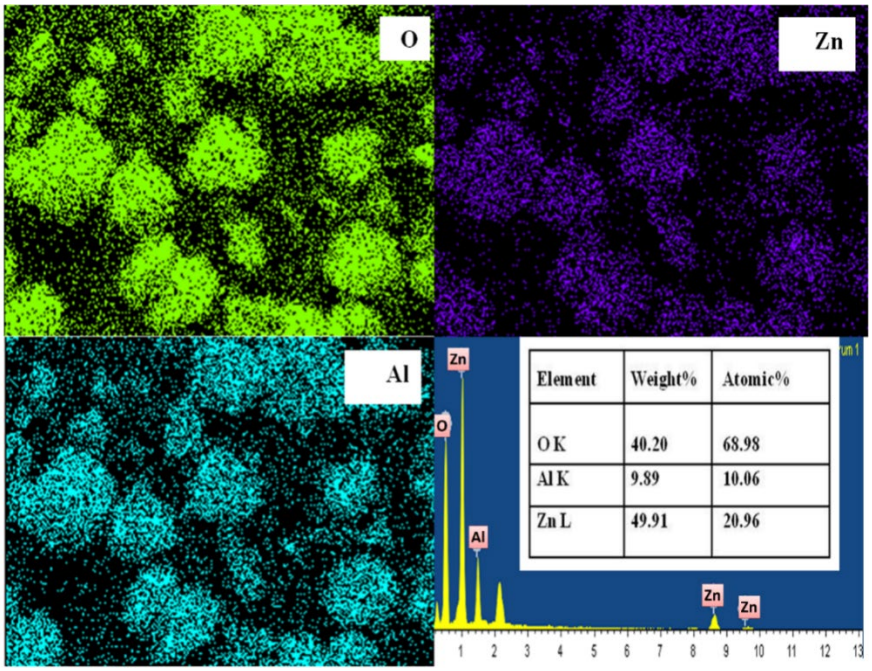

Figure 3.6: EDS spectra of as synthesized pristine Zn-Al LDH showing compositional uniformity

Dynamic light scattering (DLS) spectra of these micro composites revealed that upon increasing bismuth loading the hydrodynamic sizes gradually increases from 497 nm to 2035 nm (Fig.3.7a). Because, increasing Bi_2O_3 loading leads to enhanced extent of aggregation thereby resulted formation of larger Bi_2O_3 nanoparticles. Presence of these larger particles cause increase in the hydrodynamic size of the composites. Also, upon compare to the composite with x=2, the heterostucture with x=3 has lesser bandwidth suggesting it has a narrower particles size distribution. Variation of the surface charge densities of these hetero-composites investigated. The zeta potential of the Zn-Al LDH is −22.5 mV, Fig. 3.7 b hence revealed that has having negatively charge

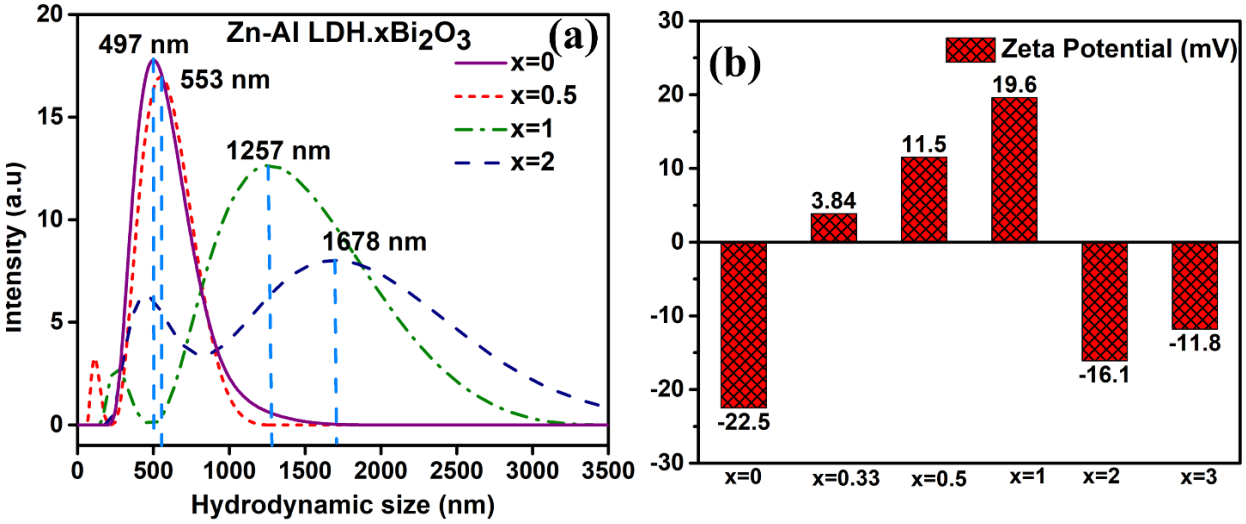

Figure 3.7: (a) DLS hydrodynamic particle size of Zn-Al LDH.xBi_2O_3 (x=0 to 2) composites and (b) variation of zeta potential of Zn-Al LDH.xBi_2O_3 (x=0 to 3) hybrid structures

surface in aqueous medium. With increase the extent of Bi_2O_3, the Bi^{3+} cations start neutralizing the negative charges. As a result, the zeta potential becomes more and more positive till x=1 (19.6 mV). Upon further increasing the amount of bismuth it can undergo hydrolysis and get converted into hydroxo anion as a result the zeta potential again changes towards negative (Fig.3.7 b).In the composite with x=3 due to higher degree of aggregation, lesser number of functional groups were exposed to the surface resulting lesser extent of hydrolysis. So, it has lesser negative zeta potential compare to the hybrid with x=2.

3.5.4 Nitrogen adsorption-desorption isotherms

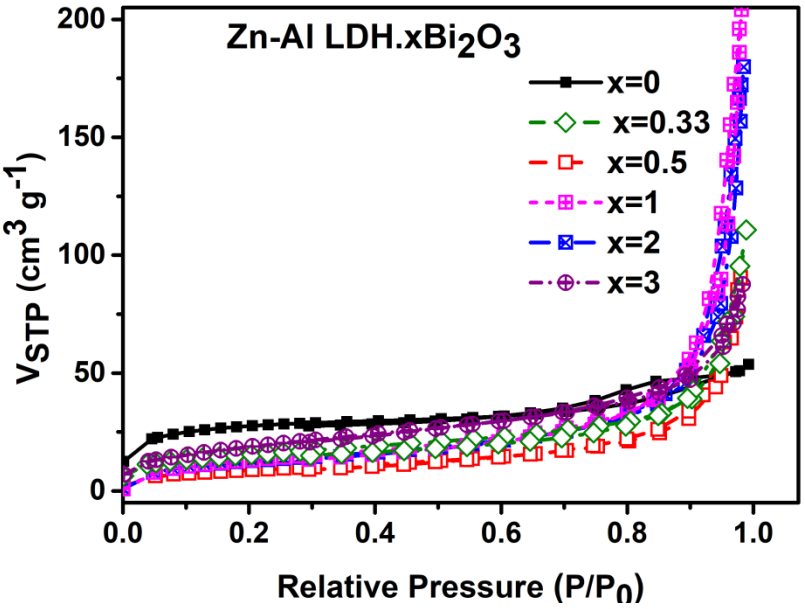

Figure 3.8: Nitrogen sorption isotherms Zn-Al LDH.xBi$_2$O$_3$ (x=0 to 3) heterostructures

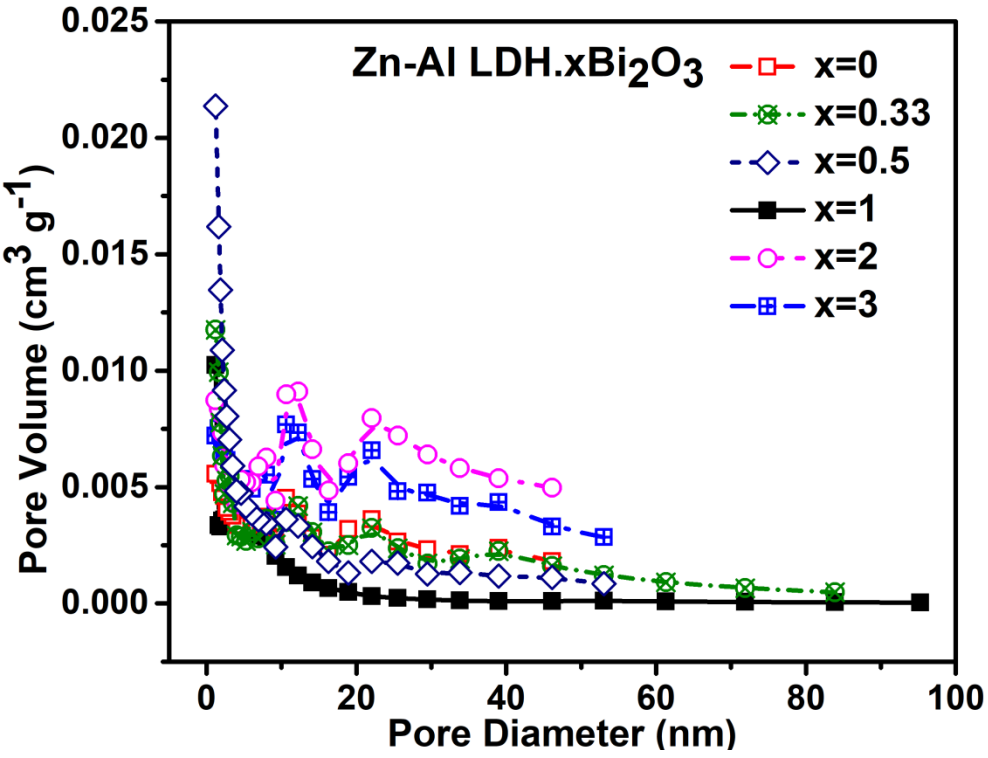

Figure 3.9: Pore size distribution curves for Zn-Al LDH.xBi$_2$O$_3$ (x=0 to 3) hybrid composites

X	S_{BET} ($cm^2\ g^{-1}$)	V_{pore} ($cm^3 g^{-1}$)	Average pore size (nm)
0	**33.9**	**0.170**	**20.09**
0.33	**54.8**	**0.171**	**12.5**
0.5	**70.5**	**0.135**	**7.69**
1	**102**	**0.082**	**3.24**
2	**49.6**	**0.316**	**25.44**
3	**48.1**	**0.278**	**23.15**

Table 3.1 Specificsurface area (S_{BET}), pore volume, and average pore size of synthesized Zn-Al LDH.xBi_2O_3 heterostructures

The nitrogen adsorption-desorption isotherms and the resultant pore size distribution of the composites revealed that the isotherms of the samples showed characteristic features of type IV isotherm, suggested the existence of mesopores in the samples that the intra-particle diffusion model may be the main rate determining step (Figs 3.7, 3.8 and Table 3.1)[51].The pristine Zn-Al LDH was having 33.9 $m^2\ g^{-1}$ surface area. Upon increasing the stoichiometric ratio of Bi_2O_3 the BET surface area initially increases and then it again decreases (Fig. 3.10). The hybrid composite with x=1 was having highest BET surface area (102 $m^2\ g^{-1}$) which is ~3 times compare to the bare analogue. This was because loading of Bi_2O_3 results two opposite effects. It increases the number of adsorption sites thereby enhancing the surface area. It also enhances the extent of aggregation, thereby limiting the availability of these active sites. Also, as suggested by DLS the particle size distribution for composite with x=3 is narrower compare to its analogue with x=2. So, there were formation of higher degree of mono-dispersed particles in x=3. So,

variation in the extent of active site blocking is less drastic. As a result, the decrease in the BET surface area between x=2 and 3 was much lesser compare to the corresponding drop between x=1 and 2.

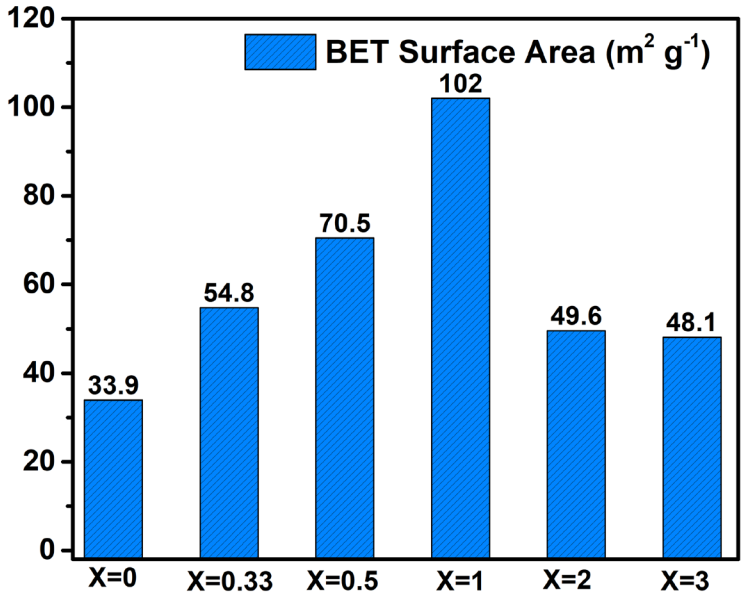

Figure 3.10: Variation of BET surface area for the Zn-Al LDH.xBi_2O_3 (x= 0 to 3) hybrid structures

3.6 Adsorption isotherms

The DCF adsorption isotherms for these material how that the sorption capacity was highest (574.81 mg g^{-1}) for the hetero-structure Zn-Al LDH.xBi_2O_3 (x=1). (Figs. 3.11, Tables 3.2 to 3.3) which was nearly 10 times higher compare to the bare LDH (57.83 mg g^{-1}). The reason for the DCF adsorption capacity was as follows: The BET surface area and zeta potential of these hybrids were two important aspects governing the DCF uptake. The pristine Zn-Al LDH exhibits lowest adsorption performance due to negative charge on the surface (-22.5 mV) and resulting in electrostatic repulsions between the anionic DCF and Zn-Al LDH. The Zn-Al LDH.xBi_2O_3 (x=1)

hybrids demonstrates a largest specific surface among all the composites. It is also having highest positive zeta potential (19.6 mV).This was beneficial for adsorbing diclofenac [52].

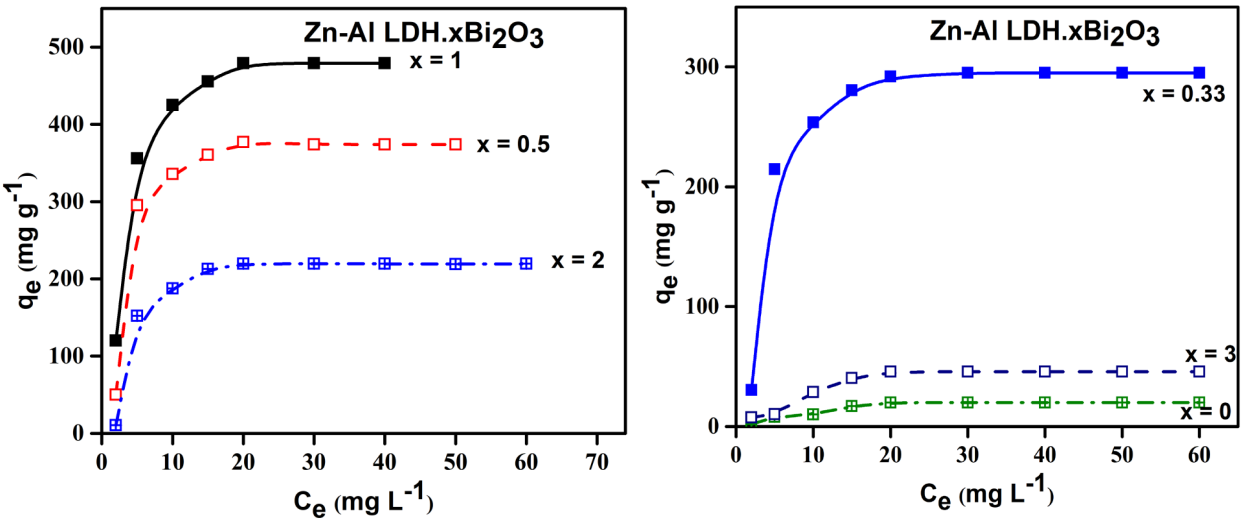

Fig.3.11. DCF adsorption isotherms of Zn-Al LDH.xBi_2O_3 a) (x=1, 0.5 and 2). b) (x=0, 0.33 and 3) micro structures at 27^0C

The Langmuir (Equation 4) and Freundlich (Equation 5) adsorption models were utilized to determine the sorption data [52-53]. The linearized forms of these models were represented below:

$$\frac{C_e}{q_e} = \frac{C_e}{q_{max}} + \frac{1}{K_L q_{max}} - - - - - - - - - (4)$$

$$\log q_e = \log K_F + \frac{1}{n} \log C_e - - - - - - - - (5)$$

x	q_{max}(mg g^{-1})	K_L	R^2
0	57.83	0.089	0.997
0.33	363.63	0.120	0.985
0.5	476.19	0.134	0.994
1	574.71	0.215	0.999
2	315.20	0.0549	0.997
3	25.09	0.084	0.998

Table 3.2 Parameters as per Langmuir asdorption isotherm models for Zn-Al LDH.xBi_2O_3 composites at 298K

X	K_F(mg g^{-1})	N	R^2
0	5.794	0.57	0.850
0.33	38.28	0.65	0.885
0.5	42.36	0.82	0.945
1	92.46	0.68	0.889
2	18.15	0.76	0.875
3	2.16	0.62	0.919

Table 3.3 Parameters as per Freundlich asdorption isotherm models for Zn-Al LDH.xBi_2O_3 hybrid structures at 298K

where q_{max} is the adsorption quantity at maximum; q_e is the adsorption capacity at equilibrium; C_e is the DCF concentration at equilibrium; K_L and K_F are the Langmuir and Freundlich constants respectively; and n is the intensity factor (Figs. 3.12, 3.13, 3.14 and Tables 3.2 and 3.3).The parameter for DCF removal using the prepared samples were listed in Table 3.3. The R^2 values suggest that the adsorption process obeyed Langmuir adsorption isotherm model which was consistent with monolayer adsorption process. The K_L values are in 0 and 1, thus confirming favorable for adsorption of DCF by these samples. As per Langmuir isotherm the maximum adsorption capacities of Zn-Al LDH.xBi_2O_3 (x=1) toward DCF is 574.71 mg g^{-1} that was almost 10 times higher compare to the pristine LDH (57.83 mg g^{-1}).

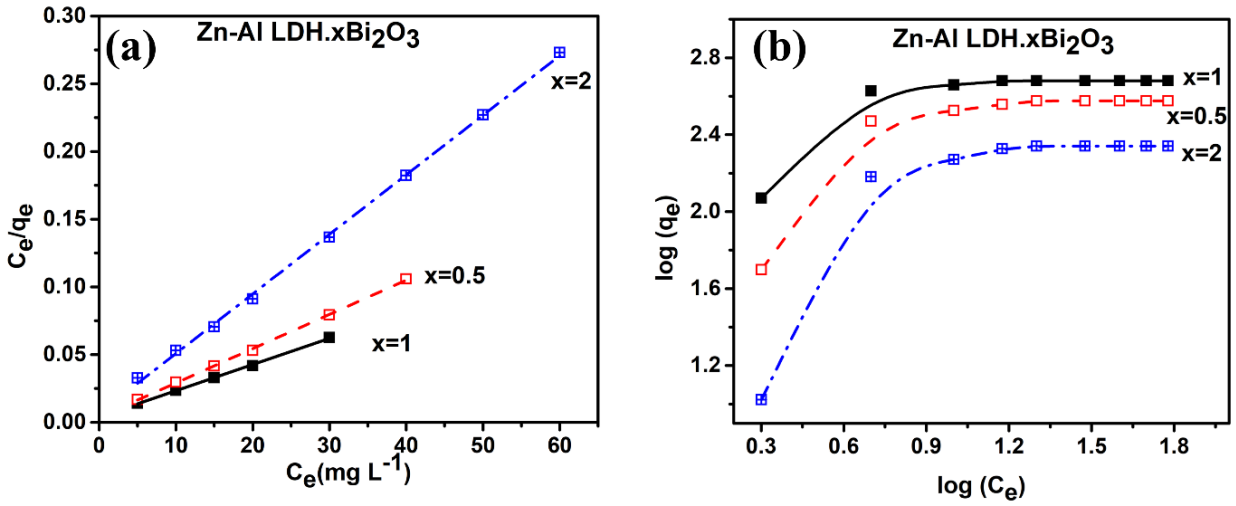

Fig.3.12. Lines fitted using the linearized Langmuir (a) and Freundlich (b) isotherm models for DCF adsorption for Zn-Al LDH.xBi_2O_3 (x = 0.5, 1,2) heterostructures

There can be two different types of interactions between DCF and the composite: (i) Electrostatic interactions of the DCF anions with the charged surface and (ii) hydrogen bonding interactions of N, O and Cl atoms of DCF with the oxide and hydroxide groups present of the surface of the adsorbent (Scheme 3.4).

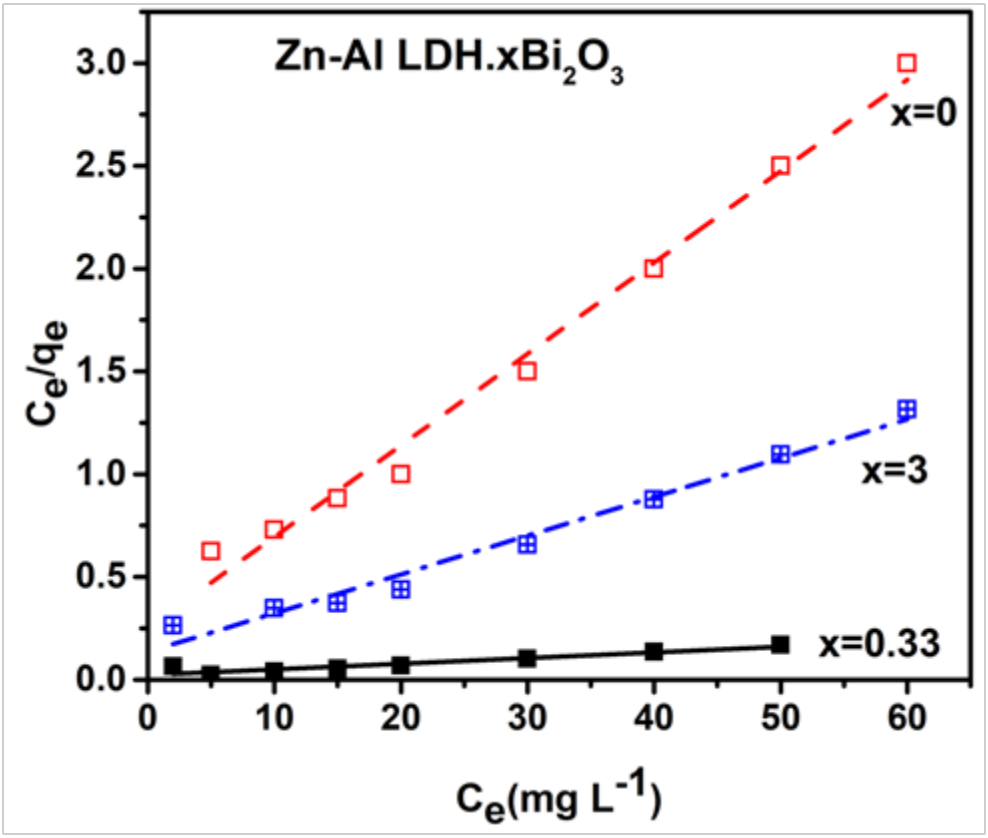

Fig.3.13. Lines fitted using the linearized Langmuir (isotherm models for DCF adsorption for for Zn-Al LDH.xBi$_2$O$_3$ (x=0, 0.33 and 3) heterostructures

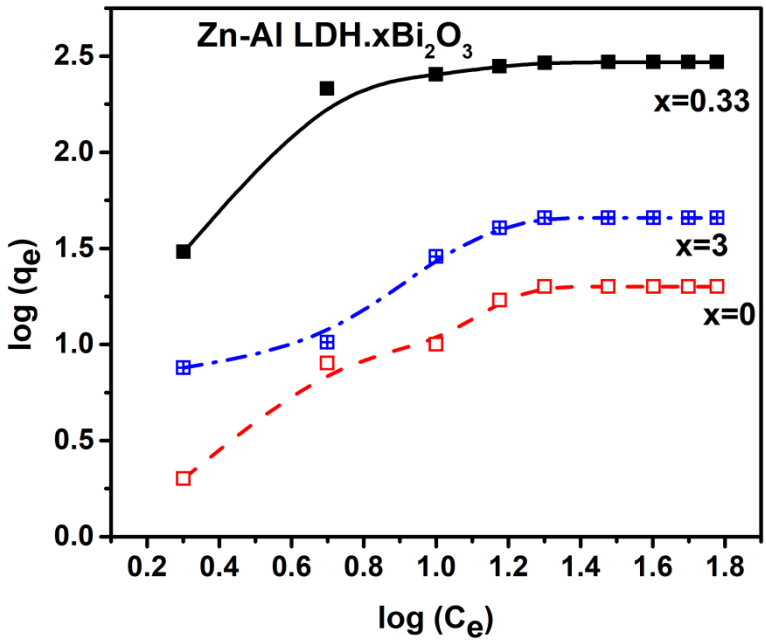

Fig.3.14. Lines fitted using the linearized Freundlich isotherm models for DCF adsorption for for Zn-Al LDH.xBi$_2$O$_3$ (x=0, 0.33 and 3) hybrid composites

X	q_e(mg g^{-1})	K_1	R^2
0	44.38	4.51×10^{-2}	0.882
0.33	299.40	6.51×10^{-2}	0.932
0.5	381.67	6.58×10^{-2}	0.903
1	487.80	6.73×10^{-2}	0.867
2	228.83	6.42×10^{-2}	0.962
3	29.56	3.50×10^{-2}	0.861

Table 3.4 kinetic parameters for the as-prepared Zn-Al LDH.xBi_2O_3hetero-structures for Diclofenac adsorption as per pseudo-first order model

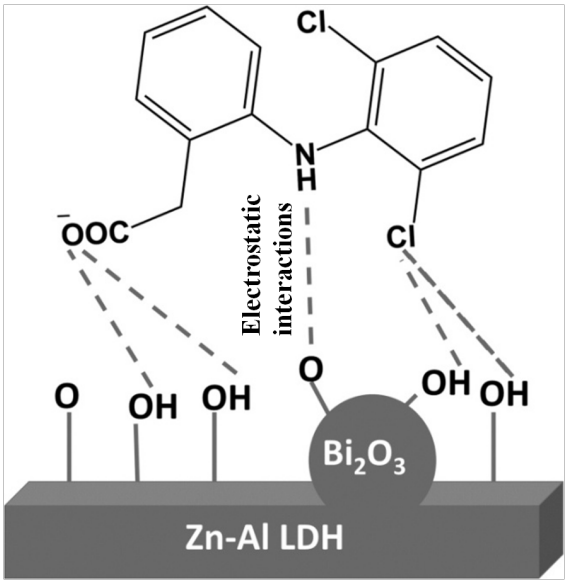

Scheme 3.4 Schematic representation of different hydrogen bonding interactions of Diclofenac with the adsorbent.

3.6.1 Adsorption Kinetics

The DCF adsorption kinetic data of prepared sample (Figs.3.15a, 3.14, 3.16 and Table 3.4) revealed that the DCF uptake capacities were improved over time and finally approach towards equilibrium. The adsorption details fitted by applying the intra-particle diffusion kinetic model (Fig.3.15 b, Table 3.4, Equation 6) where q_t is the adsorption capacity at time t, K_{di} is the interparticle diffusion rate constant and C_i is the intercept of the curve that represents the boundary layer or surface absorption effect.

$$q_t = k_{di}\sqrt{t} + C_i \quad ---------(6)$$

In Fig. 3.15b, the entire graph contains three different straight lines which is consistent with three step adsorption process.

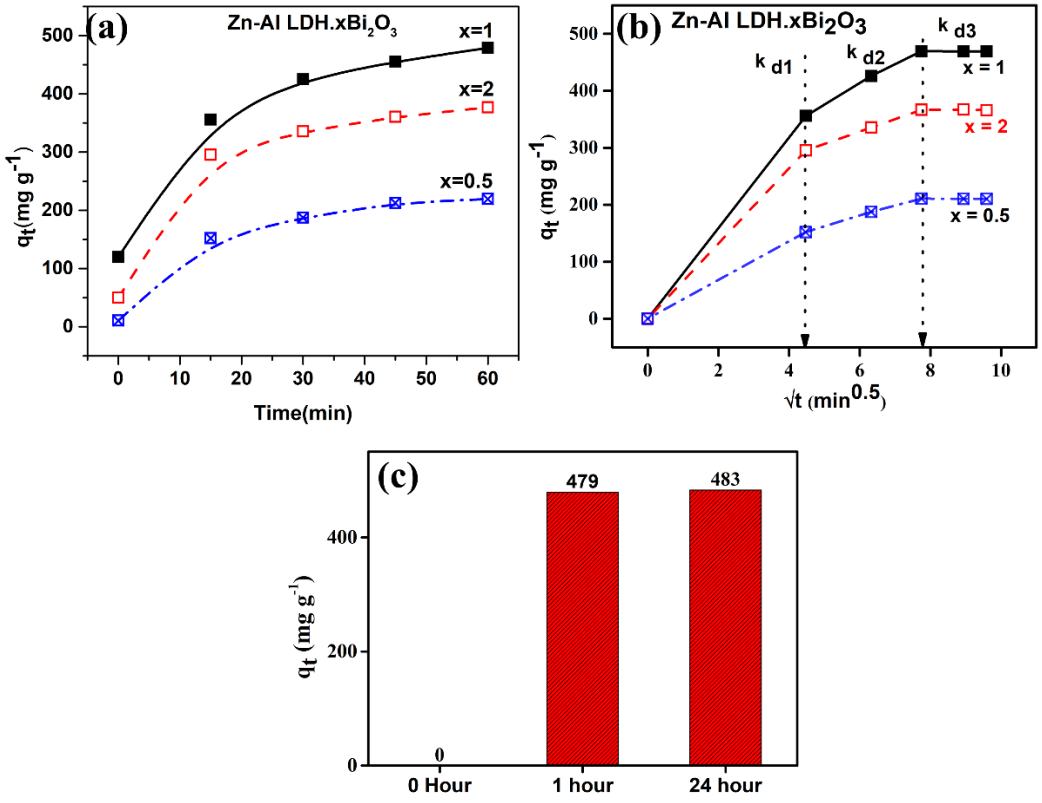

Fig.3.15.(a) Variation of DCF adsorption with time at at Room Temperature (32-35 °C) and (b) Intra-particle diffusion kinetic model and (c) Variation of DCF uptake with time for Zn-Al LDH.xBi_2O_3 (x=0.5, 1,2) heterostructures.

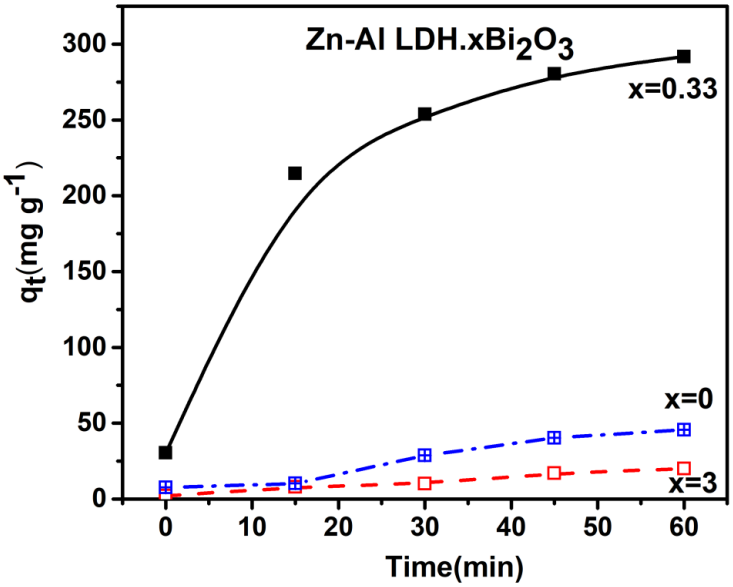

Fig.3.16. Variation in adsorption capacity with adsorption time for DCF on the as-prepared Zn-Al LDH.xBi_2O_3 (x=0, 0.33, 3) microstructures at 27

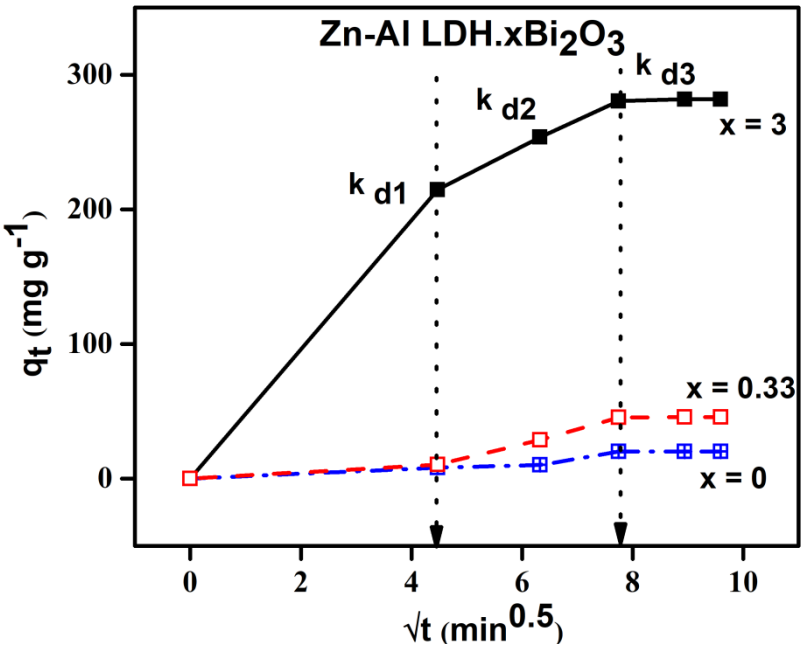

Fig.3.17 Intra-particle diffusion model for Zn-Al LDH.xBi_2O_3 (x=0, 0.33 and 3) composite.

The first step involved rapid adsorption (70-80%) on the surface of the adsorbent within a period of initial 4 min. k_{d1} (79.6) is larger in Zn-Al LDH.xBi_2O_3 (x=1) than bare LDH (2.29) due to the large specific surface area and highly positive zeta potential. Such observation suggested favorable electrostatic and other non-covalent interaction of Zn-Al LDH.xBi_2O_3 (x=1) with DCF compare to the bare analogue. The second step involves the absorption of the DCF molecules (20-30%) in the heterostructures. k_{d2} (34.7) value is larger in Zn-Al LDH.xBi_2O_3 (x=1) than in pristine LDH (10.6) due to higher surface area [54]. In the final stage is the equilibrium, the adsorption process slowly saturates to reach equilibrium. This observation suggested that the sorption process is primarily adsorption in exterior surface along with some absorption inside the pores. In order to verify the complete saturation of the sorption process, we have also performed is because upon longer control experiment by measuring the uptake capacity after a significantly long time period (24 hours). But, the sorption capacities after 1 hour (579 mg g^{-1}) and 24 hours (583 mg g^{-1}) are essentially constant (Fig 3.15c). Such observation suggested that the sorption was practically saturated after 1 hour.

To demonstrate the sorption performance more, pseudo-first-order (Equation 7), pseudo-second-order (Equation 8) kinetic models are applied [55–57].

$$\frac{t}{q_t} = \frac{1}{k_2 q_e^2} + \frac{t}{q_e} - - - - - - (7)$$

$$\log(q_e - q_t) = \log q_e - \frac{k_1 t}{2.303} - - - - - - (8)$$

The q_e and q_t represented the adsorption quantities at equilibrium and time t, similarly; k_1 and k_2 are the rate constants for pseudo-first-order and pseudo-second-order models respectively. The

fitted lines for the adsorption kinetics are displayed in Figs 3.20, 3.18, 3.19. The corresponding correlation coefficients and parameters and were showed in Table 3.4, 3.5 and 3.6. The correlation coefficient (R_2) (Table 3.2 and 3.3) values suggest that the DCF adsorption obeys pseudo second order kinetics. The determined equilibrium adsorption capacity of the pseudo-second-order model is more consistent with the measured data.

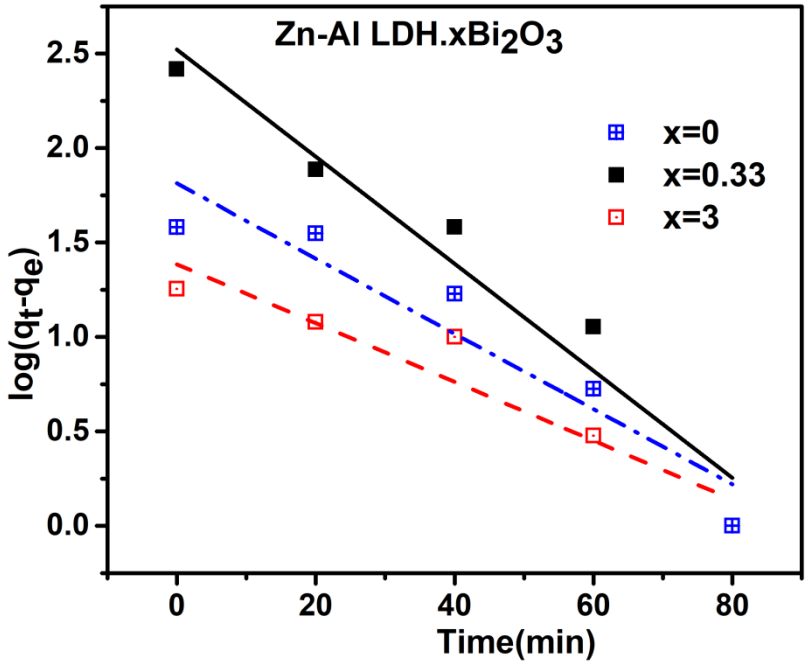

Fig.3.18.Pseudo-first-order kinetic fitting for DCF adsorption for Zn-Al LDH.xBi_2O_3 (x=0, 0.33 and 3) micro composites

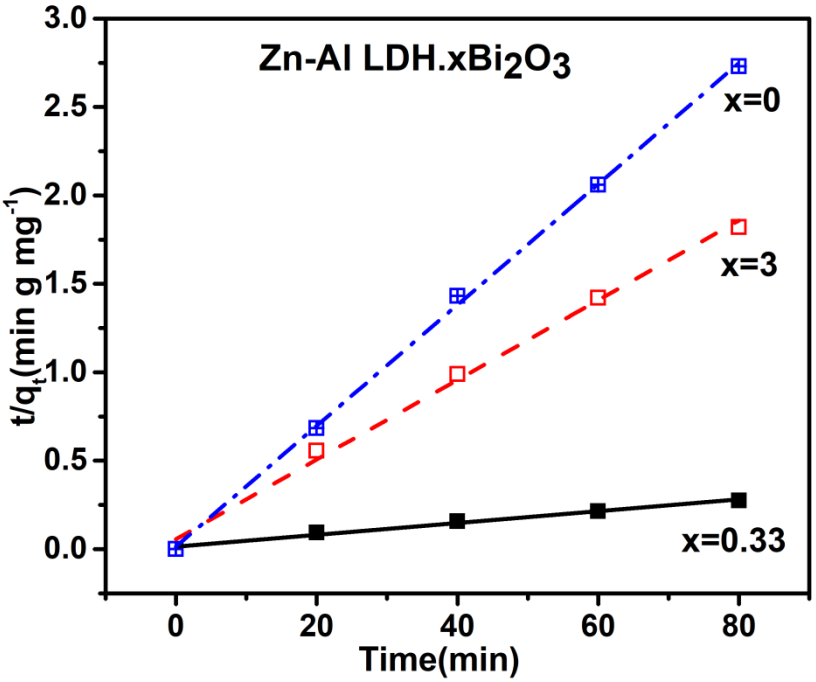

Fig.3.19.Pseudo-second-order kinetic fitting for DCF adsorption for Zn-Al LDH.xBi_2O_3 (x=0, 0.33 and 3) hybrid structures

X	**q_e (mg g^{-1})**	**K_1**	**R_2**
0	**44.38**	**82.97×10^{-2}**	**0.990**
0.33	**332.13**	**8.11×10^{-4}**	**0.985**
0.5	**395.09**	**8.37×10^{-4}**	**0.9913**
1	**520.95**	**5.38×10^{-4}**	**0.987**
2	**265.20**	**7.93×10^{-4}**	**0.974**
3	**24.24**	**90.64×10^{-4}**	**0.994**

Table 3.5 kinetic parameters for the as-prepared Zn-Al LDH.xBi_2O_3micro-structures for Diclofenac adsorption as per pseudo-second order model

X	K_{d1}	K_{d2}	K_{d3}	C_1	C_2	C_3	$(R_1)^2$	$(R_2)^2$	$(R_3)^2$
0	2.29	10.6	5.01	0	18.2	0.46	1	0.921	0.803
0.33	47.9	20.1	8.37	0	125.0	206.1	1	0.964	0.841
0.5	66.0	21.7	9.05	0	197.9	284.9	1	0.977	0.897
1	79.6	34.7	12.6	0	201.9	355.3	1	0.998	0.946
2	33.9	17.9	6.72	0	72.1	149.9	1	0.959	0.831
3	6.28	3.53	2.94	0	9.84	0.01	1	0.942	0.805

Table 3.6 Constants for the intra-particle diffusion kinetic model of the as-prepared Zn-Al LDH.xBi_2O_3 hybrid structures

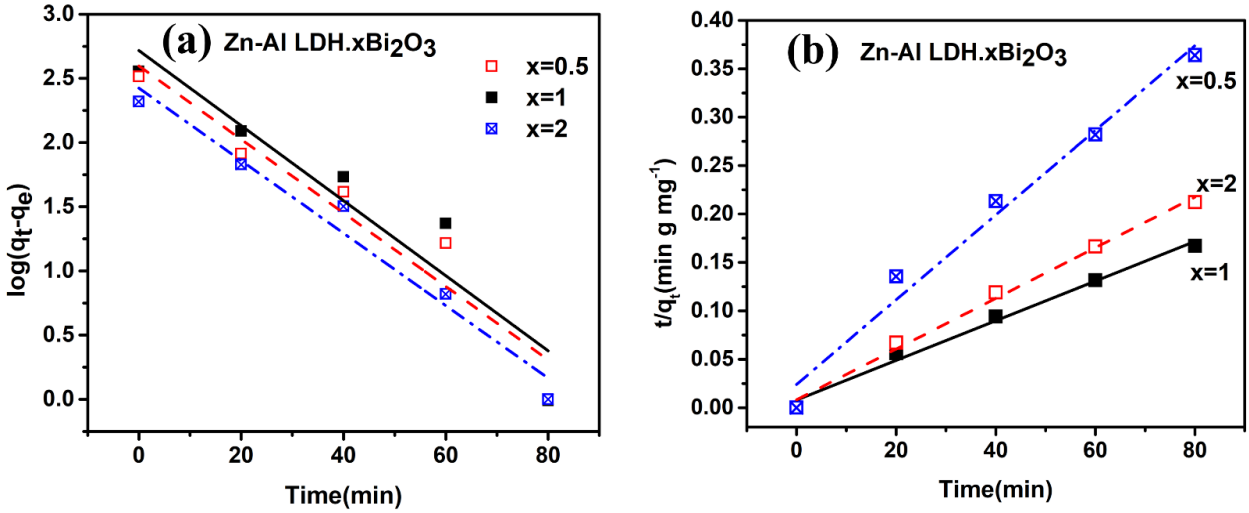

Fig.3.20.Pseudo-first-order (a) and pseudo-second-order(b) models for DCF adsorptionfor Zn-Al LDH.xBi_2O_3 (x=0.5, 1,2) heterocomposites.

3.7 Comparison of the adsorption capacities

The above adsorption studies revealed that upon increasing the relatives toichiometry of Bi_2O_3 adsorption capacity increases till x=1 and then it starts decreasing. This is because the hetero composite with x=1 is having highest positive surface charge as well as BET surface area thereby making it the most suitable adsorbent among all (Fig. 3.21).

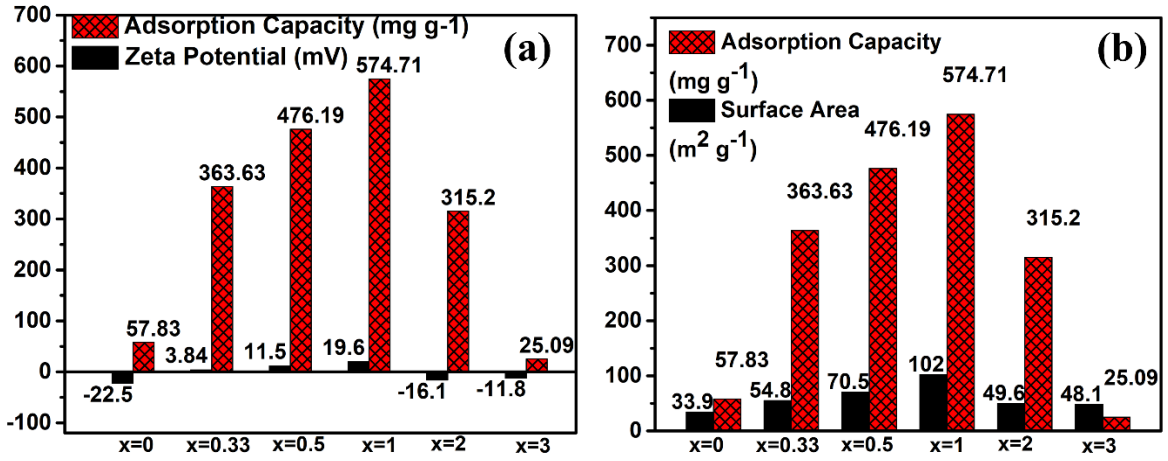

Fig.3.21.Comparitive adsorption capacity with (a) zeta potential and (b) BET Surface area of Zn-Al LDH.xBi_2O_3 (x=0 to 2) composites

Also, compare to several reported adsorbents [15, 24, 58] the composite Zn-Al LDH.xBi_2O_3 (x=1) show either comparable or higher adsorption capacity (Table 3.7)

Adsorbent	**Adsorption capacities**
Oxidized activated carbons[18]	499 mg g^{-1}
LDH-PmPD[9]	588 mg g^{-1}
Zn-Fe LDH[48]	74.50 mg g^{-1}
Zn-Al LDH.xBi_2O_3 [This work]	**574.71 mg g^{-1}**

Table 3.7: Comparative adsorption capacity of Zn-Al LDH.xBi_2O_3 (x=1) for Diclofenac Sodium (DCF) adsorbate with the recent reported litterature.

3.6.2 Regeneration of the Adsorbent

The adsorbent regeneration studies for Zn-Al LDH.xBi_2O_3 (x=1) composite reveal that 58-65% of the adsorbed molecules can be removed by one time washing the DCF adsorbed heterostructures with $NaNO_3$ solution. So, upon repeated washing process the exhausted adsorbents can be completely regenerated.So, these materials can be extremely suitable for real life application.

In this context, Bi_2O_3 loaded Zn-Al layer double hydroxide (LDH) heterostructures (Zn-Al LDH.xBi_2O_3, x= 0 to 3) have been investigated as a potential adsorbent for DCF removal. The BET surface area and zeta potential also varies significantly with extent of loading. DCF adsorption of these composites obey the Langmuir adsorption isotherm model suggesting monolayer adsorption process whereas the intra-particle diffusion model indicates that the adsorption of DCF primarily occurs on the exterior surface.The heterostructure with x=1 exhibited ~10 times higher adsorption capacity compared to bare LDH owing to its highest surface area and positive zeta potential. Due to high adsorption capacities,low cost and easy DCF removal process, these materials could act as efficient adsorbents for removal of DCF and other pollutants from waste water.

References

1. M. Wooding, E.R. Rohwer, Y. Naudé,Determination of endocrine disrupting chemicals and antiretroviral compounds in surface water: a disposable sorptive sampler with comprehensive gas chromatography–time-of-flight mass spectrometry and large volume injection with ultra-high performance liquid chromatography–tandem mass spectrometry,J. Chromatogr. A. 1496*(*2017) 122-132. https://doi.org/10.1016/j.chroma.2017.03.057.

2. C. J. Houtman, Emerging contaminants in surface waters and their relevance for the production of drinking water in Europe, J. Integr. Environ. Sci. (2010) 271-95. https://doi.org/10.1080/1943815X.2010.511648.

3. A. M. Ealias, M. P. Saravanakumar, A review on the classification, characterisation, synthesis of nanoparticles and their application, In IOP Conf. Ser. Mater. Sci. Eng. (2017) 032019. https://doi.org/10.1080/1757-899X/263/3/032019.

4. K.Li, J. Qian, P. Wang, C. Wang, J. Liu, X. Tian, B. Lu,M. Shen, Crystalline phase-dependent eco-toxicity of titania nanoparticles to freshwater biofilms, Environ. Pollut. 231(2017)1433-1441. https://doi.org/10.1016/j.envpol.2017.09.004

5. P. Wang, N. W. Menzies, P. G. Dennis, J. Guo, C. Forstner, R. Sekine, E. Lombi, P. Kappen, P. M. Bertsch, P. M. Kopittke, Silver nanoparticles entering soils via the wastewater–sludge–soil pathway pose low risk to plants but elevated Cl concentrations increase Ag bioavailability, Environ. Sci. Technol. 50 (2018) 8274-8281. https://doi.org/10.1021/acs.est.6b01180.

6. J. Lv, S. Zhang, L. Luo, J. Zhang, K. Yang, P. Christie, Accumulation, speciation and uptake pathway of ZnO nanoparticles in maize, Environ. Sci. Nano. 2(1) (2015) 68-77. https://doi.org/10.1039/C8EN00645H.

7. B. Pan, B. Xing, Applications and implications of manufactured nanoparticles in soils: a review, Eur. J. Soil Sci. 63(4) (2012) 437-456. https://doi.org/10.1007/s10646-017-1805-4.

8. T. Eichert, A. Kurtz, U. Steiner, H. E. Goldbach, Size exclusion limits and lateral heterogeneity of the stomatal foliar uptake pathway for aqueous solutes and water-suspended nanoparticles, Physiol. Plant. 134 (2008) 151-160. https://doi.org/10.1111/j.1399-3054.2008.01135.x.

9. M. S. Diniz, R. Salgado,V. J. Pereira, G. Carvalho, A. Oehmen, M. A. M. Reis,J. P. Noronha, Ecotoxicity of ketoprofen, diclofenac, atenolol and their photolysis byproducts in zebrafish, Sci. Total Environ. 505 (2015) 282-289.https://doi.org/10.1016/j.scitotenv.2014.09.103.

10. M. Patel, R, Kumar, K. Kishor, T. Mlsna, C. U. Pittman Jr., D. Mohan, Pharmaceuticals of emerging concern in aquatic systems: chemistry, occurrence, effects, and removal Methods, Chem. Rev. 119 (2019) 3510-3673. https://doi.org/10.1021/acs.chemrev.8b00299.

11. P. Kumari, R. K. Das, B. Pal, Preparation and characterization of phase pure monoclinic α-Bi_2O_3 nanoparticles and influence of $Ni^{2+}$and Cu^{2+} impregnation on their photocatalytic properties, Mat. Chem. Phys. 260 (2021), 124173.https://doi.org/10.1016/j.matchemphys.2020.124173.

12. J. Shin, J. Kwak, Y.-G. Lee, S. Kim, M. Choi, S. Bae, S.-H. Lee, Y. Park, K. Chon, Competitive adsorption of pharmaceuticals in lake water and wastewater effluent by pristine and NaOH-activated biochars from spent coffee wastes: Contribution of hydrophobic and π- π interactions, Environ. Pollut. 270 (2021) 116244. https://doi.org/10.1016/j.envpol.2020.116244.

13. Q. Zhang, R. Du, C. Tan, P. Chen, G. Yu, S. Deng, Efficient degradation of typical pharmaceuticals in water using a novel TiO_2/ONLH nano-photocatalyst under natural sunlight, J. Hazard. Mater. 403 (2021) 123582. https://doi.org/10.1016/j.jhazmat.2020.123582.

14. Y. Li, M. A. Taggart, C. McKenzie, Z. Zhang, Y. Lu, S. Pap, S. Gibb, Utilizing low-cost natural waste for the removal of pharmaceuticals from water: Mechanisms, isotherms and kinetics at low concentrations, J. Clean Prod. 227 (2019) 88-97. https://doi.org/10.1016/j.jclepro.2019.04.081.

15. T. Xiong, X. Yuan, H. Wang, Z. Wu L. Jiang, L. Leng, K. Xi, X. Cao, G. Zeng, Highlyefficient removal of diclofenac sodium from medical wastewater by Mg/Al layered double hydroxide-poly (m-phenylenediamine) composite, Chem. Eng. J. 366 (2019) 83-91. https://doi.org/10.1016/j.cej.2019.02.069.

16. M. Shalauddin, S. Akhter, W. J. Basirun, S. Bagheri, N. S. Anuar, M. R. Johan, Hybrid nanocellulose/f-MWCNTs nanocomposite for the electrochemical sensing of diclofenac sodium in pharmaceutical drugs and biological fluids, Electrochim. Acta. 304 (2019) 323-333. https://doi.org/10.3390/ph12020083.

17. H. Shao, X. Zhao, Y. Wang, R. Mao, Y. Wang, M. Qiao, S. Zhao, Y. Zhu, Synergetic activation of peroxymonosulfate by Co_3O_4 modified g-C_3N_4 for enhanced degradation of diclofenac sodium under visible light irradiation, Appl.Catal. B-Environ. 218 (2017) 810-818. https://doi.org/10.1016/j.apcatb.2017.07.016.

18. J. A. Morales-Zarate, S. P. Paredes-Carrera, L. V. Castro-Sotelo, Mixed oxides Preparation, characterization and photocatalytic activity in diclofenac degradation, of Zn/Al, Zn/Al-La and Zn-Mg/Al: Preparation, characterization and photocatalytic activity in diclofenac degradation, Rev. Mex.Ing. Quim. 17(2018) 941-953. https://doi.org/10.24275/rmiq/Cat673.

19. W. Li, B. Mu, Y. Yang, Feasibility of industrial-scale treatment of dye wastewater via bio-adsorption technology, Bioresour. Technology. 277(2019)157-170. https://doi.org/10.1016/j.biortech.2019.01.002.

20. M. A. Oturan, J. J. Aaron,Advanced oxidation processes in water/wastewater treatment: principles and applications. Crit. Rev. Env. Sci. Tec. 44(2014) 2577-2641. https://doi.org/10.1080/10643389.2013.829765.

21. A. Azimi, A. Azari, M,Rezakazemi, M.Ansarpour, Removal of heavy metals from industrial wastewaters: a review, ChemBioEng Rev. 1(2017) 37-59. https://doi.org/10.1002/cben.201600010.

22. R. Campo, G. Di Bella, Petrochemical slop wastewater treatment by means of aerobic granular sludge: effect of granulation process on bio-adsorption and hydrocarbons removal, Chem. Eng. J.378 (2019) 122083.https://doi.org/10.1016/j.cej.2019.122083.

23. F. P.Ghavi,F. Raouf,A. D. Koohi, A Review on Diclofenac Removal from Aqueous Solution, Emphasizing on Adsorption Method, Iran. J. Chem. Chem. Eng. 39(2020) 141-154. https://dx.doi.org/10.30492/ijcce.2020.33337.

24. B. Bhadra, N. Seo, P. W. S. H. Jhung, Adsorption of diclofenac sodium from water using oxidized activated carbon, Chem. Eng. J. 301(2016) 27-34. https://doi.org/10.1016/J.CEJ.2016.04.143.

25. I. M. Jauris, C. F. Matos, C. Saucier, E. C. Lima, A. J. G. Zarbin,A. S. B. Fagan, F. M. Machado, I. Zanella, Adsorption of sodium diclofenac on graphene: a combined experimental and theoretical study, Phys. Chem. Chem. Phys. 18(2016)1526-1536. https://doi.org/10.1039/C5CP05940B.

26. M. T. Rahman, T. Kameda, S. Kumagai, T. Yoshioka, A novel method to delaminate nitrate-intercalated Mg-Al layered double hydroxides in water and application in heavy metals removal from waste water, Chemosphere203(2018) 281-290. https://doi.org/10.1016/j.chemosphere.2018.03.166.

27. C. Taviot-Guého, V. Prévot, C. Forano, G. Renaudin, C. Mousty, F. Leroux, Tailoring hybrid layered double hydroxides for the development of innovative applications, Adv. Funct. Mater. 27(2018)1703868. https://doi.org/10.1002/adfm.201703868.

28. M. Richetta, P. Medaglia, A. Mattoccia, A. Varone, R. Pizzoferrato, Layered double hydroxides: tailoring interlamellarnanospace for a vast field of applications, J. Mater. Sci. Eng. 6(2017) 1000360. https://doi.org/10.4172/2169-0022.1000360.

29. M. Gong, Y. Li, H. Wang, Y. Liang, JZ. Wu, J. Zhou, J. Wang, T. Regier, F. Wei, H. Dai, An advanced Ni–Fe layered double hydroxide electrocatalyst for water oxidation, J. Am. Chem. Soc. 135 (2013) 8452-8455. https://doi.org/10.1021/ja4027715.

30. Z.-Z. Yang, J.-J. Wei, G.-M. Zeng, H.-Q. Zhang, X.-F. Tan, C. Maa, X.-C. Li, Z.-H. Li, C. Zhang, A review on strategies to LDH-based materials to improve adsorption capacity and photoreduction efficiency for CO_2, Coord. Chem. Rev. 386 (2019) 154-182. https://doi.org/10.1016/j.ccr.2019.01.018.

31. M. Laipan, J. Yu, R. Zhu, J. Zhu, A. T. Smith, H. He, D. O'Hare, L. Sun, Functionalized layered double hydroxides for innovative applications, Mater. Horiz. 7 (2020) 715-745.https://doi.org/10.1039/C9MH01494B.

32. A. Karmakar, K. Karthick, S. S. Sankar, S. Kumaravel, R. Madhu, A vast exploration of improvising synthetic strategies for enhancing the OER kinetics of LDH structures: a review, J. Mater. Chem. A. 9 (2021), 1314-1352.https://doi.org/10.1039/D0TA09788H.

33. L. Mohapatra, K. Parida, A review on the recent progress, challenges and perspective of layered double hydroxides as promising photocatalysts, J. Mater. Chem. A. 4 (2016), 10744-10766.https://doi.org/10.1039/C6TA01668E.

34. J. Sun, Y. Chen, H. Yu, L. Yan, B. Du, Z. Pei, Removal of Cu^{2+}, Cd^{2+} and Pb^{2+} from aqueous solutions by magnetic alginate microsphere based on Fe_3O_4/MgAl-layered double hydroxide, J. Colloid Interface Sci. 532(2018) 474-484. https://doi.org/10.1016/j.jcis.2018.07.132.

35. R. Zhang, Y. Ai, Z. Lu, Application of Multifunctional Layered Double Hydroxides for Removing Environmental Pollutants: Recent Experimental and Theoretical Progress, J. Environ. Chem. Eng. 2(2020)103908. https://doi.org/10.1039/C9TA13522G.

36. M. Shamsayei, Y. Yamini, H. Asiabi, Layer-by-layer assembly of layered double hydroxide/histidine/δ-MnO_2nanosheets: Synthesis, characterization, and applications, Appl. Clay Sci. 188(2020) 105540. https://doi.org/10.1016/j.clay.2020.105747.

37. Y. Yang, Z. Zheng, M. Yang, J. Chen, C. Li, C. Zhang, X. Zhang, In-situ fabrication of a spherical-shaped Zn-Al hydrotalcite with BiOCl and study on its enhanced photocatalytic mechanism for perfluorooctanoic acid removal performed with a response surface methodology, J. Hazard. Mater. 3(2020) 123070. https://doi.org/10.1016/j.jhazmat.2020.123070.

38. R. Saxena, M. Saxena, A. Lochab,Recent progress in nanomaterials for adsorptive removal of organic contaminants from wastewater, ChemistrySelect. 5(2020) 335-353. https://doi.org/10.1002/slct.201903542.

39. M. S. Hasanin, Sustainable hybrid silica extracted from rice husk with polyvinyl alcohol and nicotinic acid as multi adsorbent for textile wastewater treatment, Environ. Sci. Pollut. Res.27(2020) 26742-26749. https://doi.org/10.1007/s11356-020-09104-5.

40. E. F. Valenzuela, H. C. Menezes, Z. L. Cardeal, Passive and grab sampling methods to assess pesticide residues in water. A review, Environ. Chem. Lett. 1(2020) 1-30. https://doi.org/10.1007/s10311-020-00998-8.

41. J. Wang, Q. Zhang, F. Deng, X. Luo, D. D. Dionysiou, Rapid toxicity elimination of organic pollutants by the photocatalysis of environment-friendly and magnetically recoverable step-scheme $SnFe_2O_4/ZnFe_2O_4$nano-heterojunctions, Chem. Eng. J. 379(2020) 122264. https://doi.org/10.1016/j.cej.2019.122264.

42. J. Divya, N.J. Shivaramu, E. Coetsee, R.E. Kroon, W. Purcell, H. C. Swart, Enhanced luminescence and photocatalytic activity of Bi_2O_3: Ho^{3+} needles, J. Alloys Compd. 9(2020)155641. https://doi.org/10.1016/j.jallcom.2020.155641.

43. X. Chen, Z. Yang, L. Wang, H.Qin, Synthesis of rose-like Zn-Al-LDH and its application in zinc–nickel secondary battery, Nanotechnology. 30(2018) 015602. https://doi.org/10.1088/1361-6528/aae56e.

44. J.Singh, P. Kumari, S. Basu, Degradation of toxic industrial dyes using SnO_2/g-C_3N_4nanocomposites: role of mass ratio on photocatalytic activity, J. Photoch. Photobio. A. 371(2019) 136-143. https://doi.org/10.1016/j.jphotochem.2018.11.014.

45. R. Yuvakkumar, S. I. Hong, Structural, compositional and textural properties of monoclinic α-Bi_2O_3nanocrystals, Spectrochim. Acta A. 144(2015) 281-286. https://doi.org/10.1016/j.saa.2015.02.093.

46. X. Chen, Z. Yang, L. Wang, H. Qin, Synthesis of rose-like Zn-Al-LDH and its application in zinc–nickel secondary battery. Nanotechnology. 30(2018) 015602. https://doi.org/10.1088/1361-6528/aae56e.

47. S. J. Kerber, J. J. Brukner, A. Mattoccia, P. G. Medaglia, R. Montanari, R. Pizzoferrato, D. Scarpellini, A. Varone, S. Kaciulis, A. Mezzi, P. Soltani, A. Orsini,Surface

spectroscopy and structural analysis of nanostructured multifunctional (Zn, Al) layered double hydroxides, Surf. Interface Anal.38(2016) 514-518. https://doi.org/10.1002/sia.5973.

48. S. J. Kerber, J. J. Brukner, K. Wozniak, S. Seal, S. Hardcastle, T. L. Bar, The nature of hydrogen in x-ray photoelectron spectroscopy: General patterns from hydroxides to hydrogen bondingJ. Vac. Sci. Technol. A14, (1996) 1314-1320. https://doi.org/10.1116/1.579947.

49. Y. Shi, L. Luo, Y. Zhang, Y. Chen, S. Wang, L. Li, Y. Long, F. Jiang, Synthesis and characterization of α/β-Bi_2O_3 with enhanced photocatalytic activity for 17α-ethynylestradiol, Ceram. Int. 43 (2017) 7627-7635. https://doi.org/10.1016/j.ceramint.2017.03.057.

50. R. Boistelle, J. P. Astier, Crystallization mechanisms in solution. J.Cryst. Growth90 (1988) 14-30. https://doi.org/10.1016/0022-0248(88)90294-1.

51. W. Liu, NB. Sutton, H. H. Rijnaarts, A. A. Langenhoff, Anoxic conditions are beneficial for abiotic diclofenac removal from water with manganese oxide (MnO_2), Environ. Sci. Pollut. Res. 25(2018) 10141-10147. https://doi.org/10.1007/s11356-018-1569-2.

52. J. Skopp, Derivation of the Freundlich adsorption isotherm from kinetics, J. Chem. Educ. 86 (2009) 1341. https://doi.org/10.1021/ed086p1341.

53. O. J. Redlich, D. L. Peterson, A useful adsorption isotherm, J. Phys. Chem. 63 (1959) 1024. https://doi/pdf/10.1021/j150576a611.

54. D. C. Hurd, H. S. Pankratz, V. Asper, J. Fugate, H. Morrow, Changes in the physical and chemical properties of biogenic silica from the central equatorial Pacific; Part III, Specific pore volume, mean pore size, and skeletal ultrastructure of acid-cleaned samples, Am. J. Sci. 281 (1981) 833-895. https://doi.org/10.2475/ajs.281.7.83.

55. H. Moussout, H. Ahlafi, M. Aazza, H.Maghat, Critical of linear and nonlinear equations of pseudo-first order and pseudo-second order kinetic models, Karbala Int. J. Mod. Sci.4(2018) 244-254. https://doi.org/10.1016/j.kijoms.2018.04.001.

56. J. P. Simonin, On the comparison of pseudo-first order and pseudo-second order rate laws in the modeling of adsorption kinetics, Chem. Eng. J. 300(2016) 254-263. https://doi.org/10.1016/j.cej.2016.04.079.

57. J. Lin, L.Wang, Comparison between linear and non-linear forms of pseudo-first-order and pseudo-second-order adsorption kinetic models for the removal of methylene blue by activated carbon, Front. Env. Sci. Eng. 3(2009) 320-324. https://doi.org/10.1007/js11783-009-0030-7.

58. H. A. Younes, R. Khaled, H. M.Mahmoud, H. F. Nassar, M. M. Abdelrahman, F. I. El-Ela, M. Taha, Computational and experimental studies on the efficient removal of diclofenac from water using ZnFe-layered double hydroxide as an environmentally benign absorbent, J.Taiwan.*Inst. Chem.*Eng.102(2019) 297-311.https://doi.org/10.1016/j.jtice.2019.06.018.

Chapter 4

Enhanced photocatalytic degradation of eco-toxic pharmaceutical waste diclofenac sodium by anion loaded Cu-Al LDH·Bi_2O_3 composites

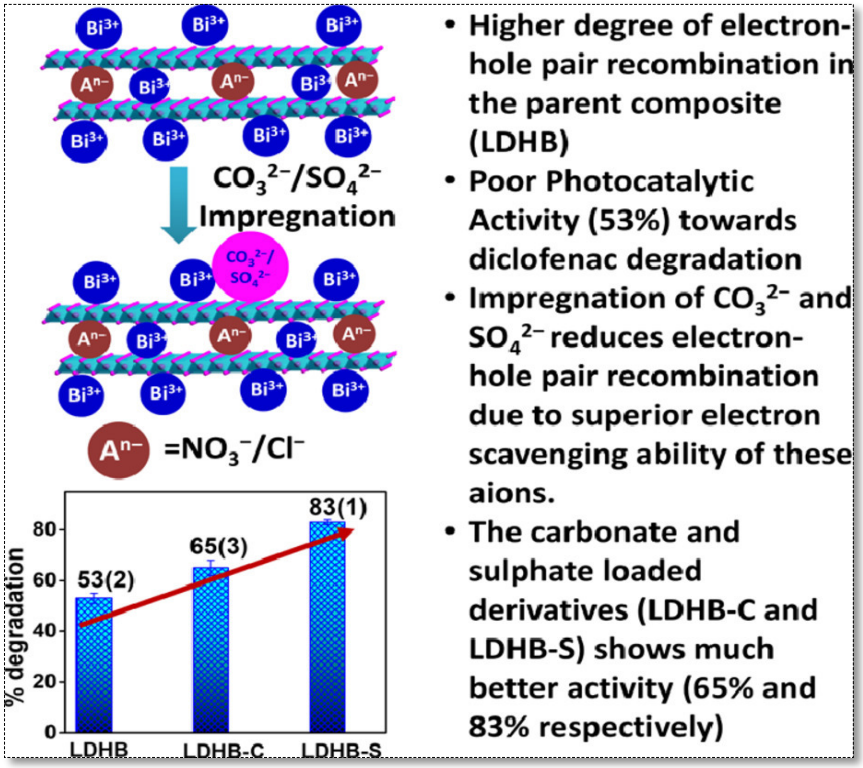

Summary

This work deals with the synthesis of anion carbonate and sulphate loaded Cu-Al LDH-Bi_2O_3 nanoparticles by solvothermal-solvent evaporation method, for efficient degradation of Diclofenac sodium i.e. a pharmaceutical drug. The as prepared nanoparticles exhibited high efficiency i.e. 65 % with carbonate loaded and 83 % with sulphate loaded.

4.1 Introduction

Drugs are micro-pollutants recognized in very small quantities. In spite of this, their harmful effects on the nature cannot be ignored, because these molecules act in living organisms [1-3].Diclofenac sodium (DCF) is one of the non-steroid anti-inflammatory drug (NSAID) that has been very often utilized to treat various chronic inflammatory and degenerative joint diseases for past few decades [4].Diclofenac is very common drug found in watery environment because of its large consumption [5-8].Due to its eco-toxicity, continuous intake of DCF can cause several adverse effects [9-11].Prolonged exposure of DCF can cause various health hazards such as epilepsy [12], psychiatric disorder [13], Kounis Syndrome [14], hallucination [15] etc. Furthermore, it contains a harmful halogenated aliphatic group that can affect the oxidation steps of Krebs cycle [16-17]. Among various physiochemical approaches electrochemical oxidation [18], adsorption [19-22], photo-Fenton process [23-24] photocatalysis [25-28] are the best method for the removal of different emerging pollutants. Layered double hydroxide (LDH) materials are class of layered clays general formula $[M(II)_{1-x}M(III)(OH)_2.]^{x+}[A_{x/n}H_2O]^{x-}$ where M(II) and M(III) are the metal cations and A is an intercalated anion. The surface charge of LDH materials can be simply tuned by changing pH of the medium as well as controlling the molar ratio of bivalent and trivalent cations.LDH materials are attracting great interests in the emerging areas such as electrochemistry, adsorption, anion exchange and photo-catalysis [29-33]. The preparation of visible light active layered double hydroxide is of great interest because of its enormous practical applications. The flexible properties of LDH plays important role in photo-catalysis. In comparison to bulk photocatalysts, layered materials showed higher activity due to high surface area and efficient separation of photogenerated electrons and holes [34-36].Zhao and co-workers reported that Zn-Al LDH possess superior removal efficiency (74.3%) towards

photo-degradation of Orange II [37]. Furthermore, the large importance of LDH materials is due to its more water absorbing capacity as these water molecules can interact with inter pore as well as outer surface [38]. However, due to the poor light absorption capacity of LDH materials several studies have been reported by combining the LDH with semiconductor that exhibited different properties. Hou and co-workers reported efficient photocatalytic degradation of rhodamine B by Bi_2MoO_6/Zn-Al LDH heterostructures [39]. TiO_2/LDH clay nanocomposites were shown to possess high photo catalytic activity (>90% efficiency) towards phenol and methylene blue removal [40] with. Similarly, Wang research group described decoration of ZnO nano-rods on Mg-Al LDH and demonstrated the adsorption as well as photo catalytic activity of different anionic substrates like acid red [41] with up to 98% efficiency. Xia et al designed a series of Zn/M–NO_3^- LDH (M =Al, Fe, Ti and Fe/Ti) and the Ti-based catalyst showed the best photo catalytic performance (98% photocatalytic efficiency) towards rhodamine B [42].

The interlayers ions play important roles in controlling the porosity layered double hydroxides. Pradhan et al. explained the effect of intercalated anion in the photo catalytic degradation [43].However, apart from controlling the interlayer distance and porosity, the exact role of these anions is not yet fully understood. Importantly there are very limited number of reports about photocatalytic degradation of DCF using LDH based photocatalysts [44]. Also, as per best of our knowledge till date there is no report on photocatalytic activity of LDH based composites towards photcatalytic DCF under visible light irradiation.

In this research, the Cu-Al LDH·Bi_2O_3 composites loaded with bivalent anions carbonate (CO_3^{2-}) and sulphate (SO_4^{2-}) has been prepared using simple wet impregnation method. Copper (II) has increased the absorbance of the composite in the visible region. We had used $CuCl_2$ instead of its nitrate analogue will as precursor because it has exerted dual role. 1) Due to

coordination ability of chloride (Cl^-) it has been stick a bit with the layers, it has been ensure that the loaded carbonate and sulphate ions has not intercalate much into the LDH layer rather remain on the external surface. So, there has been no significant change in porosity. 2) Due to higher negative charge density of chloride compare to nitrate, the surface charge has been shift towards negative side, the probability of the adsorption of the anionic pollutant DCF will have been minimal and the majority of the DCF removal process has been via photocatalytic pathway.

4.2. Experimental

4.2.1 Materials

Copper chloride dihydrate ($CuCl_2.2H_2O$, ~98 %), Aluminium nitrate nonahydrate ($Al(NO_3)_3.9H_2O$, >96%), Bismuth nitrate pentahydrate ($Bi(NO_3)_3.5H_2O$, 97%) Sodium hydroxide (NaOH,>98%), Sodium carbonate anhydrous (Na_2CO_3,99.5%) and Sodium sulphate anhydrous (Na_2SO_4,99%) all were purchased from LobaChemie. Tablets of diclofenac sodium (50 mg) (DCF) (Scheme 4.1) were obtained from Cipla pharmaceuticals. Deionized water obtained from Millipore with filtration system (40 mho cm^{-1} at 25^0 C) was used during the entire experiments. All the chemicals were used without further purification.

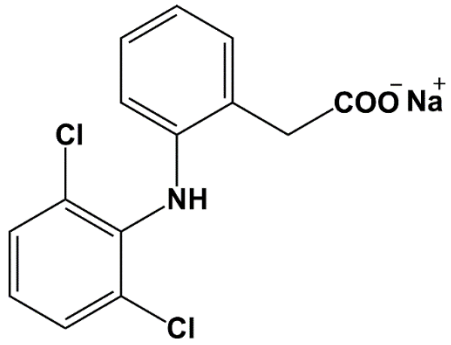

Scheme 4.1: Chemical strucutre of diclofenac sodium (DCF)

4.2.2 Preparation of Cu-Al LDH:

An aqueous solution containing $CuCl_2.2H_2O$ (1.1156 g, 6.56 mmol) and Al $(NO_3)_3.9H_2O$ (0.4689 g, 2.20 mmol) were added in a drop-wise manner to NaOH (1M) solution. The reaction mixture was stirred for 24 h and washed various times with distilled water and ethanol and followed by drying at 50°C for 6 hours [45].

4.2.3 Preparation of Cu-Al LDH·Bi_2O_3:

For the synthesis of Cu-Al LDH·Bi_2O_3 composite, 20 mg of Bi_2O_3 which was prepared using a literature procedure [46], was sonicated for 2 hours with 10 ml of ethanol to obtain a uniform suspension. Then Cu-Al LDH (20 mg) is added into it and continuously stirred for 24 hours. Then the residue was washed several times with deionized water followed by absolute ethanol dried at 50 °C for 6 hours to afford Cu-Al LDH·Bi_2O_3 composite. This composite has been referred as **LDH-B** throughout this manuscript.

4.2.4 Preparation of Carbonate and Sulphate Impregnated Hybrids Cu-Al LDH·Bi_2O_3_CO_3^{2-} and Cu-Al LDH·Bi_2O_3_SO_4^{2-}:

The carbonate (CO_3^{2-}) and sulphate (SO_4^{2-}) loaded hetreostructures were prepared by anion impregnation method. 20 mg of LDHB was stirred constantly with 10 ml of 0.01 M of Na_2CO_3 or Na_2SO_4 for 12 hours. The obtained residues were repetitively washed with deionized water and ethanol then dried at 50°C for 6 hours to obtain the anion impregnated composites Cu-Al LDH·Bi_2O_3_CO_3^{2-} and Cu-Al LDH·Bi_2O_3_SO_4^{2-}. These hybrids will be denoted as **LDHB-C** and **LDHB-S** respectively during the entire part of this manuscript.

4.3 Characterization techniques:

XRD (X-ray diffraction) measurements were performed using the X-ray diffractometer, PANALYTICAL X'Pert PRO with Cu Kα (λ=1.540Å) in 2θ range of 10–80°(scanning rate of 10

min^{-1}). The surface morphological studies as well as elemental composition are determined by scanning electron microscopy (SEM), Energy dispersive spectroscopy (SEM-EDS) respectively using JEOL JSM-7600 F microscope operated at 30 kV. The morphological and crystallographic information were further investigated by recording transmission electron microscopy (TEM) and high resolution transmission electron microscopy (HRTEM) patterns are recorded in JEOLJEM-2100 plus microscope operated at 20 kV and HRTEM, FEI Tecnai G2 F20, Netherlands operating at 200 kV respectively.Zeta potentials of the samples are measured by Zetasizer (ZEN 3600, Malvern, U.K.). Specific surface areas are determined by measuring the sorption isotherms using BELSORP MINI-II instrument.The oxidation states and the chemical environments were determined by XPS (X-ray photoelectron spectroscopy) singKratos axis ultra with DLD system (Al (ka) source- 1486.7eV).The concentration of DCF in the solutions is determined by measuring the absorbance value at 275 nm using Shimadzu UV-2600 spectrophotometer.

4.4 Optical Properties

The diffused reflectance spectra (DRS) was of all three composites were recorded by using DRS, Avantes spectrometer in the range 350-800 nm to monitor the UV-Visible absorption properties and the band gap. In order to monitor photoluminescence (PL) spectra 1mg of the individual heterostructures was sonicated with 5 ml deionized water to afford uniform suspensions. Then the PL of these suspensions was recorded by Perkin-Elmer LS55 spectro-fluorimeter upon exciting them with 329 nm incident light.

4.5 Photo catalytic activities

The photocatalytic behavior of the pristine composite (**LDHB**) as well as the anion impregnated derivatives (**LDHB-C** and **LDHB-S**) were carried out by treating 5 mL of pharmaceutical waste

i.e. DCF (50 mg L^{-1}) with 10mg of each catalyst for various time intervals under visible light illumination (50 $mWcm^{-2}$) with vigorous stirring. Prior to each photocatalytic reaction, the individual reaction mixtures were stirred under dark for 30 minutes to achieve adsorption-desorption equilibrium. Then the catalyst was removed by centrifugation (at 5000 rpm for 10 min) at regular intervals and the concentration of DCF in the solution was determined by measuring absorbance at 275 nm using Shimadzu UV 2600 spectrometer. The percentage degradation(%D) was calculated by the equation 1 [46].

$$\% D = \frac{A_0 - A}{A_0} \times 100 \quad ----------(1)$$

Where A_0 and A are the initial and final absorbance of DCF at 275 nm.

4.6 Result and Discussions

4.6.1 Structure and Morphology:

The crystallinity and phase purity of the as-prepared pristine Cu-Al LDH·Bi_2O_3 composite (**LDHB**) and the anion impregnated analogues Cu-Al LDH·Bi_2O_3_CO_3^{2-} (**LDHB-C**) and Cu-Al LDH·Bi_2O_3_SO_4^{2-} (**LDHB-S**) were confirmed by X-ray diffraction (XRD) patterns (Fig. 4.1). The diffraction patterns of these hetrostructures consists of the characteristic peaks correspond to (121) and (041) lattice planes of the monoclinic α-Bi_2O_3 phase (JCPDS card No. 00-041-1449) as well as the (001), (009) and (015) of the crystallographic planes of rhombohedral Cu-Al LDH phase [46, 47, 48]. It was also observed that the peaks correspond to α-Bi_2O_3 phase were having higher intensity than Cu-Al LDH signals. Because due to higher atomic number bismuth has higher X-ray scattering co-efficient than Copper and Aluminum. Absence of any other extra signal confirmed the phase purity of these composites. The XRD patterns of the carbonate impregnated analogue (**LDHB-C**) showed no noteworthy shift of the peak position compare to

its parent LDH. Whereas in case of the sulphate impregnated derivative (**LDHB-C**) the peaks correspond to (001), (009) and (015) crystallographic plane of LDH shifts slightly towards higher 2θ values suggesting slight contraction along crystallographic *c* axis. Such observation was quite surprising because intercalation of sulphate anions should lead to expansion of the interlayer spacing it was having larger size compare to nitrate/chloride ions. This can be probably due to interaction of the sulphate ions with water and hydroxyl groups. The sulphate anions can undergo hydrogen bonding interactions to break the giant hydrogen bonded water chain to cause slight reduction in crystallographic *c* axis length. In case of **LDHB-C**, larger basicity of carbonate anions can cause de-protonation of water molecules and OH groups that enhances the repulsion between the LDH layers to compensate any such shrinkage.

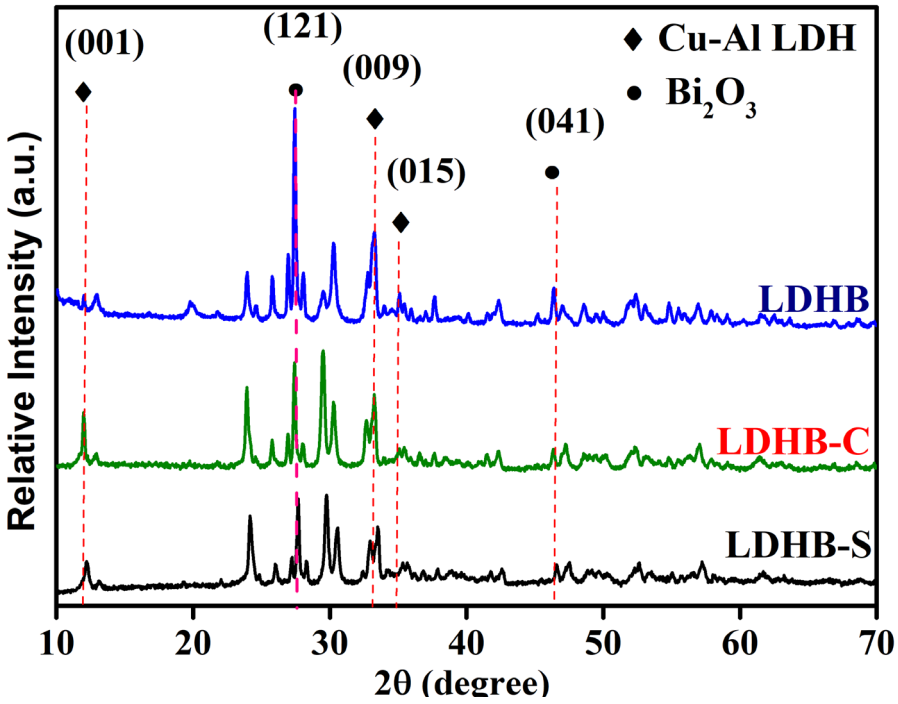

Fig.4.1. XRD patterns of the parent and anion impregnated composites

To investigate the morphology and crystallinity further, the HRTEM studies were performed for **LDHB** (Fig.4.2) and **LDHB-S** (Fig.4.3). The TEM images of the parent composite (**LDHB**)

revealed that it is having irregular platelet like structure. The images contain both gray and black portions which were correspond to the Cu-Al LDH matrix and α-Bi_2O_3 respectively. The lattice fringes correspond to (121) lattice plane of α-Bi_2O_3 was also observed. The TEM images of sulphate impregnated hybrid (**LDHB-S**) also show similar morphology as well as color contrast. In this case the lattice fringes were consistent with the (015) plane of Cu-Al LDH. In the selected area electron diffraction (SAED) patterns the characteristic diffraction spots correspond to the (121) and (041) lattice planes of α-Bi_2O_3 as well (001), (009) and (015) crystallographic planes of Cu-Al LDH were observed. Such observations support formation of the Cu-Al LDH·Bi_2O_3 binary hybrids.

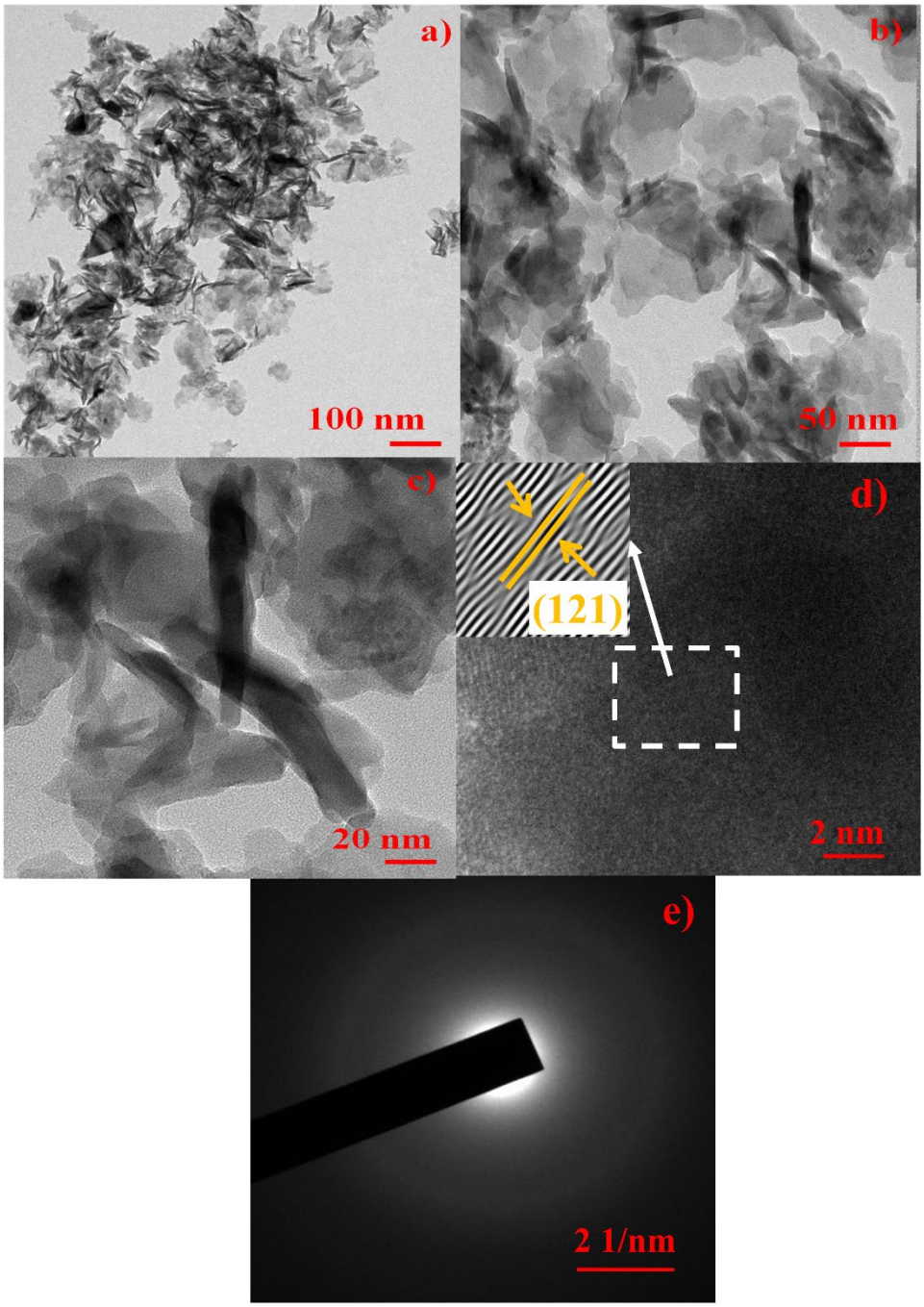

Fig. 4.2: HR-TEM images (a-c) and their corrosponding (d-e) lattice fringes and f) SAED pattern of the Cu-Al LDH·Bi_2O_3 composite (**LDHB**)

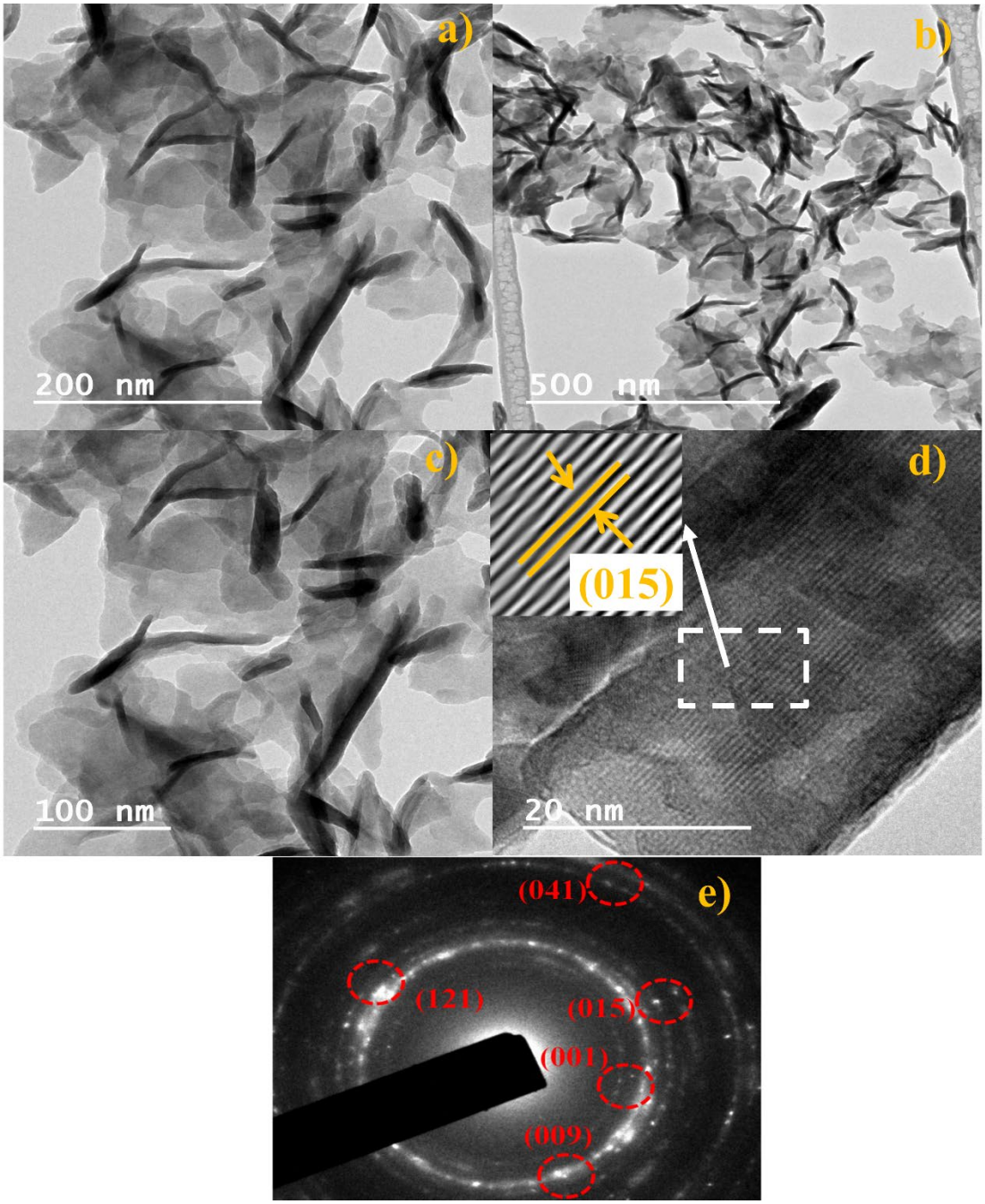

Fig. 4.3. HR-TEM images (a-c), lattice fringes(d) and SAED pattern (e) for Cu-Al LDH·Bi_2O_3_SO_4^{2-} (**LDHB-S**).

Both the anion impregnated hybrids **LDHB-C** (-10.3 mV) and **LDHB-S** (-5.9 mV) were having more negative zeta potential than the original one, **LDHB** (-2.6 mV) suggesting adsorption of

these anions in the exterior surface (Fig. 4.4). The carbonate loaded hybrid (**LDHB-C**) is having most negative zeta potential among all.

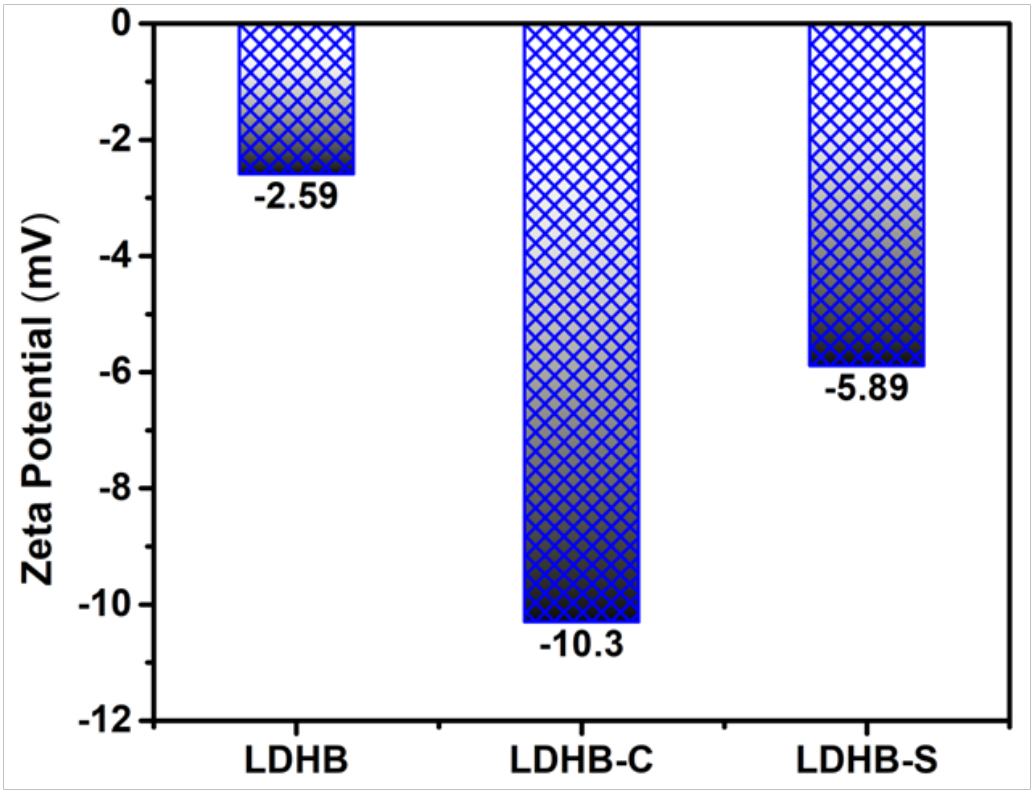

Figure 4.4: Zeta potential values of the parent and anion loaded heterostructures

Because the some of the hydroxyl (OH) groups can undergo de-protonation in presence of basic carbonate anions to increase the negative charge density in the surface.

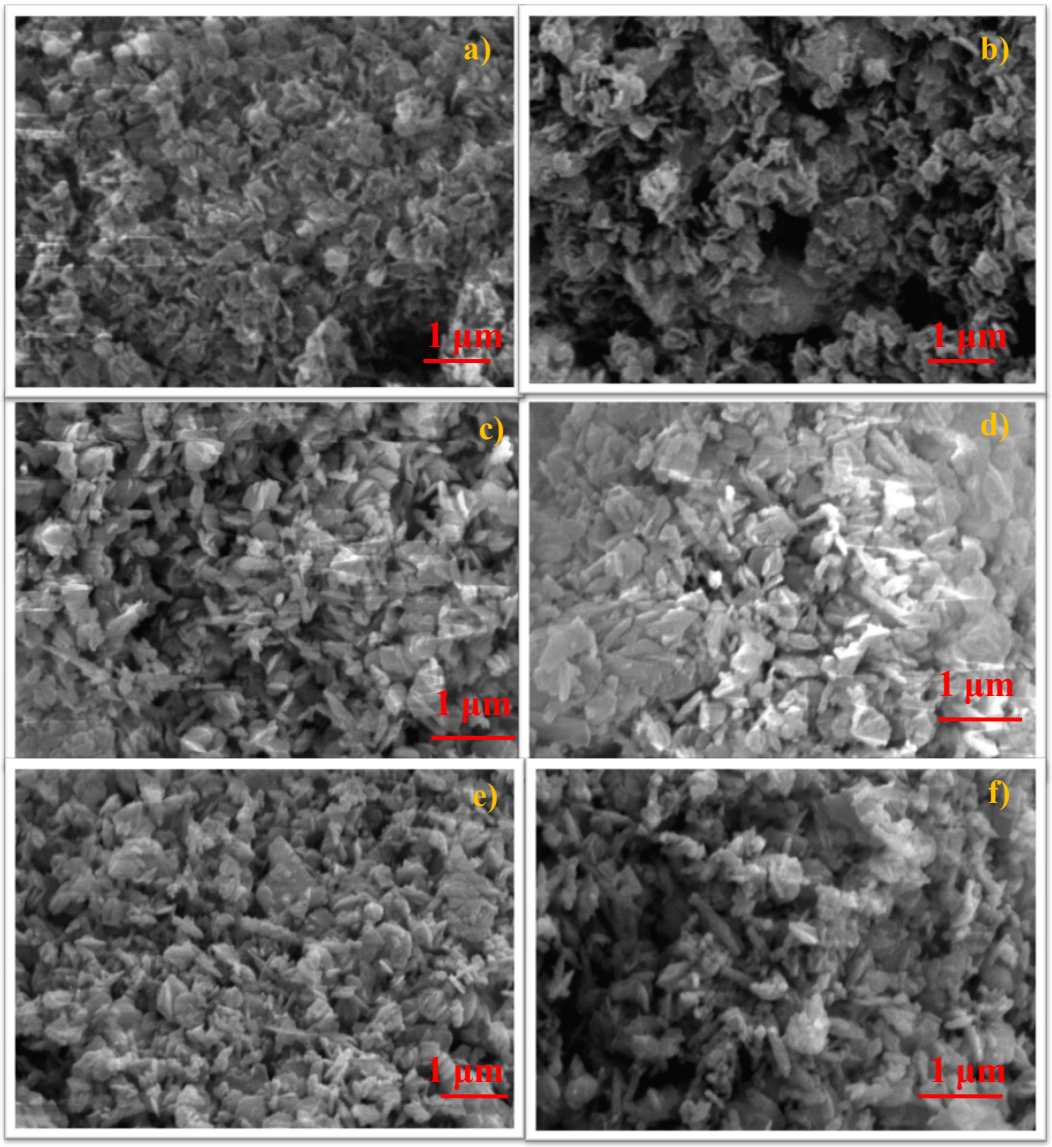

Fig. 4.5 SEM images for (a-b) **LDHB**, (c-d) **LDHB-C** and (e-f) **LDHB-S**.

The Scanning electron microscopy of prepared samples is shown in Fig. 4.5. All the samples display the similar morphological shape and unordered irregular clusters of agglomerated particles within the range in micrometers. It can be demonstrated that there is no significantly change in the surface properties after loading with carbonate and sulphate anions. The corresponding energy dispersive X-ray scattering (EDS) mapping (Figs. 4.6 and 4.7-4.8) of samples with different samples indicates that all the major elements (Cu, Al, Bi, O) as well as C

(**LDHB-C**) and S (for **LDHB-S**) were uniformly dispersed over the whole surface. Apart from that there are no extra peaks present in the EDS map thereby confirming the absence of any other element in these hybrids.

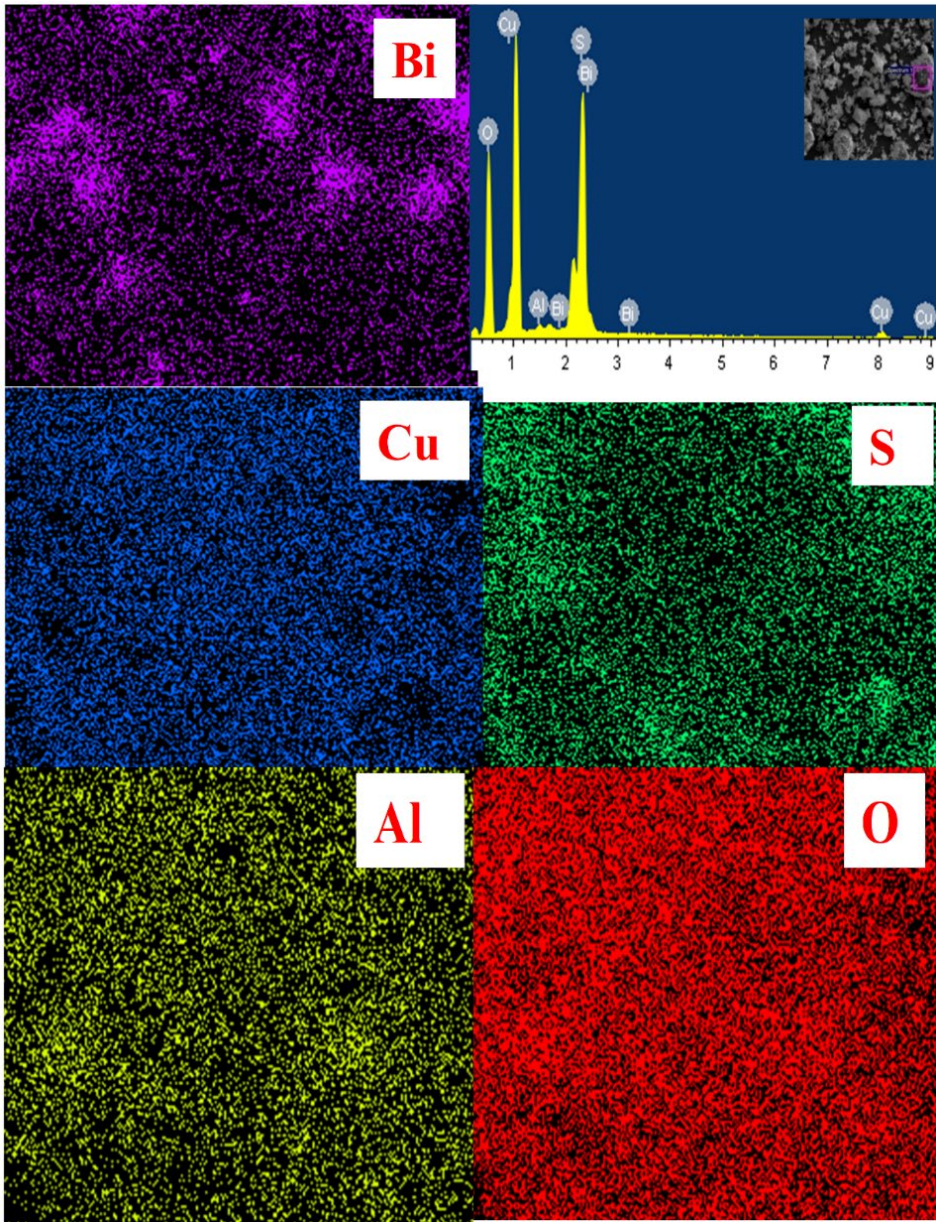

Figure.4.6. EDS mapping for **LDHB-S** sample.

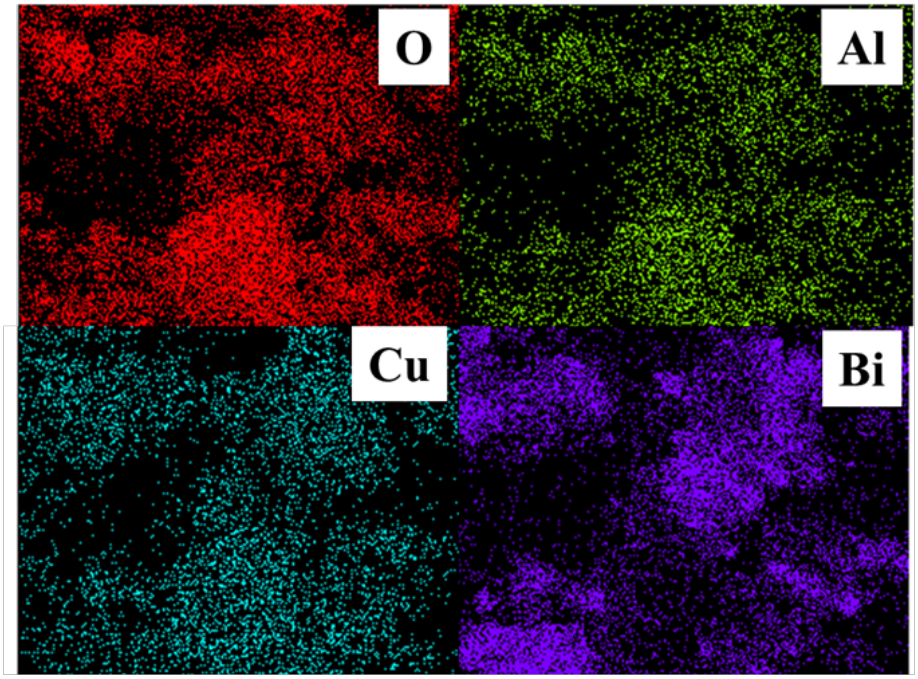

Figure.4.7. EDS mapping for pristine **Cu-Al LDH·Bi_2O_3 (LDHB)** sample.

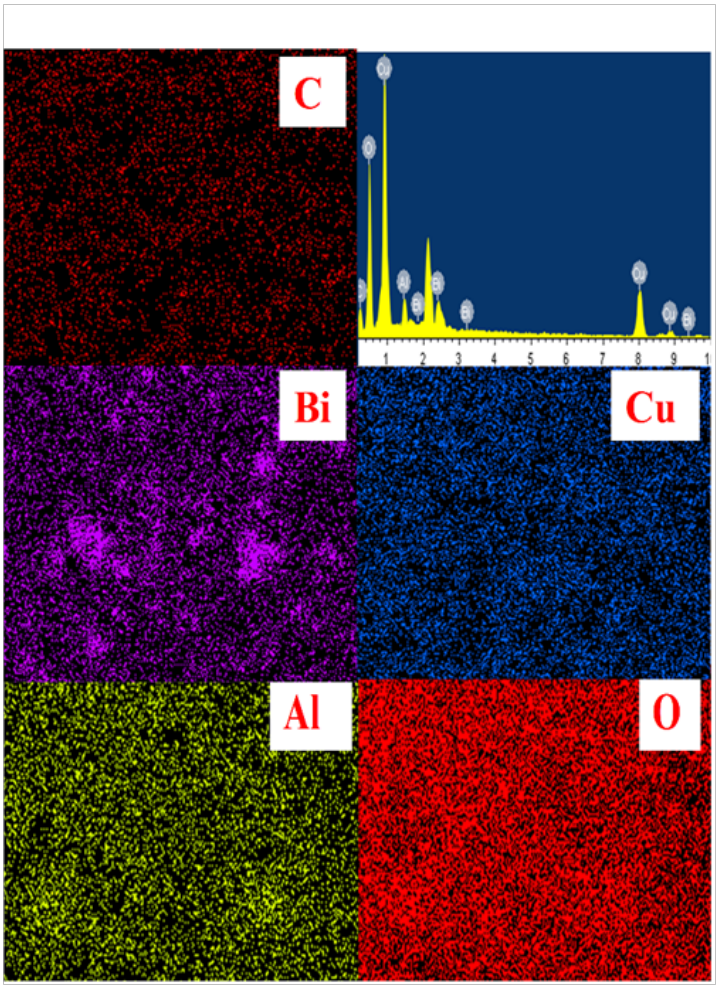

Figure.4.8. EDS mapping for **Cu-Al LDH·Bi_2O_3_CO_3^{2-} (LDHB-C)** sample.

4.6.2 XPS Studies

The oxidation state and the chemical environment of the fundamental elements were further studied by X-Ray photoelectron spectroscopy (XPS). The XPS spectra of Cu-Al LDH·Bi_2O_3 composite (**LDHB**) is shown in Fig.4.9. The Cu $2p_{3/2}$ and $2p_{1/2}$ signals at 934.6 and 954.4 respectivelyare characteristic of Cu(II)-hydroxide species (Fig. 4.9a) [49]. The prominent shake up satellite signals at 939.1, 943.5, 958.8 and 962.6 eV are consistent with the presence of 3d9 open shell of Cu(II) [50]. The O1s signals at 531.3and 531.9eV can be ascribed as presence of metal-hydroxo (M−OH) bonding whereas the signal 536.4 eV clearly suggests the presence of adsorbed water molecules (Fig. 4.9b) [51, 52]. The Al 2p signals at 73.9 and 77.1 eV confirms presence ofAl (III)−OH and Al(III)−O species respectively(Fig. 4.9 c) [53]. The formation of α-Bi_2O_3 phase and +3 oxidation state of bismuth is consistent with the presence of $4f_{7/2}$ (158.7eV) and $4f_{5/2}$ (164.0 eV) signals(Fig. 4.9 d) [54].

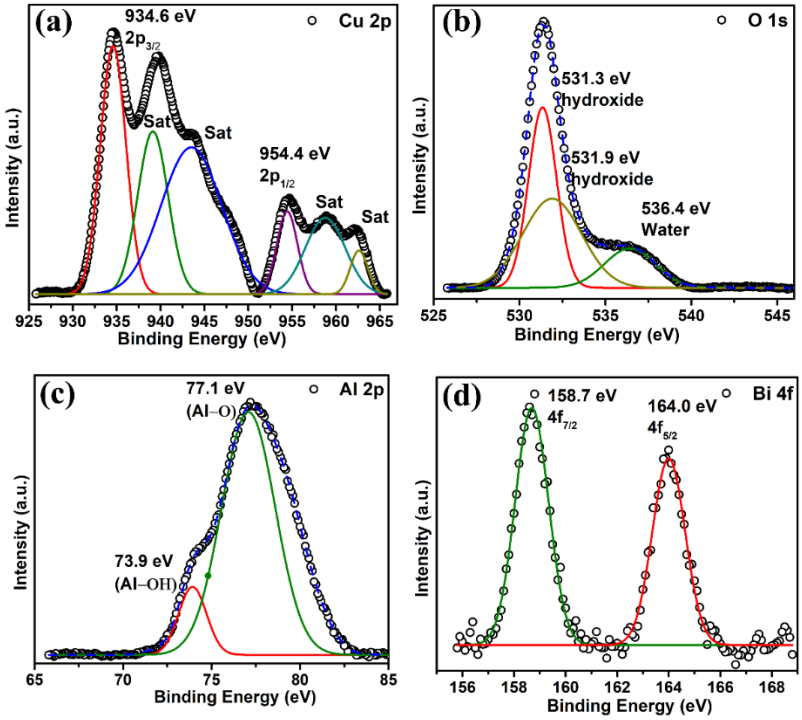

Fig. 4.9. a) Cu 2p b) O 1s c) Al 2p and d) Bi 4f XPS Patterns for the pristine **LDHB** sample.

The XPS of **LDHB-S** (Fig. 4.10) also reveals the characteristic signals of the respective elements. The$2p_{3/2}$ and $2p_{1/2}$ peaks at 934.2 and 954.2 eV along with a strong satellite signals at 941.1 and 961.4 eV can be ascribed as presence of Cu (II). The Bi $4f_{7/2}$ (158.5eV), $4f_{5/2}$ (163.8 eV) and Al 2p (77.5 eV) XPS patterns are practically identical as the parent composite thereby confirming of similar oxidation state and chemical environment for these two elements. Interestingly, the presence of avery weak signal at 168.5 eV is consistent with the presence of a very small quantity of sulphate anions primarily in the external surface of **LDHB-S** [55]. Also the O 1s signals (Fig. 4.10 b) correspond to hydroxide (531.2 e V) and water (533.4 e V) shift towards slightly lower binding energies. Such observation suggest that there are increase the negative charge densities on these oxygen atoms resulting decrease in binding energy which can be attributed to the hydrogen bonding interactions between sulphate ions with hydroxyl groups and water molecules. Such observation is quite consistent with XRD.

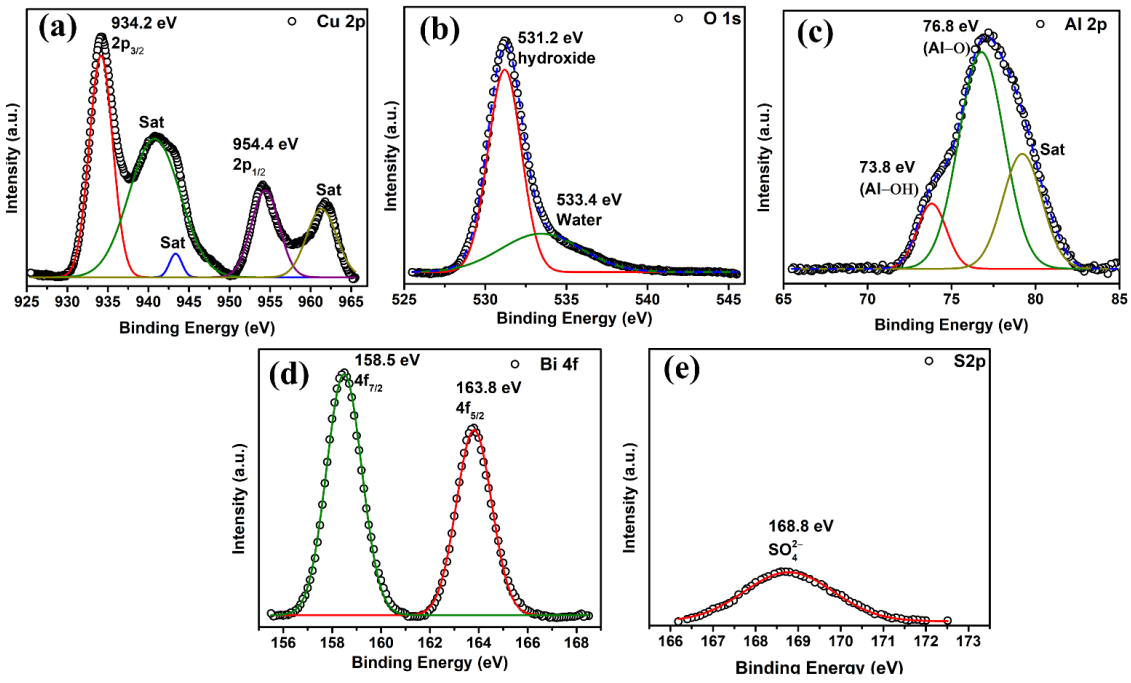

Fig. 4.10. a) Cu 2p b) O 1s c) Al 2p d) Bi 4f and e) S 2p XPS Patterns for the sulphate loaded composite (**LDHB-S**).

4.6.3 Optical Properties

The solid state diffused reflectance spectra (DRS) of the parent composite (**LDHB**) as well as the anion impregnated analogues (**LDHB-C** and **LDHB-S**) reveal that they show broad absorption band over the whole visible region (Fig. 4.11a). Furthermore, the Tauc plots [58] (Fig. 4.12) of **LDHB**(1.77 eV), **LDHB-C** (1.74 eV) and **LDHB-S** (1.76 eV) suggest that all these three as narrow band gap semiconductors (band gap <1.8 eV). Due to such optical properties, these hetereo-structrures can act as efficient photocatalyst in presence of visible light.

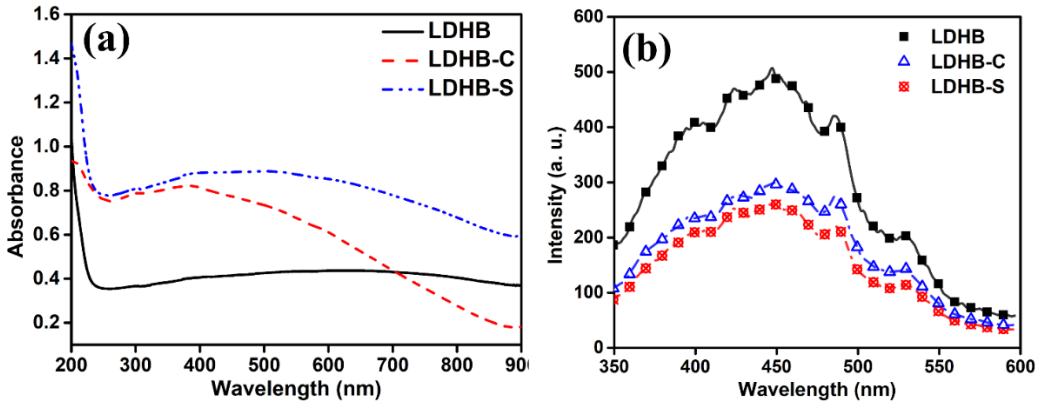

Fig. 4.11 a) UV-Visible and b) Photoluminscence spectra of different composites.

In order to understand the electron-hole pair recombination and trapping process photoluminescence (PL) spectra of these three composites were recorded by exciting them at 329 nm. The PL of **LDHB** shows several peaks around 400, 424, 447, 486 and 530 nm (Fig. 4.11b). It's to be noted that the both anion impregnated hybrids **LDHB-C** and **LDHB-S** is having significantly lower emission intensity compare to their pristine analogue. The PL intensity is lowest in LDHB-S, suggesting the highest amount of emission quenching due to lowest extent of electron hole-pair recombination. Here the sulphate anions can act as an efficient electron scavenger due to high oxidation state of sulphur (+6). In case of carbonate the oxidation state of C is +4 so, its PL quenching ability is relatively smaller compare to sulphate.

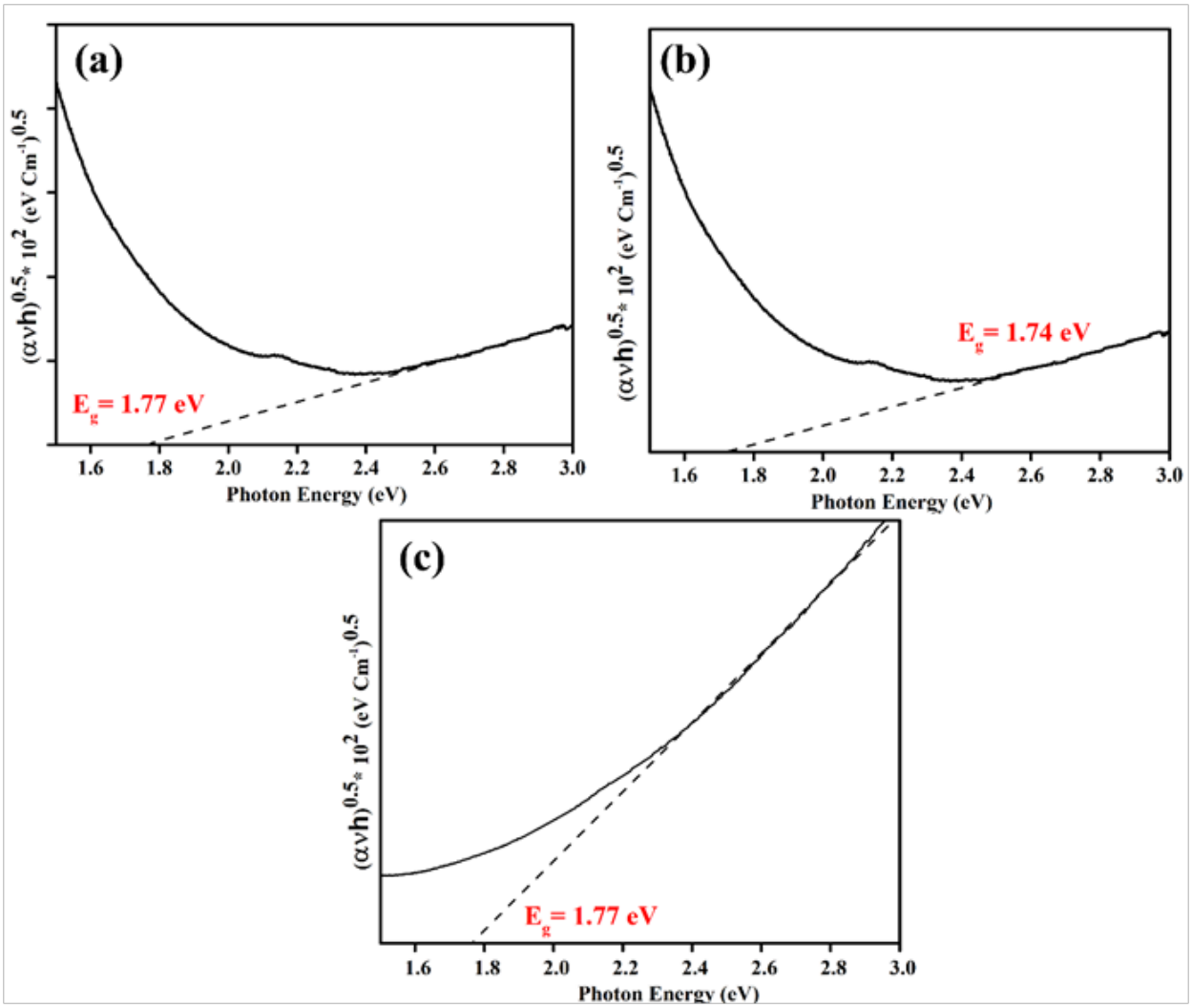

Figure 4.12: Tauc Plots of (a) **LDHB**(b) **LDHB-C** and (c) **LDHB-S** hybrids

In order to further confirm the PL quenching is happening due to sulphate, we have performed a control experiment. The PL was monitored after adding different amount of 0.01M Na_2SO_4 solution to a suspension of **LDHB** in water (Fig.4.13). Interestingly from a certain threshold amount (600 µL) PL intensities are decreased with increasing the volume of Na_2SO_4 solution. In order to cause a significant amount of sulphate adsorption of the surface, addition of amount of 0.01M Na_2SO_4 solution is required. Such observation gives a clearer evidence about that the suphate is actually responsible for PL quenching though capture of photogenerated electron.

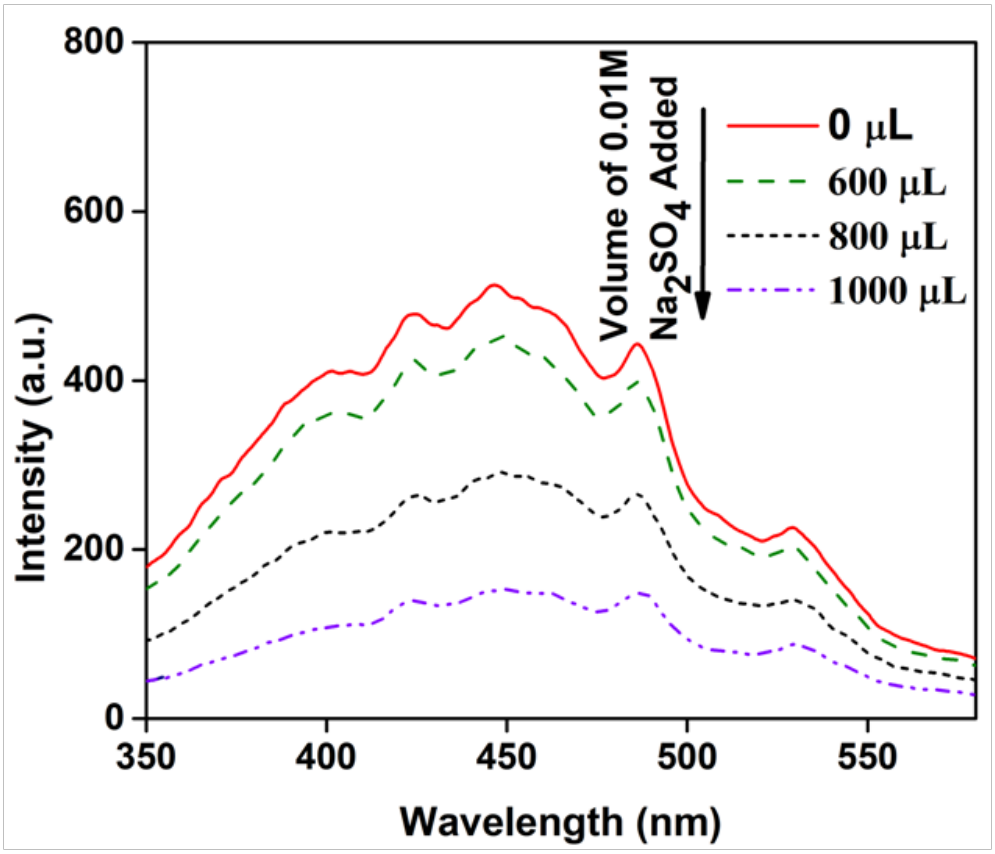

Fig. 4.13: Variation of photluminscience spectra upon adding different amount of 0.01M Na_2SO_4 solution.

4.6.4 Nitrogen Sorption Isotherms

In order to understand the changes in the specific surface areas upon anion loading, BET sorption isotherms of all these composites were recorded. All these heterostructures shows type IV sorption behavior thereby suggesting presence of mesopores (Fig. 4.14a). Interestingly the anion exchanged hybrids **LDHB-C** (35 m^2 g^{-1}) and **LDHB-S** (40.5 m^2 g^{-1})are hiving much larger specific surface area than the parent analogue **LDHB** (5.87 m^2 g^{-1})(Fig. 4.14 b). Such observation suggests enhancement of guest binding sites upon anion loading.

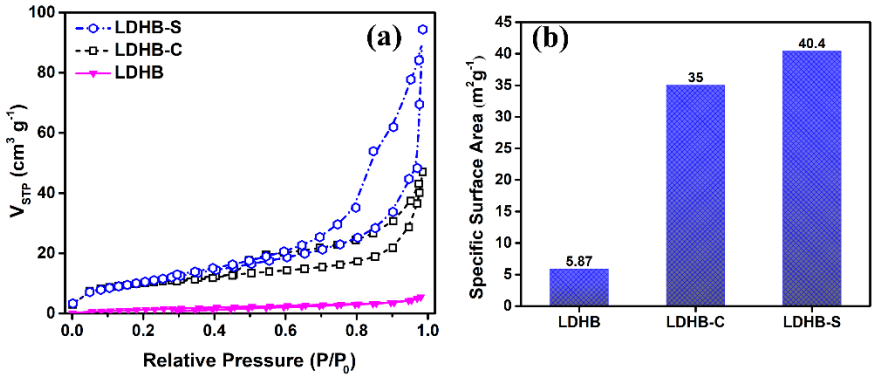

Fig. 4.14 a) Nitrogen sorption isotherms of **LDHB**, **LDHB-C** and **LDHB-S** b) variation of specific surface areas for **LDHB**, **LDHB-C** and **LDHB-S**

4.7 Photocatalytic properties:

Photodegradation efficiency of the parentCu-Al LDH·Bi_2O_3 hybrid (**LDHB**) and the anion loaded derivatives Cu-Al LDH·Bi_2O_3_CO_3^{2-}(**LDHB-C**) and Cu-Al LDH·Bi_2O_3_SO_4^{2-} (**LDHB-S**) were evaluated by photo catalytic diclofenac sodium (DCF) removal under the visible light irradiation and monitored by measuring absorbance at 275 nm (Fig. 4.15 a). In all three cases the extent of adsorption is minimum as indicated by negligible changes in absorbance of the filtrate even after stirring it in dark with for 30 minutes with different composites. Because due to negative zeta potential values, these heterostructures cannot adsorb the anionic pollutant DCF substantially. But upon visible light irradiation the absorbance of the filtrate decreases. The decrease in absorbance is highest for the sulphate impregnated catalyst (**LDHB-S**) whereas the original hybrid (**LDHB**) shows lowest drop in peak intensity. The compare to the prisitine composite, **LDHB** shows 53(2)% photodegradation efficiency towads DCF after 50 minutes. The relatively low photocatalytic efficiency of **LDHB** is due to higher rate of electron-hole pair recombination as indicated by PL. Interestingly the anion loaded derivatives **LDHB-C**{65(3)%} and **LDHB-S**{83(1)%} shows significantly higher photodegradation efficiency towards DCF

(Fig. 4.15b). So, the sulphate loaded heterostructure (**LDHB-S**) is acting as most efficient photocalyst towards DCF degradation. Such enhancement of photocatalytic activity is consistent with the lesser degree charge recombination as well as increase in external surface areaupon anion impregnation. Here the suphate and carbonate anions can act as efficient electron scavengers and consume more number of photogenerated electrons to decrease the electron-hole pair recombination rate and enhance the charge carrier life-time as noticeable by PL.Moreover **LDHB-S** is having highest specific surface area that also boosts its photocatalytic activity.

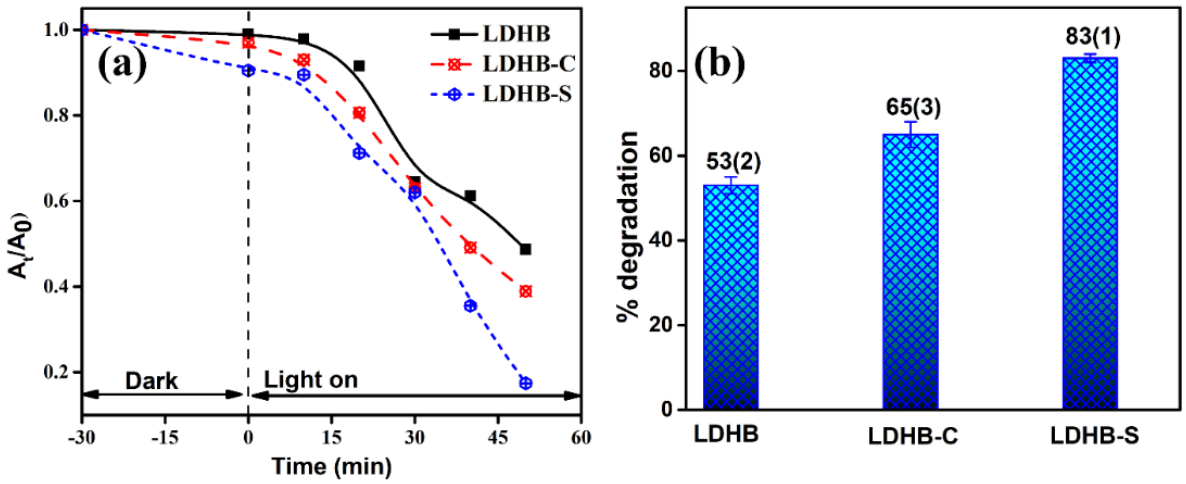

Fig. 4.15 a) variation of absorbance (A_t/A_0) vs time under dark and in presence of visible light irradiation and b) comparison of photocatalytic efficiencies towards DCF degradation for different LDH based catalysts

In all three cases the photo-degradation process obeys pseudo-first order kinetic model (Fig. 4.16 a, Table 4.1) (equation 2)

$$2.303 \log \frac{C_0}{C_t} = kt \text{----------(2)}$$

Where C_0 = the Initial Concentration of DCF, C_t= Concentration of DCF at time t and k= pseudo-first order rate constant. The rate constant values are determined to be 0.01497, 0.01962 and 0.03005 min^{-1} for **LDHB**, **LDHB-C** and **LDHB-S** respectively (Fig. 4.15 b). Such

observation again suggests that impregnation of sulphate and carbonate anions increases the photocatalytic

Sample	K_1	R^2
LDHB	**1.497×10^{-2}**	**0.916**
LDHB-C	**$1..962\times10^{-2}$**	**0.961**
LDHB-S	**3.005×10^{-2}**	**0.908**

Table 4.1 kinetic parameters for the as-prepared as well as the anion loaded hetero-structures fowards DCF photodegradation as per pseudo-first order model

efficiency due to higher external surface area and lesser extent of the electron-hole pair recombination.. Notably, the sulphate loaded catalyst (**LDHB_S**) is having shorter reaction time, comparable or better photocatalytic efficiency and higher rate constant value compare to several reported catalysts towards DCF degradation (Table 4.1) [26-28].

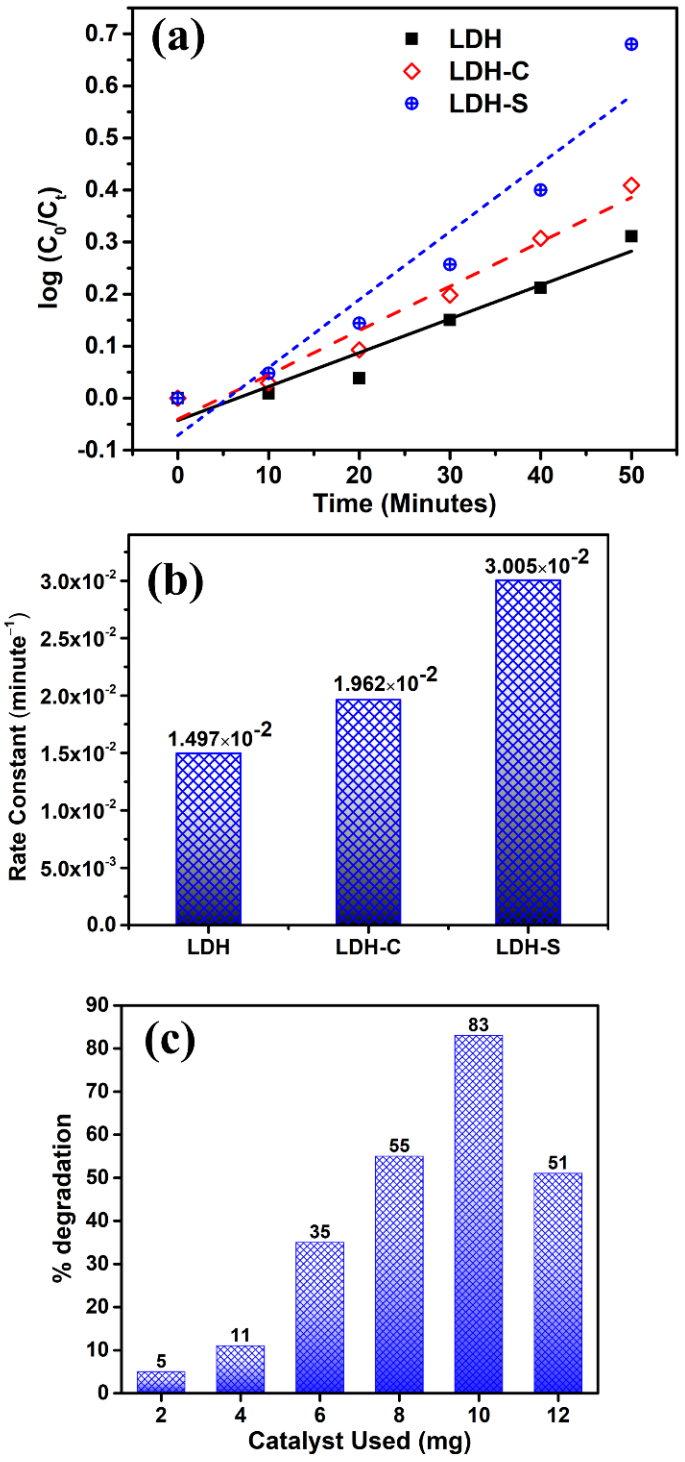

Fig. 4.15 a) Pseudo first order kinetic for DCF degradation in presence of different photocatalysts and b) Variation of the psedo first order rate constant for different heterostructures c) Effect of catalyst(**LDHB-S**) loading on photocatalytic activity

Table 4.2: Comparative photodegradationefiiciency of **Cu-Al LDH·Bi_2O_3_SO_4^{2-} (LDHB-S)** towards Diclofenac Sodium (DCF) under visible light irradiationwith the recent reported litterature.

Photo catalyst	**Photocatalytic Efficiency (%)**	**Time (minutes)**	**Pseudo First Order Rate Constant, k = (min^{-1})**	**References**
TiO_2-CdS heterojunction	86	240	2.316×10^{-2}	[26]
Molecularly imprinted TiO2	62.5	300	-	[27]
$CuBi_2O_4/Ag_3PO_4$	82	240	1.62×10^{-2}	[28]
Cu-Al LDH·Bi_2O_3_SO_4^{2-} (LDHB-S)	83	50	3.005×10^{-2}	This Work

4.7.1 Effect of Catalyst Loading

In order to avoid surplus of catalyst usage, we have varied the amount of catalyst and examined the change in photocatalytic activity towards DCF degradation (Fig 4.15c). We have added different amount of **LDHB-S** (2-12 mg) to the reaction mixture and monitored the variation in degradation efficiency. Upon increasing the catalyst amount up to 10 mg the photocatalytic activity improves due to increase in number of active sites for photodegradation reaction. But upon further increase in catalyst loading the photodegradation efficiency drops. This is probably due to aggregation of the heterostructures at higher concentration which reduces the availability of reactive sites thus leading to decrease in photocatalytic activity.

4.8 FT-IR spectra

In order to further confirm the photodegradation process the FT-IR spectra of pure DCF before and after the photcatalytic reactions in presence of **LDHB-C** and **LDHB-S** have been recorded (Fig. 4.16). The IR spectra of DCF showed clear peaks at 1572.66 cm^{-1} due to carbonyl (–C=O) stretching vibrational mode in carboxylate ion, broad band at 3340 cm^{-1} corresponds to N–H stretching of secondary amines and the peak at 745 $cm^{-1}$is a characteristic of the C–Cl stretching mode[27]. The peaks at 2918 and 2844 $cmcm^{-1}$ cab be ascribed as the N–H stretching motions. The FT-IR spectra also shows a prominent signal ~1510 cm^{-1}T due to aromatic C=C stretching. After the degradation these peaks are either disappeared completely or diminished substantially suggesting decomposition of DCF molecules in presence of the photocatalysts.

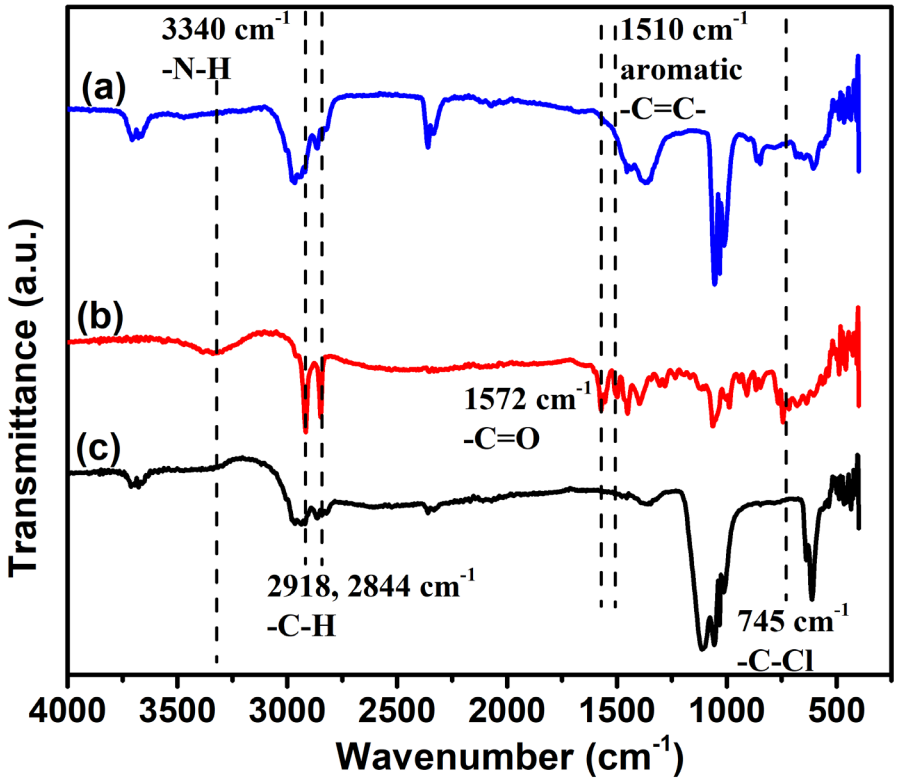

Fig.4.16. FTIR spectra of a) DCF+**LDHB-C** (after degrdation), b) pure DCF c) DCF+ **LDHB-S** (after degradation)

4.9 Recyclability Studies

Moreover, the stability and recyclability of a catalyst is extremely important for potential real life application. The reusability of the sulphate impregnated catalyst (**LDHB-S**) was examined by isolating it from the reaction mixture and using it again for the next reaction. The catalyst **LDHB-S** shows 83%, 79%, 76% and 75% photodegradation efficiency towards DCF from first to fourth cycle (Fig. 4.17). So there is only 8% decrease in catalytic activity from the initial cycle therebye confirming the stability of the catalyst as well as ruling out any possibility of catalyst leaching during the reaction.

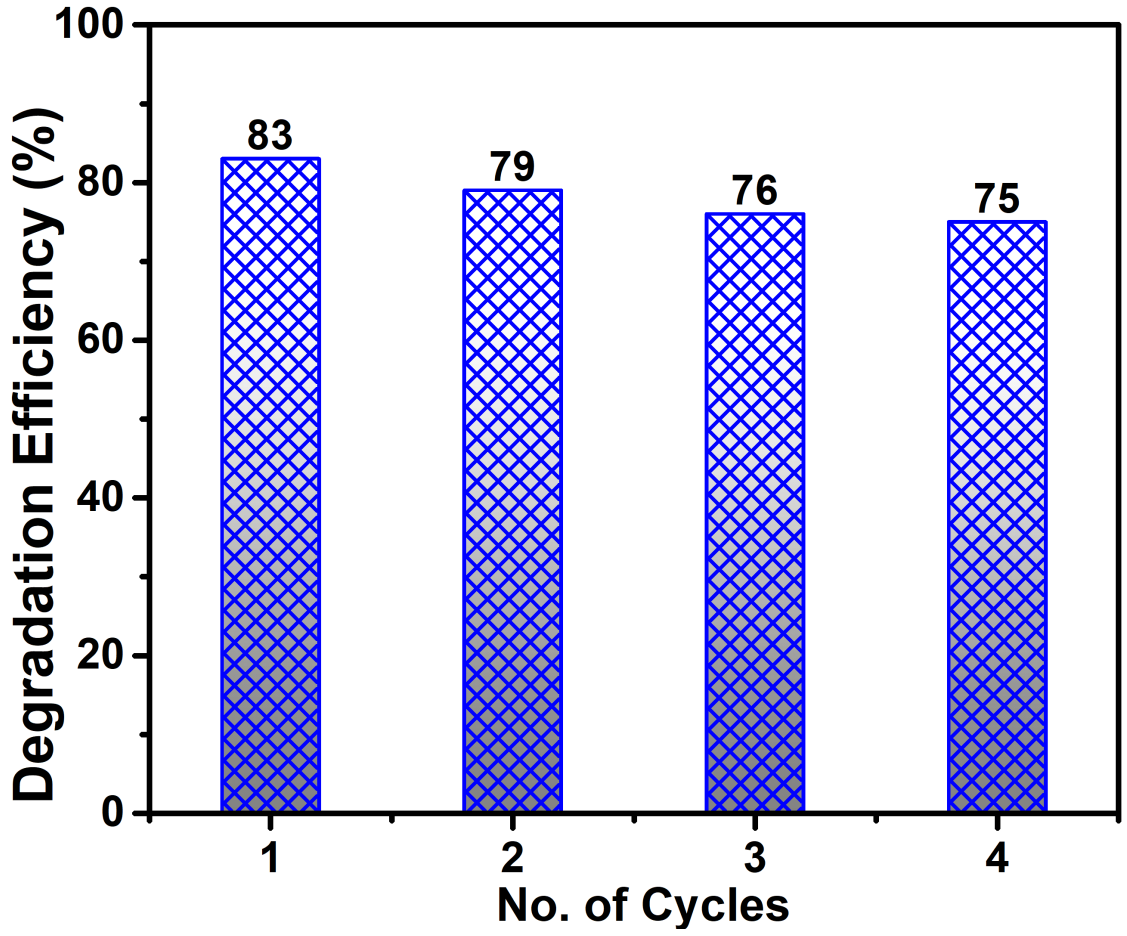

Fig. 4.17 Recyclibilty of **LDHB-S** catalyst towards photocatalytic DCF degradation under visible light irradiation for four cosecutive catalytic reactions.

4.10 Conclusion

In summary we have prepared different Cu-Al LDH·Bi_2O_3based composites and evaluated their photocatalytic activity towards DCF degradation. XRD studies of the anion loaded composites (**LDHB-C** and **LDHB-S**)do not give any clear indication of intercalation of these anions. In **LDHB-S** there is contraction along crystallographic *c* axis probably due to breakage of hydrogen bonded water chain owing to hydrogen bonding interaction of sulphate anions withwater molecules and hydroxyl groups. Such interactionshave been also confirmed through XPS.Compare to pristine Cu-Al LDH·Bi_2O_3 hybrid (**LDHB**) the anion loaded derivatives (**LDHB-C** and **LDHB-S**) shows significantly higher photocatalytic activity due to smaller degree of electron-hole pair recombination and higher specific surface area. The carbonate and sulphate ions are acting as electron-scavenger to reduce the probability of charge recombination. Such observation suggests that in LDH materials apart from controlling the porosity and electrokinetic parameters, the anions can also play other important roles to determine their catalytic activity. Furthermore, these catalyst shows excellent recyclability towards photocatalytic degradation of DCF under visible light irradiation. Therefore, the current work has opened a new dimension in the area of enhancing the photocatalytic activity of layer-double hydroxides by loading them with different anions and their application towards waste-water treatment.

.

References

1. RamakrishnanB, MegharajM, VenkateswarluK, SethunathanN, NaiduR.Mixtures of environmental pollutants: effects on microorganisms and their activities in soils, Rev Environ ContamToxicol 2011;211:120.

2. DeblondeT, Cossu-LeguilleC, HartemannP. Emerging pollutants in wastewater: A review of the literature, Int JHyg Environ Health 2011;214:442-448.

3. KhanNA, KhanSU, AhmedS, FarooqiIH, Yousefi M, MohammadiAA, ChanganiF. Recent trends in disposal and treatment technologies of emerging-pollutants-A critical review, Trend Anal Chem 2020;122:115744.

4. AtzeniF, MasalaIF, Sarzi-PuttiniP. A Review of chronic musculoskeletal pain: central and peripheral effects of diclofenac, Pain Ther 2018;7:163-177.

5. StültenD, ZühlkeS, LamshöftM, SpitellerM. Occurrence of diclofenac and selected metabolites in sewage effluents, Sci Total. Environ 2008;405:310-316.

6. HebererT. Occurrence, fate, and removal of pharmaceutical residues in the aquatic environment: a review of recent research data, ToxicolLett 2002;131:5.

7. LonappanL, BrarSK, DasRK, VermaM, SurampalliRY.Diclofenac and its transformation products: Environmental occurrence and toxicity - A review, Environ. Int. 2016;96:127-138.

8. ZhangY, GeißenSU, GalC. Carbamazepine and diclofenac: removal in wastewater treatment plants and occurrence in water bodies, Chemosphere 2008;73:1151-61.

9. FuQ, FedrizziD, KosfeldV, SchlechtriemC, GanzV, DerrerS, RentschD, HollenderJ. Biotransformation Changes Bioaccumulation and Toxicity of Diclofenac in Aquatic Organisms, Environ SciTechnol 2020;54:4400-4408

10. AygünD, KaplanS, Odaci E, OngerME, Altunkaynak ME. Toxicity of non-steroidal anti-inflammatory drugs: a review of melatonin and diclofenac sodium association, HistolHistopathol 2012;27:417-436.

11. ŻurJ, PińskiA, WojcieszyńskaD, Smułek W, GuzikU.Diclofenac Degradation—Enzymes, Genetic Background and Cellular Alterations Triggered in Diclofenac-Metabolizing Strain Pseudomonas moorei KB4, Int J MolSci 2020;18:6786.

12. Vieira V, Glassmann D, Marafon P, Pereira P, Gomez R, Coitinho AS. Effect of diclofenac sodium on seizures and inflammatory profile induced by kindling seizure model. Epilepsy Res 2016;127:107–13.

13. Gupta D, Javali M, Pradeep R, Mehta A, Acharya P, Srinivasa R. Acute confusional state induced by diclofenac: Report and review of literature. Neurol India 2019;67:858–61.

14. [Cagliyan CE, Balli M, Tekin K, Turkmen S, Tanboga IH. Kounis syndrome triggered by diclofenac sodium injection which leads to myocardial infarction and cardiac arrest. J Cardiol Cases 2013;8:17–9.

15. Tang KL, Teoh YL, Khairul Anwar H, Fong JY. A Case of Probable Diclofenac-Induced Acute Meningism in a Healthy Adolescent. Int J ClinPediatr 2020;9:20–3.

16. SingerK, DettmerK, UngerP, SchönhammerG, Renner K, PeterK, SiskaPJ, BerneburgM, HerrW, OefnerPJ, KarrerS, KreutzM, DatzE. Topical Diclofenac Reprograms Metabolism and Immune Cell Infiltration in Actinic Keratosis, Front Oncol 2019;9:605.

17. NiklasJ, NoorF, HeinzleE. Effects of drugs in subtoxic concentrations on the metabolic fluxes in human hepatoma cell line Hep G2, ToxicolApplPharmacol 2009;240:327-336.

18. Castañeda-JuárezM, Martínez-MirandaV, Almazán-SánchezPT, Linares-HernándezI, Santoyo-TepoleF, Vázquez-MejíaG. Synthesis of TiO_2 catalysts doped with Cu, Fe, and Fe/Cu supported on clinoptilolite zeolite by an electrochemical-thermal method for the degradation of diclofenac by heterogeneous photocatalysis, JPhotochemPhotobiol A 2019;380:111834.

19. BhadraBN, Seo PW, JhungSH. Adsorption of diclofenac sodium from water using oxidized activated carbon, ChemEng J 2016;301:27-34.

20. KumariP, Pal B, DasRK. Superior adsorptive removal of eco-toxic drug diclofenac sodium by Zn-Al LDH.xBi_2O_3 layer double hydroxide composites, Appl Clay Sci 2021;208:106119.

21. BoukhalfaN, BoutahalaM, DjebriN. Synthesis and characterization of ZnAl-layered double hydroxide and organo-K10 montmorillonite for the removal of diclofenac from aqueous solution, AdsorpSciTechnol 2017;35:20-36.

22. YounesHA, KhaledR, Mahmoud HM,NassarHF, Abdelrahman MM, El-ElaFI, TahaM. Computational and experimental studies on the efficient removal of diclofenac from

water using ZnFe-layered double hydroxide as an environmentally benign absorbent, JTaiwan. InstChemEng2019;102:297-311.

23. GiriAS, Golder AK. Fenton, photo-fenton, H_2O_2 photolysis, and TiO_2photocatalysis for dipyrone oxidation: drug removal, mineralization, biodegradability, and degradation mechanism, IndEngChem Res 2014;53:1351-1358.

24. Wang Q, Tian S, Long J, Ning P, Use of Fe (II) Fe (III)-LDHs prepared by co-precipitation method in a heterogeneous-Fenton process for degradation of Methylene Blue, Catal Today 2014;224:41-48.

25. Shao H, Zhao X, WangY, MaoR, WangY, QiaoM, ZhaoS, ZhuY. Synergetic activation of peroxymonosulfate by Co_3O_4 modified g-C_3N_4 for enhanced degradation of diclofenac sodium under visible light irradiation, ApplCatal B-Environ 2017;218:810-818.

26. MugunthanE, Saidutta MB, JagadeshbabuPE.Photocatalytic degradation of diclofenac using TiO_2-CdS heterojunction catalysts under visible light irradiation, Environ SciPollut Res 2021;28:18186-18200.

27. de EscobarCC, RuizYPM, dos SantosJHZ, Ye L.Molecularly imprinted TiO_2photocatalysts for degradation of diclofenac in water, Colloid Surf A PhysicochemEng Asp 2018;538:729-738.

28. ChenX, YuC, ZhuR,LiN, ChenJ,LinQ,XuS, ChenX, WangH.Photocatalytic performance and mechanism of Z-Scheme $CuBi_2O_4$/Ag_3PO_4 in the degradation of diclofenac sodium under visible light irradiation: Effects of pH, H_2O_2, and $S_2O_8^{2-}$, Sci Total Environ 2020;711:134643.

29. ZhangH, NengziLC, WangZ, LiX, ZhangB, ChengX. Construction of Bi_2O_3/CuNiFe LDHs composite and its enhanced photocatalytic degradation of lomefloxacin with persulfate under simulated sunlight, J Hazard Mater 2020;83:121236.

30. KaurH, SinghS, PalB.A brief review on modified layered double hydroxides for H_2 production through photoinduced H_2O splitting, Environ NanotechnolMonitManag 2021;16:100451.

31. SeftelEM, PuscasuMC, Mertens M, CoolP, CarjaG. Assemblies of nanoparticles of CeO_2–ZnTi-LDHs and their derived mixed oxides as novel photocatalytic systems for phenol degradation, ApplCatal B-Environ 2014;150:157-166.

32. PrasadC, TangH, Liu W. Magnetic Fe_3O_4 based layered double hydroxides (LDHs) nanocomposites-recent review of progress in synthesis, properties and applications, J Nanostructure Chem 2018;4:393-412.

33. HirataN, TadanagaK, TatsumisagoM.Photocatalytic O_2 evolution from water over Zn–Cr layered double hydroxides intercalated with inorganic anions, Mater Res Bull 2015;62:1-4.

34. MengY, Luo W, XiaS, NiZ., Preparation of Salen–metal complexes (metal= Co or Ni) intercalated ZnCr-LDHs and their photocatalytic degradation of Rhodamine B, Catalysts 2017;5:143.

35. MohapatraL, ParidaKM. A review on the recent progress, challenges and perspective of layered double hydroxides as promising photocatalysts. J MaterChem A 2016;28:10744-10766.

36. WuY, GongY, LiuJ, ChenT, LiuQ, ZhuY, NiuL, LiC, LiuX, SunCQ, XuS. Constructing NiFe-LDH wrapped Cu_2O nanocubeheterostructurephotocatalysts for enhanced photocatalytic dye degradation and CO_2 reduction via Z-scheme mechanism, J Alloys Compd 2020;831:154723.

37. ZhangL, XiongZ, LiL, BurtR, ZhaoXS Uptake and degradation of Orange II by zinc aluminum layered double oxides, J. Colloid Interface Sci 2016;469:224-230.

38. YunSK, PinnavaiaTJ. Water content and particle texture of synthetic hydrotalcite-like layered double hydroxides, Chem Mater 1995;7:348-354.

39. LiH, DengQ, LiuJ, Hou W, DuN, ZhangR, TaoX. Synthesis, characterization and enhanced visible light photocatalytic activity of Bi_2MoO_6/Zn–Al layered double hydroxide hierarchical heterostructures, CatalSciTechnol 2014;4:1028-1037.

40. SeftelEM, NiarchosM, MitropoulosC, MertensM, Vansant EF, CoolP.Photocatalytic removal of phenol and methylene-blue in aqueous media using TiO_2@ LDH clay nanocomposites. Catal Today 2015;252:120-127.

41. YuanS, LiY, ZhangQ, WangH, ZnOnanorods decorated calcined Mg–Al layered double hydroxides as photocatalysts with a high adsorptive capacity, Colloid Surf APhysicochemEng Asp2009;348:76-81.

42. Xia SJ, Liu FX, Ni ZM, Xue JL, Qian PP. Layered double hydroxides as efficient photocatalysts for visible-light degradation of Rhodamine B, J Colloid Interface Sci 2013;405:195-200.

43. Baliarsingh N, Parida KM, Pradhan GC. Effects of Co, Ni, Cu, and Zn on photophysical and photocatalytic properties of carbonate intercalated MII/Cr LDHs for enhanced photodegradation of methyl orange, IndEngChem Res 2014;53:3834-3841.

44. BarreraA, PadillaF, TzompantziF, ArizagaGGC, RamosE, Pérez-HernándezR, CasillasJE, López-GaonaA, Castillo-RodríguezJC.Influence of W^{6+}cations on the photocatalytic activity of Zn^{2+} Al^{3+} W^{6+} layered double hydroxides in the degradation of diclofenac, Fuel 2020;280:118621.

45. WangQ, O'HareD. Recent advances in the synthesis and application of layered double hydroxide (LDH) nanosheets, Chem Rev 2012;112:4124-55.

46. KumariP, Das RK, Pal B. Preparation and characterization of phase pure monoclinic α-Bi2O3 nanoparticles and influence of Ni^{2+} and Cu^{2+} impregnation on their photocatalytic properties, Mater ChemPhys 2021;260:124173.

47. YuvakkumarR, HongSI. Structural, compositional and textural properties of monoclinic α-Bi_2O_3 nanocrystals, SpectrochimActa 2015;144:281-286.

48. YusufS, MohebA, Dinari M. Green phenol hydroxylation by ultrasonic-assisted synthesized Mg/Cu/Al-LDH catalyst with different molar ratios of Cu^{2+}/Mg^{2+}, Res ChemIntermed 2021;47:1297-1313.

49. FuN, ZhangS, Ma Y, YangZ, LiuW. Diatomite/Cu/Al layered double hydroxide hybrid composites for polyethylene degradation, RSC Adv 2020;10:9808-9813.

50. LiuY,LiuY,ShiH,WangH,ChengSH-S,BianH,KamruzzamanM,CaoL,ChungCY,LuZ.Cobalt-copper layered double hydroxide

nanosheets as high performance bifunctional catalysts for rechargeable lithium-air batteries JAlloys Compd2016;688:380-387.

51. KerberSJ,BruknerJJ, MattocciaA, MedagliaPG, MontanariR, PizzoferratoR, ScarpelliniD, Varone A, KaciulisS, MezziA, SoltaniP, OrsiniA, Surface spectroscopy and structural analysis of nanostructured multifunctional (Zn, Al) layered double hydroxides, Surf Interface Anal 2016;38:514-518.

52. KerberSJ,BruknerJJ, WozniakK, SealS, HardcastleS, BarTL.The nature of hydrogen in x-ray photoelectron spectroscopy: General patterns from hydroxides to hydrogen bondingJ VacSciTechnol 1996;14:1314-1320.

53. HanW, ZhangS, LuJ, MaY, FuN, WuY, Liu W, MeiD. Cu/Al layered double hydroxide by co-precipitation with high anti-UV performance in waterborne varnish, ChemLett 2019;48:866-869.

54. ShiY, LuoL, ZhangY, ChenY, WangS, LiL, LongY, JiangF.Synthesis and characterization of α/β-$Bi_2O_3$with enhanced photocatalytic activity for 17α-ethynylestradiol, Ceram Int 2017;43:7627-7635.

55. WangJ, YangH, GuanC, LiuJ, ChenZ, LiangP, ShenZ. Space-confinement and chemisorption co-involved in encapsulation of sulfur for lithium–sulfur batteries with exceptional cycling stability, J MaterChem A 2017;5:24602-24611.

Chapter 5

Superior cooperative adsorption of methylene blue and naproxen by Ni-Al LDH.xBi_2O_3 layered double hydroxide composites

Summary

This work deals with the preparation and characterization of Bi_2O_3 loaded Ni-Al layer double hydroxides (Ni-Al LDH.xBi_2O_3) hetero-composites for superior adsorptive removal of multi-component drug and dye in waste water. It found that absorption capacity of Ni-Al LDH.xBi_2O_3 displayed high adsorption properties in comparison to bare LDH material.

5.1 Introduction

Recently, rapid demand for pharmaceuticals had increased due to growth in population and advancement in medicines [1-2]. However, antibiotics, non-steroidal, anti-inflammatory drugs such as naproxen (NPX) etc are beneficial for human health for e.g. saving kidneys, livers [3]. But their use is less than average value of 30%. Previous research reports show that they have continuously polluted our aquatic system and further these entered into the human body and caused certain major life threatening effects [4]. Since the risk of these pharmaceuticals is very high for environment and humans. Therefore extensive efforts has been made to remove them from the water. Among all methods like electro coagulation, ion exchange, advanced oxidation, photocatalysis and precipitation, adsorption is considered to be an effective approach because of its high feasibility, and large efficiency over a wide range[5-7]. Large number of adsorbents has been published by researcher for the efficient removal of dye and pharmaceutical pollutant from

water [8] But low regeneration, adsorption and high cost adsorbent is still a big challenge. So, cost effective and high adsorption capacity material is urgent.

Layered double hydroxides are from the class of hydrotalcites having anion exchanged properties [9-10]. These types of materials have three dimensional layered structures with positive charge surface layers and anions are intercalated in between them [11-12]. These materials had attracted large attention in the field of adsorption because of their high surface area, porous structure and anion exchangeable properties [13-14]. The surface properties like charge can be easily varied of these LDH materials by varying divalent and trivalent anion concentration. Recently, Qi Kang et al prepared (EPIDMA/bentonite) catalysts to determine the adsorption properties of three dyes i.e. Scarlet, Violet 3R and Eosin Y [15]. They found that EPIDMA /bentonitrite showed maximum adsorption in the case only when all the three are mixed together. Zubair Hasan et al. reports the single component system for the adsorption of naproxene and clofibric acid using MIL-101s [16]. The high adsorption properties were observed with ED-MIL-101 both for the adsorption rate and adsorption capacity. Joanna La ch et. al reports the efficient removal of naproxen sodium using carbon sorbent i.e. microporous (WG-12 and F-300) and micro-mesoporous (ROW 08 Supra) activated carbons [17]. The maximum efficiency has been achieved by carbon F-300. O.s. Chan et al showed the single and multicomponent acid dye adsorption equlilbrium studies on tyre demineralization activated carbon [18]. It has been found that the Langmuir and freundlich model does well consistent with the multicomponent system. Dipshikha et al. prepared NiAl LDH by sonochemical method to improve the adsorption of dye congo red and confirming the interaction of anionic dye with LDH surface [19]. Among all studies, adsorption has been seen in one component system only. Very few studies has been reported for mixed dye and pharmaceutical system. To our best knowledge till now no studies

have been done on multicomponent system. Therefore, this studies majorly focus on the idea of mixing methylene blue dye with pharamaceutical waste naproxen using water as a solvent in order to check single layer and multilayer adsorption properties. We have choosen nitrate salts to prepare LDHs, due to the reason that nitrate salts completely ionize into water and release sufficient amount of nickel in comparison to chloride, acetate etc. Furthermore, nitrate is not a coordinating anion due to this it does not stick to the layers of LDH resulting their availability for host guest interactions. Further, among all the transition series Ni (II) has outstanding ability to coordinate and activate unsaturated substrates e.g. double bond, triple bond etc and another is transformation of pi electronic system. Also, Al(III) exhibits large stability. So, in this way both will result in the formation of large area available for the interaction of host with the guest i.e. adsorbent with the substrate molecules.

In this research, the Ni-Al LDH .xBi_2O_3 composites were prepared by simple co-precipitation method. The material possesses layered structure. Meanwhile anionic pollutant NPX and positive charge pollutant MB and its mixture using water as a solvent is choosen as targeting pollutant. The adsorption performance of this mixture was investigated using Ni-Al LDH .x.Bi_2O_3 (x=1, 2). The isotherm and kinetic model were investigated in adsorption in single and multi-component mixture. The Langmuir and frendulich models are discussed. The Ni-Al LDH.xBi_2O_3 composite show efficient absorption properties towards multi-component system in comparison to single ones, therefore resulting that it can behave as suitable adsorbent for removal wastewater.

5.2 Materials and Methods

5.2.1 Chemicals

Nickel nitrate hexa-hydrate Ni $(NO_3)_2.6H_2O$ (~98%), $Al(NO_3)_3.9H_2O$ (>97%), Bismuth nitrate pentahydrate $Bi(NO_3)_3.5H_2O$(98%), and sodium hydroxide NaOH (>98%) all are purchased from Loba chemie. Tablets of naproxen are purchased from local pharmacy (RPG Life Sciences ltd.). Deionized water obtained from Millipore with filtration system (40 mho cm^{-1} at 25^0C) was used during the whole experiments. All the chemicals were used without further purification.

5.2.2 Synthesis of Ni-Al LDH:

A solution containing mixture of Ni $(NO_3)_2.6H_2O$ (1.1156 gm) and Al $(NO_3)_3.9H_2O$ (0.4689 gm) was mixed drop-wise to NaOH (1M) solution. The resulting mixture was kept for stirring for 24 h at room temperature. After 24 h of stirring the mixture was washed with deionized water and ethanol for several times and finally dried at 50°C for 6-8 hours(20) .

5.2.3 Preparation of Ni-Al LDH.xBi_2O_3 (x =1, 2) composite

For the synthesis of Ni-Al LDH-x.Bi_2O_3, (x=1) composite, 0.3 g of prepared bismuth trioxide is added to 15 ml of ethanol and sonicated for 2 hours in order to prepare uniform suspension. Further, 0.2 g of prepared Ni-Al LDH is added to the above solution and then stirred this mixture for 24 hours in order to obtain composite. Then, the resulting mixture is dried at 50 °C for 6 hours. Similarly, another sample (x=2) is prepared by changing the amount of Bi_2O_3(21).

5.2.4 Characterization techniques:

X-ray diffraction analysis were done using, X'Pert PRO having Cu Kα (λ=1.540Å) in 2θ range of 10–80° (scanning rate of 10 min^{-1}). The surface morphological properties as well as elemental composition are determined by scanning electron microscopy (SEM), Energy dispersive spectroscopy (SEM-EDS) respectively using JEOL JSM-7600 F microscope operated at 30 kV.

The morphological information was further investigated by recording high resolution transmission electron microscopy (HRTEM) in JEOLJEM-2100 plus microscope operated at 20 kV. Zeta potential and hydrodynamic size are analyzed by Zetasizer (ZEN 3600, Malvern, U.K.). The oxidation states of respective elements are recorded by XPS (X-ray photoelectron spectroscopy) Kratos axis ultra with DLD system (Al (ka) source- 1486.7eV).The concentration of NPX and MB in the solutions is determined by measuring the absorbance value using Shimadzu UV-2600 spectrophotometer.

5.2.5 Preparation of dye and drug mixture

For the preparation of wastewater, mixture of dye and drug (MB and NPX) is prepared by mixing 2.5 ml of 50 ppm stock solution of NPX and 2.5 ml of 25 ppm stock solution of MB.

5.2.6 Adsorption experiments

Adsorption studies are performed by mixing 0.01 g of synthesized samples with 10 ml of adsorbate solution in a conical flask. Then the flasks are placed on magnetic stirrer in order to process adsorption experiment. After certain regular intervals, the solutions are centrifuged at 5000 rpm for 10 minutes and finally at different time intervals adsorption efficiency will be calculated by the given equation (1).

$$q_t = \frac{(C_0 - C_t)V}{W}$$

where C_0 (mg L^{-1}) represents the initial adsorption concentration at time t =0, Ct (mg L^{-1}) C_t (mg L^{-1}) represents the concentration at time t, V is adsorbate solution in liters, W is the adsorbent mass taken in grams, q_t represents adsorption capacity at different time intervals.

The isotherms experiments are done by mixing 0.01 gm of prepared materials with 5 mL of adsorbate solution having concentration (10-60 mg L^{-1}). The mixture is kept for stirring using magnetic stirrer for 4-5 h at room temperature in order to obtain equilibrium. Finally, the residual concentration of NPX and MB is obtained. The adsorption equilibrium capacity is determined by using the equation (2).

$$q_e = \frac{(C_0 - C_e)V}{W}$$

Where C_e (mgL^{-1}) and C_0 (mg L^{-1}) is the equilibrium concentration at time t and at t=0 respectively. V (L) is adsorbate solution, W (g) is the adsorbent mass, and q_e (mg g^{-1}) is the adsorption at equilibrium.

5.3 Results and discussions

5.3.1 XRD analysis

X-ray patterns (XRD) for the synthesized materials with variation in Bi_2O_3 composition are shown in Fig.5.1. The patterns obtained for the samples are well matched with the monoclinic phase of alpha Bi_2O_3 with (JCPDS: 00-041-1449) having major peaks that are inconsistent with the planes (111),(041) and (212)(21). The planes (006), (012) and (018) are the major peaks of Ni-Al LDH [22]. Beside this, no extra phase was observed. As there is no sharp peak between 5~10 º.Therefore, planes starts located after 20º.

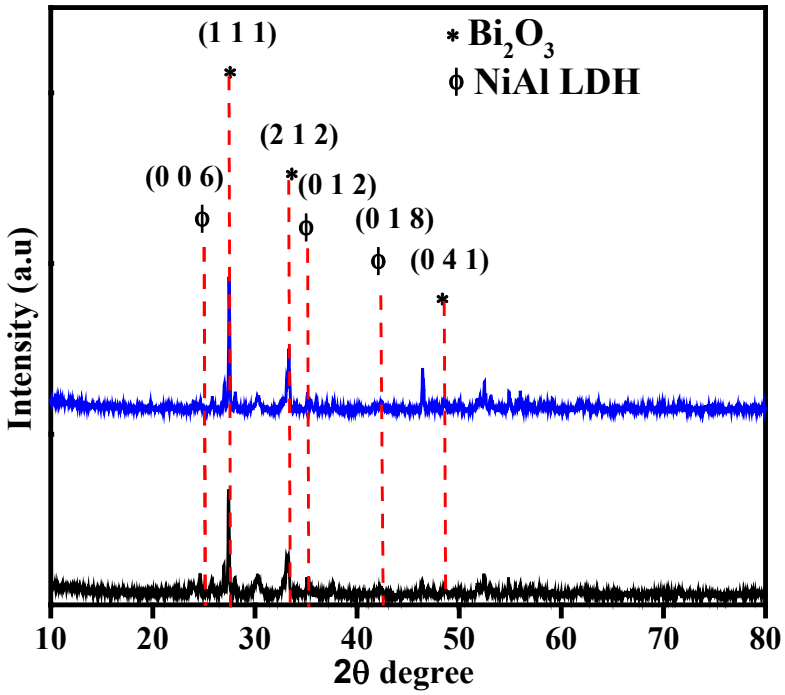

Fig. 5.1. X-ray diffraction patterns of Ni-Al LDH x.Bi_2O_3 (x=1) and (x=2) composites.

It has been clearly seen in the fig that after Bi_2O_3 loading there will be increase in the intensities of peaks which can be referred as dilution effect. Further, the peaks shown in the figure confirmed that there will be noticeable reduction in the relative intensities due to the presence of small amount of Bi_2O_3. This result indicates the formation of Ni-Al LDH-Bi_2O_3 composite. The crystallize size of Ni-Al LDH-Bi_2O_3 material was estimated by Scherer equation is 50.2 nm.

HRTEM images of Ni-Al LDH.xBi_2O_3 (x =1) and Ni-Al LDH-.xBi_2O_3 (x =2) is shown in the Fig.5.2 and 5.3 respectively. Both the structure showed the spherical shaped morphology of Bi_2O_3 and these sphere are uniformly spread over the surface of Ni-Al LDH layers. Fig. 5.2 (d) indicating the lattice planes (012) and (006). Similarly, Fig.5.3(c) indicates the (012) and (006) lattice planes indicating the formation of Ni-Al LDH. No peak was observed in the SAED pattern for Bi_2O_3 due to the low amount of Bi_2O_3. Moreover, the lattice planes (006) and (012) are perfectly matched with the lattice fringes having d-spacing value (0.308) and (0.371). The

crystalline size was found to be 3.25 nm and 5.84 nm for x = 1, 2 respectively. The size increases from 3.25 to 5.84 nm can also be seen in the Fig.5.2 (b) and Fig. 5.3(b).

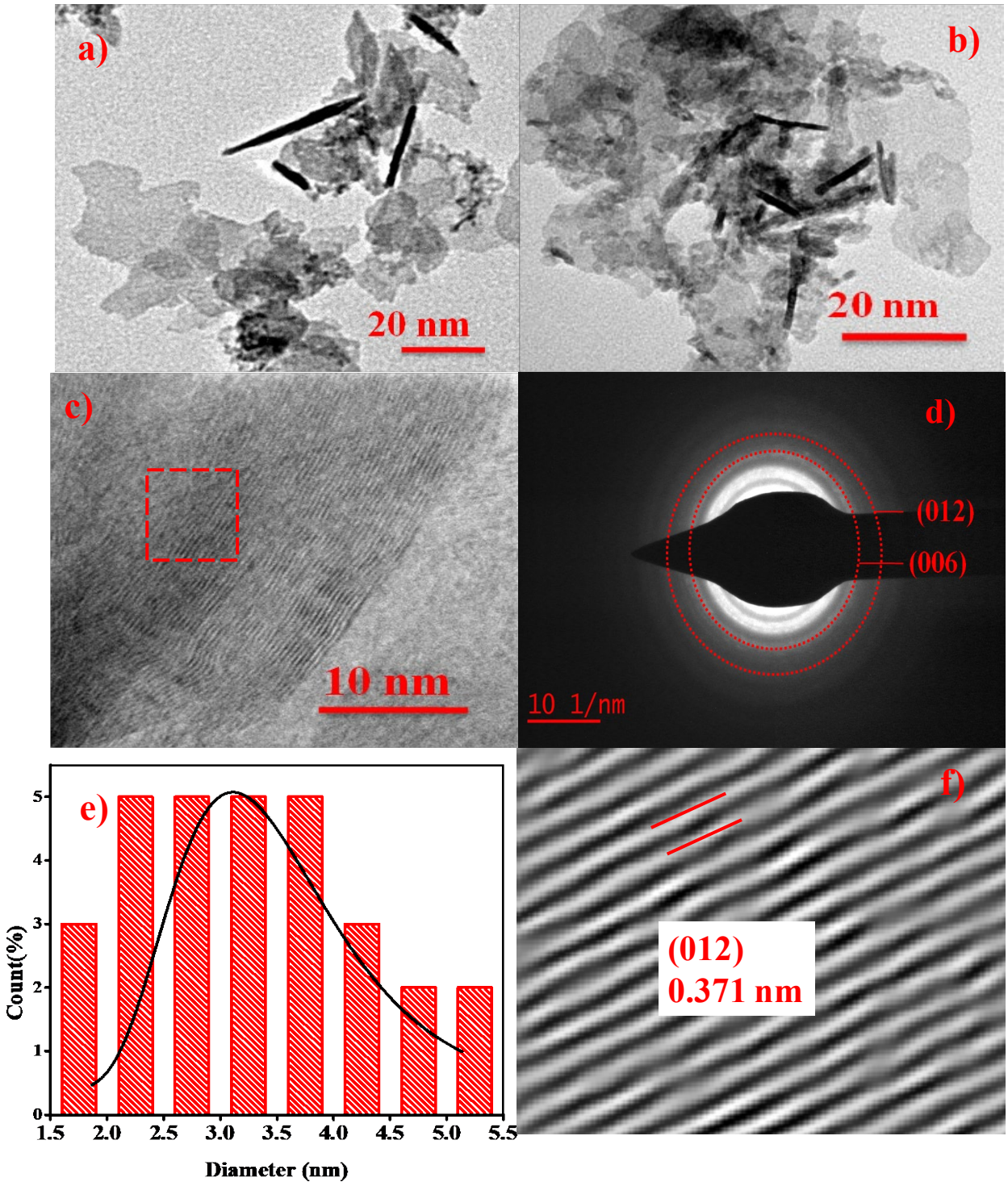

Fig.5.2. (a-c) HRTEM images d) SAED e) particle size distribution curve and f) lattice fringes of Ni-Al LDH.Bi_2O_3

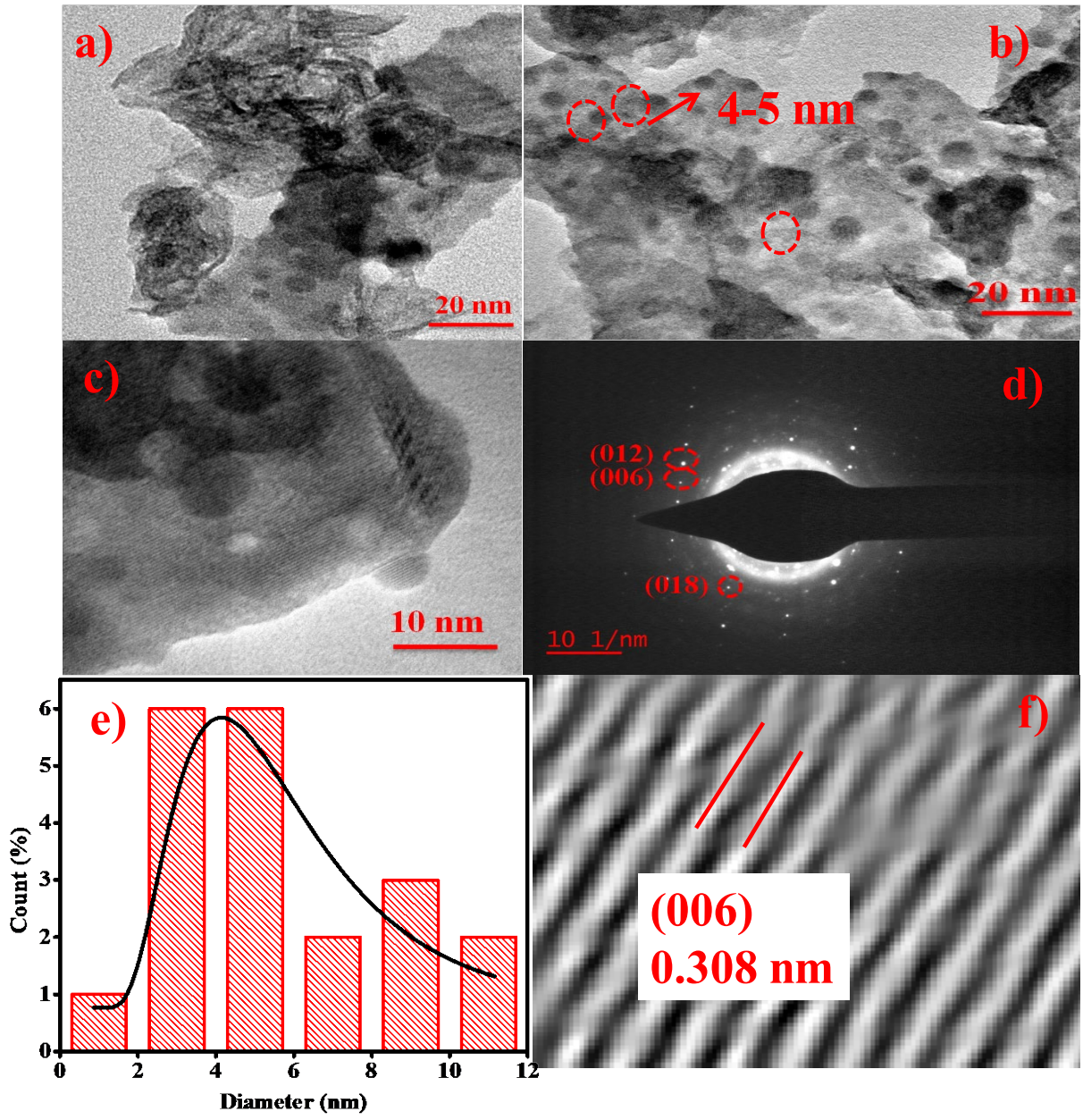

Fig.5.3. (a-c) HRTEM images d) SAED e) particle size distribution curve and f) lattice fringes of Ni-Al LDH.$2Bi_2O_3$

Fig 5.4, 5.5 displays the XPS spectrum of Ni-Al LDH-.xBi_2O_3 (x=1,2) respectively a) Ni 2p b) Bi 4f and c) O1s d) Al 2p. The peak Ni $2p_{3/2}$ (855.9 -857.1 eV) shows the Ni $(OH)_2$ and peak position at (861.5-861.6) eV of Ni $2p_{3/2}$ represents the satellite peak of $Ni(OH_2)$ and the peak of Ni $2p_{1/2}$ with binding energy at (873.3-873.4) eV represents the Nickel is in its oxide form with +2 valence state i.e NiO and the peak at(878.9 -879.8) eV shows the satellite peak [23]. The binding energies of Bi $4f_{7/2}$ (158.7eV) and $4f_{5/2}$ (164.0 eV) can be referred as Bi_2O_3 indicating the presence of Bi^{3+} ions [24] . The peak position of Al 2p after deconvulation in Fig. 5.4. showed Al $2p_{3/2}$ (73.9 eV) and Al 2p1/2 (74.5eV) indicates the peaks of Al-O and Al-OH i.e Al-oxyhydroxide and Al-hydroxide linkage and Al ions occupy the tetrahedral and octahedral sites [25]. Further, in Fig. 5.5. Al 2p shows peak positions at higher binding energy 76.77 and 77.48 eV which might be ascribed to larger number of oxygen sites are available for metal (Bi) binding , therefore increases binding energy.. Therefore the peak positions at lower and higher binding energy is due to Al-O and Al-OH bonding in AlO_6.

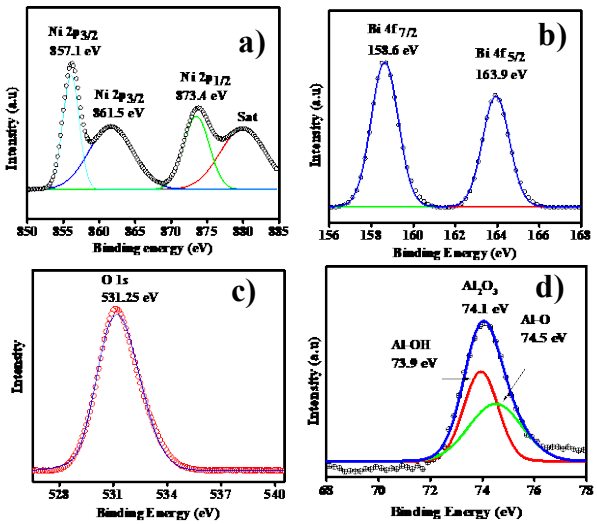

Fig.5.4. a)Ni 2p, b) Bi 4f, c) O 1s and d) Al 2p XPS spectra of Ni-Al LDH. Bi_2O_3 composite.

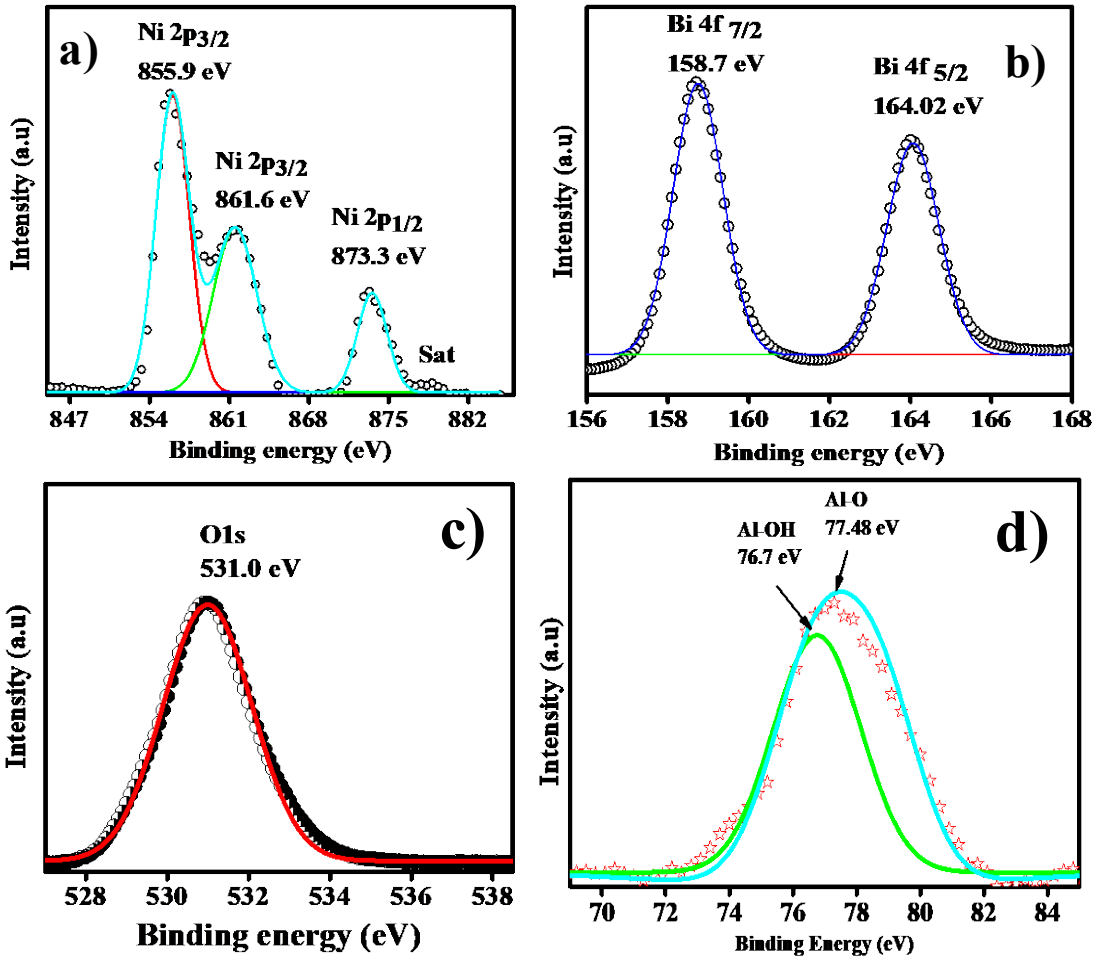

Fig 5.5. a)Ni 2p, b) Bi 4f, c) O 1s and d) Al 2p XPS spectra of Ni-Al LDH-2.Bi_2O_3 heterostructures

5.3.2 Morphology

The scanning electron microscopy of prepared samples is shown in fig.5.6 (a-b) of Ni-Al LDH-Bi_2O_3 (1:1), (c-d) of Ni-Al LDH-Bi_2O_3 (1:2) nanostructures. The images show the irregular morphology with sphere type clusters agglomerated together and particle size range in between the micrometers. It has been clearly seen that there is no change in the morphological properties after doubling the Bi_2O_3 nanoparticles ratio. Similarly EDS spectrum of Ni-Al LDH.x Bi_2O_3 (x = 1, 2) heterostructured is shown in the Fig (5.7a) and fig (5.7b) . This spectrum shows the

presence of Ni, Al, Bi and O elements in both the samples and their atomic weight percent shows that there is no extra peak observed for any other element indicating that the sample is pure in

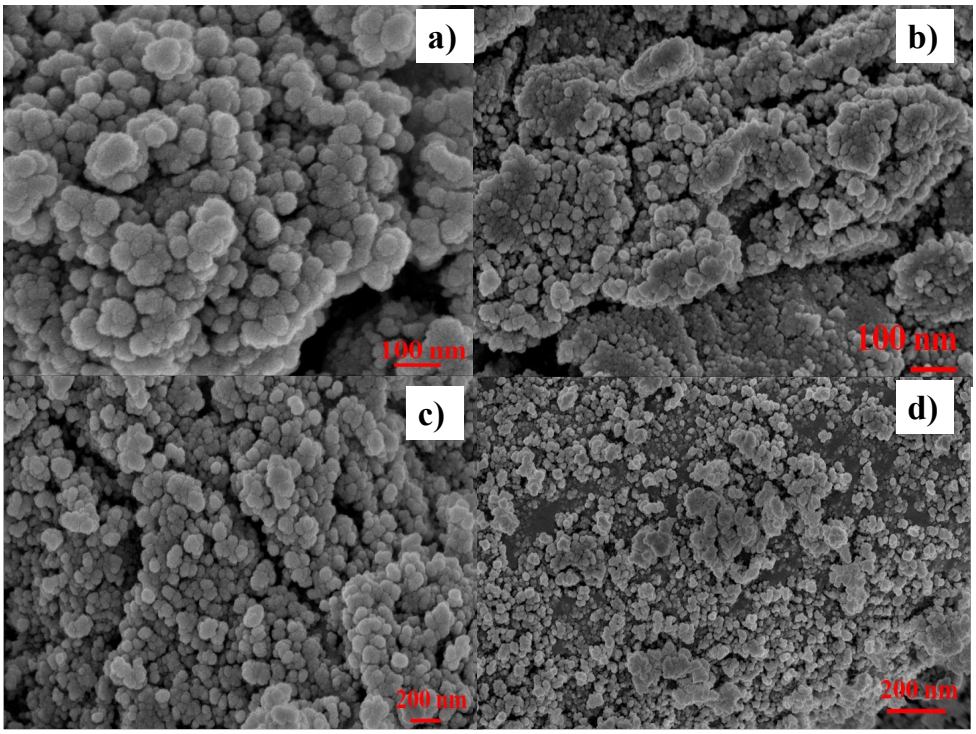

Fig.5.6.(a-b) FESEM images of Ni-Al LDH.xBi_2O_3. (x=1) and (c-d), (x=2) hybrids.

nature. These studies confirm the formation of hetero-structure of Ni-Al LDH.xBi_2O_3 and therefore good foe adsorption performance. Further, the elemental mapping (Fig 5.8) indicating that Bi_2O_3 particles are uniformly dispersed over the surface of Ni-Al LDH.

Dynamic light scattering of the prepared microstructures (Fig.5.9a) indicates that size of pure Ni-Al LDH is 491 nm. After bismuth incorporation the size increases gradually from 491 nm to 739 nm. As from the results it can be demonstrated that spherical size of Bi_2O_3 nanoparticles starts increasing which is in consistent with HRTEM image. In comparison to bare, Ni-Al LDH-Bi_2O_3 (1:1) exhibits larger size i.e. 693 nm which suggest that there is Bi_2O_3 particles plays a significant role. Presence of Bi_2O_3 particles on the surface of LDH increases the hydrodynamic size.

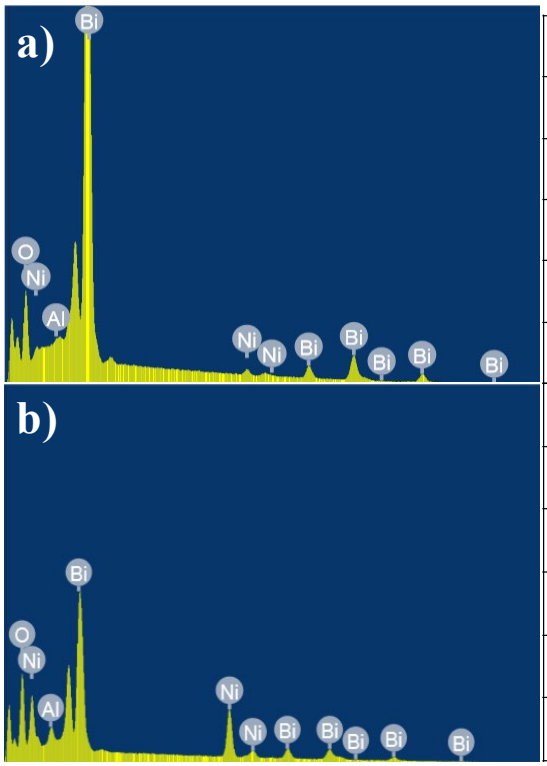

Element	Weight %	Atomic %
O K	34.20	77.52
Al K	1.80	2.42
Ni K	20.16	12.45
Bi M	43.83	7.61
Total	100.00	

Element	Weight %	Atomic %
O K	24.780	80.25
Al K	0.16	0.31
Ni K	1.32	1.16
Bi M	73.74	18.28
Total	100.00	

Fig.5.7. EDS spectrum of Ni-Al LDH.xBi_2O_3 (x = 1, 2) heterostructured showing compositional uniformity

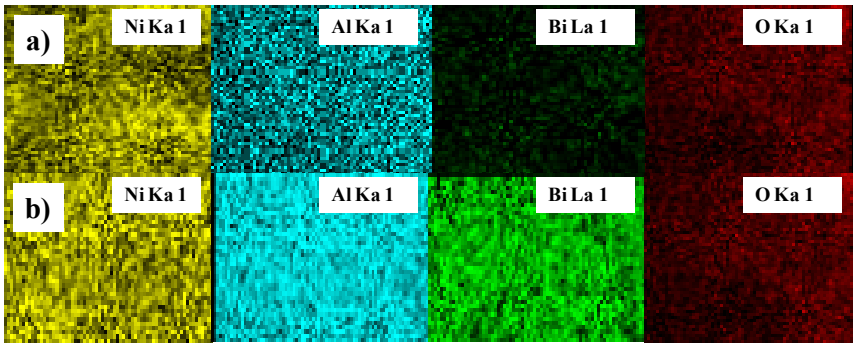

Fig.5.8. Elemental mapping of a) NALB1 b) NABL2 showing compositional uniformity.

The variation in the surface properties of prepared samples has been investigated in fig. 5.9 (b).The zeta potential value of pure Ni-Al LDH is -24.9 mV which demonstrates that the pure LDH has negative surface charge in aqueous solvent. By increasing the amount of Bi_2O_3, the bismuthate ions (Bi^{3+}) will starts neutralizing the negative charge. After that it will starts increasing gradually and the value become less negative for prepared sample i.e -6.65 mV for Ni-Al LDH-Bi_2O_3 (1:1) and 8.79 mV for Ni-Al LDH-Bi_2O_3 (1:2).

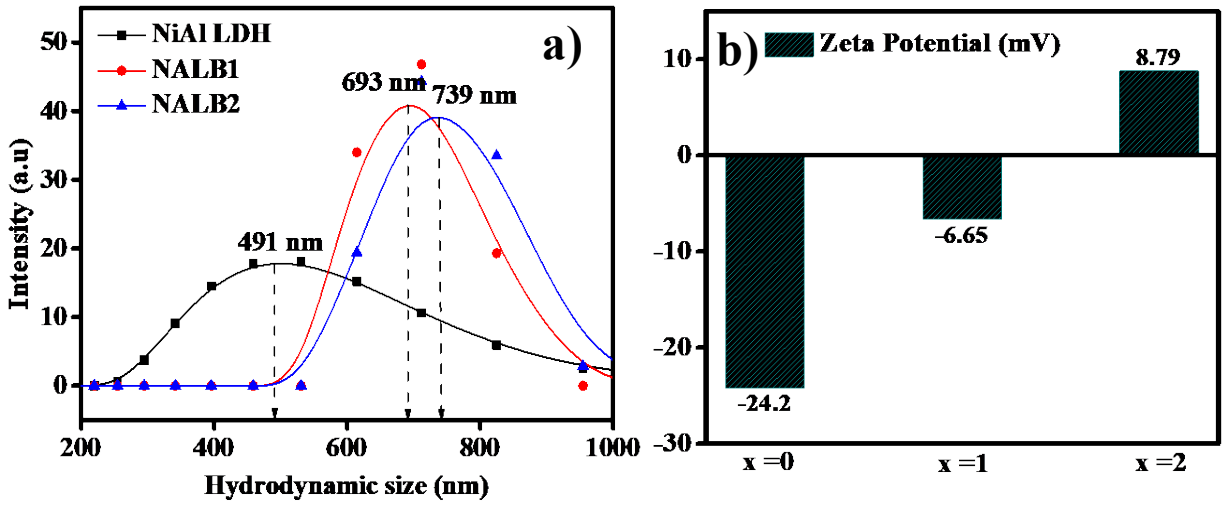

Fig.5.9. DLS hydrodynnamic particle size of Ni-Al LDH.x Bi_2O_3 (x=1,2) composite and b) variation of zeta potential of Ni-Al LDH .x Bi_2O_3 (x=1,2) heterostructures.

5.4 Adsorption isotherms

The variation in the absorbance spectra has been shown in fig.5.10. The NPX in mixture displays highest adsorption capacity is 77% in case of Ni-Al LDH-Bi_2O_3 (1:2) which is almost double in comparison to when it is bare and 72% with MB in case of Ni-Al LDH-Bi_2O_3 (1:1). The reason for NPX and MB adsorption is due to the following reason: the zeta potential i.e. -6.65 mV of Ni-Al LDH-Bi_2O_3 (1:1) and 8.79 mV for Ni-Al LDH-Bi_2O_3 (1:2). The NPX exhibits more

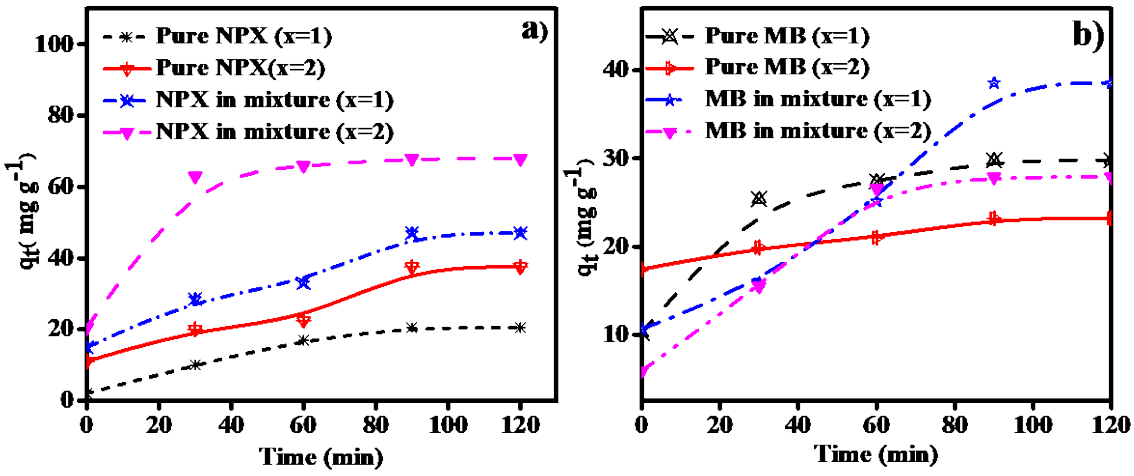

Fig.5.10. Variation in adsorption capacity a) NPX b) MB using different nanocatalysts.

adsorption capacity in case of mixture of MB and NPX using Ni-Al LDH-Bi_2O_3 (1:2) catalyst. As this catalyst has positive surface charge, therefore due to electrostatic interaction s between the NPX substrate and catalyst, this will attract more substrate molecule towards itself because of negative surface charge properties of NPX molecule. Therefore, it will absorb more towards the 1:2 catalyst in comparison to 1:1. NPX , shows more adsorption properties when it is in mixture with MB in comparison to when it is in bare form. As 1:1 catalyst has a negative surface charge , still NPX adsorb to a large extent , this might be due to reason that , as the surface is negative charge and firstly MB molecules will attract towards the negative surface and neutralize the catalyst surface . After that second layer of NPX, will get adsorbed on the neutralized surface and that will enhanced the adsorption capacity which is nearly 53 % in comparison to bare. Similarly the MB shows adsorption capacity i.e. 72 % in case of Ni-Al LDH-Bi_2O_3 (1:1). The reason behind is negative surface charge i.e. -6.65 mV. The MB exhibits maximum adsorption in case of when it is present in mixture with NPX followed by when it is present alone. The higher adsorption capacity in this case is due to its negative zeta potential value which will attract more substrate molecules of MB towards itself and showed greater adsorption. And the surface with positive charge will repel the MB molecules and therefore shows lesser adsorption capacity. But

in case of 1:2 , when the MB is present with NPX solution firstly, NPX molecules will develop a negative charge by forming layer and then on the negative surface, these MB molecules will gets attracted and show the adsortion 53%.

The Langmuir [26] and Freundlich [27]fig.5.11 and 5.12. adsorption models and their adsorption parameters table 5.1 ,5.2,5.3 and 5.4 were studied to determine the data. The equations for the linearlized forms of these models are given below:

$$\frac{C_e}{q_e} = \frac{C_e}{q_{max}} + \frac{1}{K_L q_{max}}$$

$$\log q_e = \log K_F + \frac{1}{n} \log C_e$$

where q_{max} represents the adsorption quantity at maximum; q_e shows adsorption capacity at equilibrium; C_e is the NPX and MB concentration at equilibrium; K_L represents the Langmuir constant and K_F is Freundlich constants respectively; where n is the intensity factor. The parameter for NPX and MB removal using the prepared samples are displayed in Table 5.1 and Table 5.2. The R^2 values indicate that the adsorption process follow Langmuir adsorption isotherm model. Also its K_L value lies in between 0 and 1. The R^2 value displays that the adsorption process does not follows Freundlich isotherm model. As Langmuir model is monovalent / single layer model and freundlich is multilayered. So adsorption here follows monovalent / single layer adsorption as it is evident with the zeta potential values .Due to the electrostatic interaction between the adsorbate and adsorbent first layer will form after that layer will change the surface charge properties second substrate molecule will a adsorbed on the surface and vice versa.

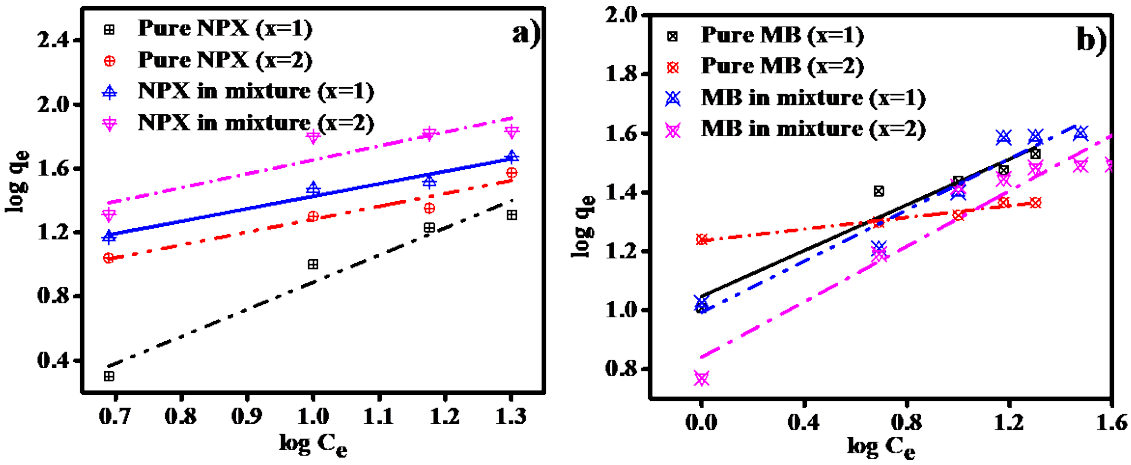

Fig.5.11. Lines fitted using the linearized Langmuir isotherm models for a) NPX b) MB adsorption using Ni-Al LDH.xBi_2O_3

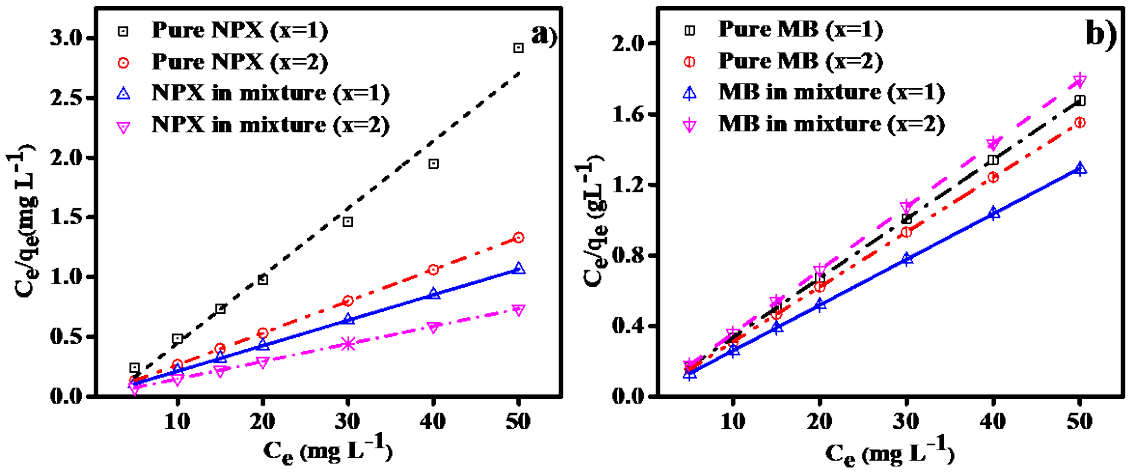

Fig.5.12. Lines fitted using the Freundlich isotherm models for a) NPX b) MB adsorption using Ni-Al LDH.xBi_2O_3

Ni-Al LDH.xBi_2O_3	q_{max}(mg g-1)	K_L	Substrate	R^2
x=1	29.79	0.0080	Methylene Blue	0.9501
x=2	32.20	0.0081	Methylene Blue	0.9523
x=1	38.71	0.0075	Methylene Blue in mixture	0.9845
x=2	27.94	0.0068	Methylene Blue in mixture	0.9953

Table 5.1 Parameters as per Langmuir asdorption isotherm models for Ni-Al LDH.xBi_2O_3 hybrid structures at 298K for methylene blue.

NiAl LDH-.xBi_2O_3	q_{max}(mg g^{-1})	K_L	Substrate	R^2
x=1	17.72	0.4807	Naproxen	0.881
x=2	37.63	0.0075	Naproxen	0.791
x=1	46.97	0.0035	Naproxen in mixture	0.692
x=2	68.02	0.01246	Naproxen in mixture	0.783

Table 5.2 Parameters as per Langmuir asdorption isotherm models for Ni-Al LDH.xBi_2O_3 hybrid structures at 298K for naproxen.

Ni-Al LDH .xBi_2O_3	K_F	n	Substrate	R^2
x=1	1.105	0.589	Naproxen	0.945
x=2	1.599	1.243	Naproxen	0.905
x=1	1.905	1.284	Naproxen in mixture	0.913
x=2	2.376	1.152	Naproxen in mixture	0.978

Table 5.3 Parameters as per Freundlich asdorption isotherm models for Ni-Al LDH.xBi_2O_3 hybrid structures at 298K for naproxen.

Ni-Al LDH .xBi_2O_3	K_F	n	Substrate	R^2
x=1	23.06	0.02	Methylene Blue	0.9987
x=2	40.04	0.14	Methylene Blue	0.9854
x=1	49.55	0.16	Methylene Blue in mixture	0.9658
x=2	68.54	0.11	Methylene Blue in mixture	0.9782

Table 5.4 Parameters as per Freundlich asdorption isotherm models for Ni-Al LDH.xBi_2O_3 hybrid structures at 298K for methylene blue.

5.4.1 Adsorption Kinetics

To demonstrate the adsorption performance more, pseudo-first-order [28], pseudo-second-order [29-30], kinetic models are applied.

$$\frac{t}{q_t} = \frac{1}{k_2 q_e^2} + \frac{t}{q_e}$$

$$\log(q_e - q_t) = \log q_e - \frac{k_1 t}{2.303}$$

The q_e and q_t represent the adsorption capacity at equilibrium and time t, k_1, k_2 are the rate constants of pseudo-first-order and pseudo-second-order kinetics. The linearlized fitted lines for the adsorption kinetics are displayed in Figs5.13 and 5.14. The corresponding correlation factors and their respective parameters and are given in Table 5.5 ,5.6,5.7 and 5.8 The correlation coefficient value (R^2) suggest that NPX follows pseudo second order kinetics and the pseudo first order kinetics in case of MB. The resultant data indicated that the determined adsorption data in case of NPX is consistent with the pseudo second order kinetics and for for MB it is more consistent with the pseudo first order model.

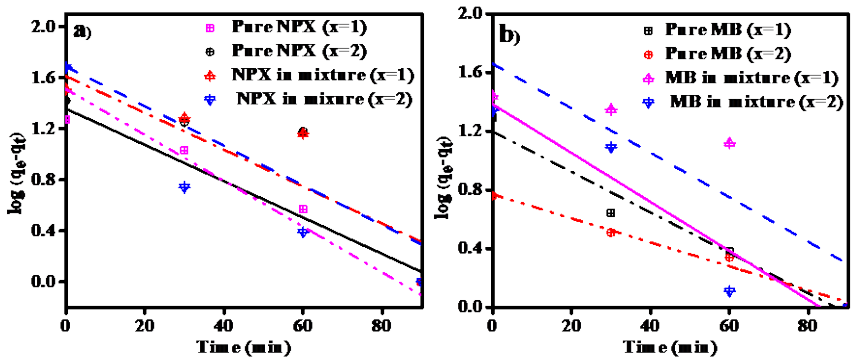

Fig.5.13.Pseudo-first-order (a) naproxen (b)methylene blue models for as prepared nanostructures.

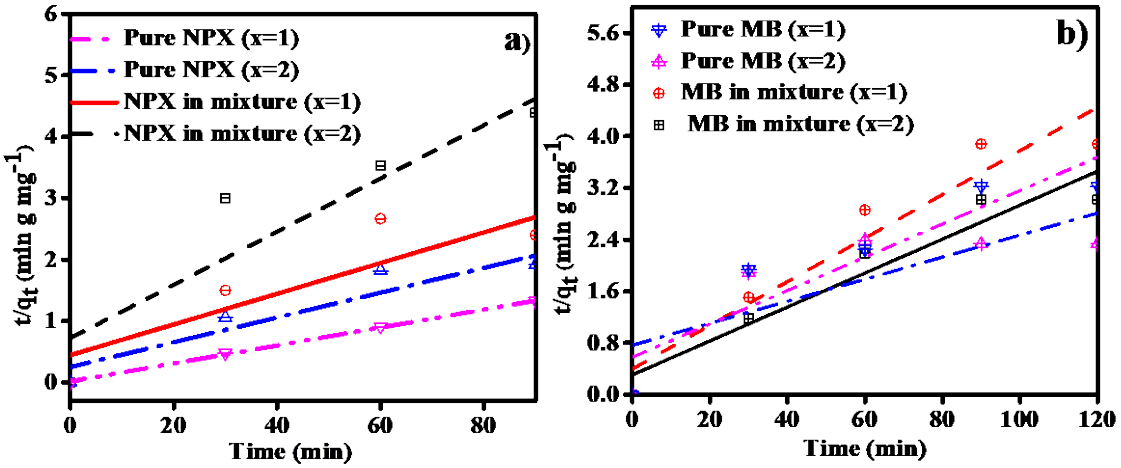

Fig.5.14.Pseudo-second-order (a) naproxen (b) methylene blue models for as prepared Ni-Al LDH.xBi_2O_3 nanostructures

Ni-Al LDH .xBi_2O_3	q_e(mg g-1)	K_1	Substrate	R^2
x=1	15.78	3.1×10^{-2}	Methylene Blue	0.9489
x=2	5.88	1.8×10^{-2}	Methylene Blue	0.8523
x=1	45.70	3.4×10^{-2}	Methylene Blue in mixture	0.9565
x=2	24.26	3.8×10^{-2}	Methylene Blue in mixture	0.9123

Table 5.5 kinetic parameters for the as-prepared Ni-Al LDH.xBi_2O_3 hetero-structures for methylene blue using pseudo-first order model.

Ni-Al LDH .xBi$_2$O$_3$	q_e(mg g-1)	K_1	Substrate	R^2
x=1	22.80	3.2×10^{-2}	Naproxen	0.9071
x=2	32.43	3.2×10^{-2}	Naproxen	0.9071
x=1	48.64	3.4×10^{-2}	Naproxen in mixture	0.9071
x=2	40.98	3.9×10^{-2}	Naproxen in mixture	0.9123

Table 5.6 kinetic parameters for the as-prepared Ni-Al LDH.xBi$_2$O$_3$ hetero-structures for naproxen using pseudo-first order model.

Ni-Al LDH .xBi$_2$O$_3$	q_e(mg g-1)	K_1	Substrate	R^2
x=1	38.08	2.2×10^{-3}	Methylene Blue	0.809
x=2	29.61	2.8×10^{-3}	Methylene Blue	0.843
x=1	58.65	0.3×10^{-3}	Methylene Blue in mixture	0.825
x=2	38.74	1.1×10^{-3}	Methylene Blue in mixture	0.836

Table 5.7 kinetic parameters for the as-prepared Ni-Al LDH.xBi$_2$O$_3$ hetero-structures for methylene blue using pseudo-second- order model.

Ni-Al LDH .xBi$_2$O$_3$	q_e(mg g-1)	K_1	Substrate	R^2
x=1	22.80	3.2×10^{-2}	Naproxen	0.9071
x=2	32.43	3.2×10^{-2}	Naproxen	0.9071
x=1	48.64	3.4×10^{-2}	Naproxen in mixture	0.9071
x=2	40.98	3.9×10^{-2}	Naproxen in mixture	0.9123

Table 5.8 kinetic parameters for the as-prepared Ni-Al LDH.xBi$_2$O$_3$ hetero-structures for napeoxen using pseudo-second- order model

The q_{max} values in bar plot with different as prepared nanocatalyst were shown in fig. 5.15.

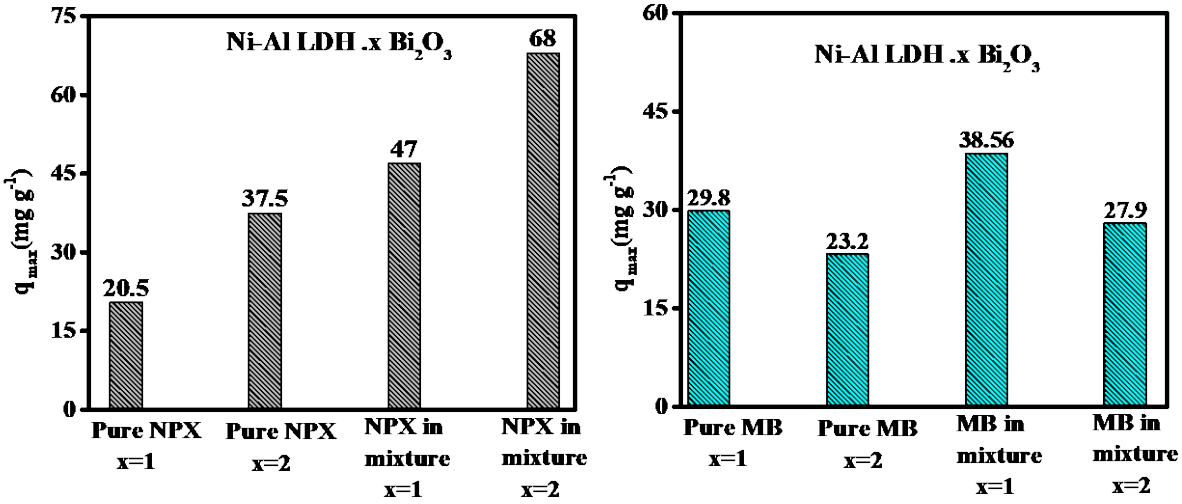

Table 5.15 Adsorption capacity values for the as-prepared Ni-Al LDH.xBi$_2$O$_3$ hetero-structures for naproxen and methylene blue.

5.5. Conclusion

In summary, here we report simple co-precipitation method to synthesize the NiAl-Bi_2O_3 heterostructures. The NALB-1 exhibits negative surface charge thereby favour MB adsorption to a great extent and NALB-B exhibits positive surface, therefore resulting favourable adsorption of NPX. After multilayer formation, in case of mixture both will get attracted towards to their respective surface and resulting favourable adsorption in comparison to the bare ones. Both the substrate follows freundlich adsorption isotherm because it is multilayer adsorption not single layer. Further, NPX follows second order kinetics and MB follows pseudo first order model. Such structure property correlation can be extremely beneficial for designing new generation materials for water treatment. Also, considering the simpler synthetic route, low cost and high adsorption capacity these materials can act as superior adsorbent compare to conventional analogues for better removal of pharmaceutical and dye contaminants.

References

1. Rasheed T, Bilal M, Nabeel F, Adeel M, Iqbal HMN. Environmentally-related contaminants of high concern: Potential sources and analytical modalities for detection, quantification, and treatment. Environ Int. 2019 Jan 1;122:52–66.
2. Katheresan V, Kansedo J, Lau SY. Efficiency of various recent wastewater dye removal methods: A review. J Environ Chem Eng [Internet]. 2018;6(4):4676–97. Available from: https://doi.org/10.1016/j.jece.2018.06.060
3. Cycon M, Borymski S, Zolnierczyk B, Piotrowska-Seget Z. Variable effects of non-steroidal anti-inflammatory drugs (NSAIDs) on selected biochemical processes mediated by soil microorganisms. Front Microbiol [Internet]. 2016;7(DEC). Available from: www.frontiersin.org
4. Bashir I, Lone FA, Bhat RA, Mir SA, Dar ZA, Dar SA. Concerns and Threats of Contamination on Aquatic Ecosystems. 2020; Available from: https://doi.org/10.1007/978-3-030-35691-0_1
5. Qasem NAA, Mohammed RH, Lawal DU. Removal of heavy metal ions from wastewater: a comprehensive and critical review. npj Clean Water [Internet]. 2021;4(1). Available from: https://doi.org/10.1038/s41545-021-00127-0
6. Barakat MA. New trends in removing heavy metals from industrial wastewater. Arab J Chem. 2011 Oct 1;4(4):361–77.

7. Ambaye TG, Vaccari M, van Hullebusch ED, Amrane A, Rtimi S. Mechanisms and adsorption capacities of biochar for the removal of organic and inorganic pollutants from industrial wastewater. Int J Environ Sci Technol [Internet]. 2021;18(10):3273–94. Available from: https://doi.org/10.1007/s13762-020-03060-w
8. Chikri R, Elhadiri N, Benchanaa M, El Y. Efficiency of Sawdust as Low-Cost Adsorbent for Dyes Removal. 2020; Available from: https://doi.org/10.1155/2020/8813420
9. Velasco JI, Ardanuy M, Antunes M. Layered double hydroxides (LDHs) as functional fillers in polymer nanocomposites. Adv Polym Nanocomposites Types Appl. 2012;91–130.
10. Hong J, Zhang W, Wang Y, Zhou T, Xu R. Photocatalytic reduction of carbon dioxide over self-assembled carbon nitride and layered double hydroxide: The role of carbon dioxide enrichment. ChemCatChem. 2014;6(8):2315–21.
11. Daniel S, Thomas S. Layered double hydroxides: fundamentals to applications. Layer Double Hydroxide Polym Nanocomposites. 2020;1–76.
12. Ye H, Liu S, Yu D, Zhou X, Qin L, Lai C, et al. Regeneration mechanism, modification strategy, and environment application of layered double hydroxides: Insights based on memory effect. Coord Chem Rev. 2022 Jan 1;450:214253.
13. Johnston AL, Lester E, Williams O, Gomes RL. Understanding Layered Double Hydroxide properties as sorbent materials for removing organic pollutants from environmental waters. J Environ Chem Eng. 2021 Aug 1;9(4):105197.
14. Zhao Y, Jia X, Waterhouse GIN, Wu LZ, Tung CH, O'Hare D, et al. Layered Double Hydroxide Nanostructured Photocatalysts for Renewable Energy Production. Adv Energy Mater. 2016 Mar 23;6(6).
15. Kang Q, Zhou W, Li Q, Gao B, Fan J, Shen D. Adsorption of anionic dyes on poly(epicholorohydrin dimethylamine) modified bentonite in single and mixed dye solutions. Appl Clay Sci. 2009 Aug 1;45(4):280–7.
16. Seo PW, Khan NA, Hasan Z, Jhung SH. Adsorptive Removal of Artificial Sweeteners from Water Using Metal-Organic Frameworks Functionalized with Urea or Melamine. ACS Appl Mater Interfaces [Internet]. 2016;8(43):29799–807. Available from: www.acsami.org
17. Lach J, Szymonik A. Adsorption of naproxen sodium from aqueous solutions on commercial activated carbons. J Ecol Eng [Internet]. 2019 Nov 1 [cited 2022 Jan 11];20(10):241–51. Available from: http://www.journalssystem.com/jeeng/Adsorption-of-naproxen-sodium-from-aqueous-solutions-on-commercial-activated-carbons,113419,0,2.html
18. Chan OS, Cheung WH, McKay G. Single and multicomponent acid dye adsorption equilibrium studies on tyre demineralised activated carbon. Chem Eng J [Internet]. 2012;191:162–70. Available from: http://dx.doi.org/10.1016/j.cej.2012.02.089
19. Bharali D, Deka RC. Adsorptive removal of congo red from aqueous solution by sonochemically synthesized NiAl layered double hydroxide. J Environ Chem Eng [Internet]. 2017;5(2):2056–67. Available from: http://dx.doi.org/10.1016/j.jece.2017.04.012
20. Kumari P, Das RK, Pal B. Enhanced photocatalytic degradation of eco-toxic pharmaceutical waste diclofenac sodium by anion loaded Cu-Al LDH·Bi2O3 composites. J Taiwan Inst Chem Eng [Internet]. 2021;129:227–36. Available from: https://doi.org/10.1016/j.jtice.2021.07.023

21. Kumari P, Pal B, Das RK. Superior adsorptive removal of eco-toxic drug diclofenac sodium by Zn–Al LDH·xBi2O3 layer double hydroxide composites. Appl Clay Sci [Internet]. 2021;208(November 2020):106119. Available from: https://doi.org/10.1016/j.clay.2021.106119
22. Guo Y, Liu X, Wang X, Iqbal A, Yang C, Liu W, et al. Carbon dot/NiAl-layered double hydroxide hybrid material: facile synthesis, intrinsic peroxidase-like catalytic activity and its application. RSC Adv. 2015;5(116):95495–503.
23. Shao D, Li P, Wang D, Zhao C, Zhao C. High OER performance Ni(OH)2 with hierarchical structure. J Solid State Electrochem [Internet]. 2019;23(7):2051–60. Available from: https://doi.org/10.1007/s10008-019-04299-1
24. Fan H, Wang G, Hu L. Infrared, Raman and XPS spectroscopic studies of Bi2O3-B2O3-Ga2O3 glasses. Solid State Sci. 2009 Dec 1;11(12):2065–70.
25. Ogugua SN, Ntwaeaborwa OM, Swart HC. Luminescence, structure and insight on the inversion degree from normal to inverse spinel in a ZnAl(2-x)Fex3+O4system. Bol la Soc Esp Ceram y Vidr [Internet]. 2021;60(3):147–62. Available from: https://doi.org/10.1016/j.bsecv.2020.02.005
26. Keskin Avci S, Erucar I. Porous Materials. Compr Energy Syst. 2018 Feb 7;2–5:182–203.
27. Singh NB, Susan ABH. Polymer nanocomposites for water treatments. Polym Nanocomposites Energy Environ Appl A Vol Woodhead Publ Ser Compos Sci Eng. 2018 Jan 10;569–95.
28. Kalonia DS, Simonelli AP. Analysis of Consecutive Pseudo-First-Order Reactions I: An Evaluation of Available Methods to Calculate the Rate Constants from Co-Product or Co-Reactant Data. J Pharm Sci. 1988 Dec 1;77(12):1055–61.
29. Ho YS, McKay G. Pseudo-second order model for sorption processes. Process Biochem. 1999 Jul 1;34(5):451–65.
30. Shaaban M, Abid M. Biochar as a sorbent for organic and inorganic pollutants. Sorbents Mater Control Environ Pollut. 2021;189–208.

Conclusion and future aspects

In summary here we report simple methodology to enhance the adsorption capacity of LDHs (Cu-Al, Ni-Al and Zn-Al) based hybrid micro-composites. The pristine LDH is having negative/positive surface charge thereby resulting unfavorable adsorption of anionic/cationic adsorbate such as NPX, DCF. The adsorption process follows Langmuir and frendulich adsorption isotherm. Thus , the current findings revealed that physiochemical properties of Bi_2O_3 were improved by loading different LDHs or metal ions. Such LDH-Bi_2O_3 based nanomaterials may be efficient materials for the degradation and adsorption of harmful environment pollutants. Therefore, the current work had opened a new dimension in the area of enhancing the photo catalytic activity of layered double hydroxide by loading on the surface of Bi_2O_3 and their applications towards waste-water treatment. In this way, detailed study had been done, but there are still few points which could be followed to extend the research work.

There are large varieties of LDH such as Cu-Zn, Fe-Al, Zn-Fe that are cost effective and exhibit efficient photochemical properties. There are variety of substrate molecules present such as paracetamol, ibufron etc. We had determined the surface properties of LDH based nanomaterials. However, the study of effect of LDH based nanocomposites can be further continued for hydrogen production and reduction reactions as well.

List of publications

1. **Pooja Kumari, Raj Kumar Das and Bonamali Pal,** Preparation and characterization of phase pure monoclinic α-Bi_2O_3 nanoparticles and influence of Ni^{2+} and Cu^{2+} impregnation on their photocatalytic properties. Materials Chemistry and Physics. 2021 Feb 15;260:124173. **IF (4.09)**

2. Pooja Kumari, Bonamali Pal and Raj Kumar Das, Superior adsorptive removal of eco-toxic drug diclofenac sodium by Zn–Al LDH· xBi_2O_3 layer double hydroxide composites. Applied Clay Science. 2021 Jul 1;208:106119. **IF (5.46)**

3. Pooja Kumari, Raj Kumar Das and Bonamali Pal, Enhanced photocatalytic degradation of eco-toxic pharmaceutical waste diclofenac sodium by anion loaded Cu-Al LDH· Bi2O3 composites. Journal of the Taiwan Institute of Chemical Engineers. 2021 Dec 1;129:227-36**. IF (5.87)**

4. Pooja Kumari, Bonamali Pal and Raj Kumar Das Superior cooperative adsorption of methylene blue and naproxen by Ni-Al LDH.xBi_2O_3 layered double hydroxide composites

(Manuscript under preparation)

Other Publications

1.Sakshi Bhardwaj, Diksha Sharma, Pooja Kumari and Bonamali Pal , Influence of photodeposition time and loading amount of Ag co-catalyst on growth, distribution and photocatalytic properties of Ag@TiO_2 nanocatalysts. Optical Materials. 2020 Aug 1;106:109975. **(IF = 3.08)**

Conferences and workshops attended

1. Pooja Kumari and Bonamali Pal, 12th National conference on Chemical and Environmental Sciences: Advanced Innovations-2020 (CESAI-2020), Punjabi University, Patiala, 19-20 February, 2020.

2. Pooja Kumari and Bonamali Pal, Effective research planning and execution using Scopus and Science direct, University of Jammu , 17 December,2021

Materials Chemistry and Physics 260 (2021) 124173

Contents lists available at ScienceDirect

Materials Chemistry and Physics

journal homepage: www.elsevier.com/locate/matchemphys

Preparation and characterization of phase pure monoclinic α-Bi_2O_3 nanoparticles and influence of $Ni^{2+}$and Cu^{2+} impregnation on their photocatalytic properties

Pooja Kumari, Raj Kumar Das, Bonamali Pal *

School of Chemistry and Biochemistry, Thapar Institute of Engineering and Technology, Patiala, 147004, Punjab, India

HIGHLIGHTS

- Improved optical and photocatalytic properties of Ni^{2+} and Cu^{2+} loaded Bi_2O_3 catalysts.
- Greater quenching of emission peak intensities of photocatalysts.
- Superior degradations of naproxen and fuchsin blue under visible light irradiations.

GRAPHICAL ABSTRACT

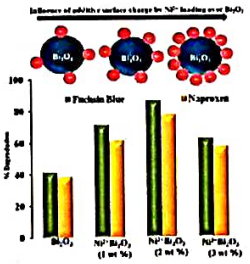

ARTICLE INFO

Keywords:
Impregnated Bi_2O_3
Visible light active
Optical properties
Photocatalytic activity
Naproxen
Fuchsin blue

ABSTRACT

Nowadays, pharmaceutical waste, Naproxen (NPX) as well as the dye fuchsin blue (FB) become hazardous pollutant due to their toxic behavior. Because of toxicity, the efficient removal of them from water has become one of the most vital challenge. Yet, due to high cost, low degradation efficiency, of the known catalyst restrict their real life applications. In this perspective, metal ions impregnated (Ni^{2+} and Cu^{2-}) Bi_2O_3 heterostructures have been investigated as a potential material for photocatalytic degradation of NPX and FB. These materials are synthesized by simple wet-impregnation method and thoroughly characterized by various methods such as XRD, DLS, SEM, EDS, HRTEM, XPS, etc. The diffraction patterns confirm formation of phase pure α-Bi_2O_3 nanoparticles. The zeta potential (−25 mV) of Bi2O3 nanoparicles confirms presence of negatively charges oxide groups in its surface that can act as anchors for divalent anions. The impregnated hybrids shows considerably smaller zeta potential values (−15 and −17 mV for Ni^{2+}-Bi_2O_3 and Cu^{2+}-Bi_2O_3 respectively). The XPS studies reveal presence of surface bound divalent metal ions. The adsorption edge of Ni^{2+}-Bi_2O_3 and Cu^{2+}-Bi_2O_3 nanostructures were shifted slightly towards lower frequency. The photoluminescence spectrum impregnated materials shows significant quenching compare to pristine Bi_2O_3. suggesting lesser degree electron-hole recombination upon metal loading. Due to the photocatalytic degradation efficiencies of both Ni^{2+}-Bi_2O_3 (87% for FB and 79% for NPX) and Cu^{2+}-Bi_2O_3 (73% for FB and 70% for NPX) heterostructures are significantly higher compare to the pristine one (43% for FB and 40% for NPX). The photodegradation process obeys the pseudo first order kinetics. Due to simpler synthesis and enhanced activity metal ion loaded Bi_2O_3 photocatalysts can be potential photo-catalysts for removing NPX and FB from wastewater.

* Corresponding author.
E-mail address: bpal@thapar.edu (B. Pal).

https://doi.org/10.1016/j.matchemphys.2020.124173
Received 2 August 2020; Received in revised form 11 November 2020; Accepted 12 December 2020
Available online 15 December 2020

Applied Clay Science 208 (2021) 106119

Contents lists available at ScienceDirect

Applied Clay Science

journal homepage: www.elsevier.com/locate/clay

Research Paper

Superior adsorptive removal of eco-toxic drug diclofenac sodium by Zn–Al LDH·xBi_2O_3 layer double hydroxide composites

Pooja Kumari, Bonamali Pal, Raj Kumar Das *

School of Chemistry and Biochemistry, Thapar Institute of Engineering and Technology, Patiala 147004, Punjab, India

ARTICLE INFO

Keywords:
Diclofenac sodium adsorption
Layer double hydroxides
Zn-Al LDH·xBi_2O_3 composites
Reversal of zeta potential
Pharmaceutical waste removal

ABSTRACT

Recently, efficient removal of eco-toxic pollutant diclophenac sodium (DCF) from wastewater is emerging as crucial problem. However, low adsorption capacity, high cost of conventional adsorbents limits their utility. In this context, Bi_2O_3 loaded Zn–Al layer double hydroxide (LDH) heterostructures (Zn–Al LDH·xBi_2O_3, x = 0 to 3) have been investigated as a potential adsorbent for DCF removal. These materials are prepared by solvothermal-solvent evaporation method, and systematically characterized by several techniques e.g. XRD, SEM, EDS, HRTEM, XPS, BET and DLS etc. The XRD patterns confirms formation of both LDH and α-Bi_2O_3 phases. The flower-like morphology is evident by SEM. XPS and EDS confirm Bi_2O_3-LDH composite. Higher Bi_2O_3 loading leads to increase in the hydrodynamic sizes of the composite structure. The BET surface area and zeta potential also varies significantly with extent of loading. DCF adsorption of these composites obey the Langmuir adsorption isotherm model suggesting monolayer adsorption process whereas the intra-particle diffusion model indicates that the adsorption of DCF primarily occurs on the exterior surface. The heterostructure with x = 1 exhibited ~10 times higher adsorption capacity compared to bare LDH owing to its highest surface area and positive zeta potential. Due to high adsorption capacities, low cost and easy DCF removal process, these materials could act as efficient adsorbents for removal of DCF and other pollutants from waste water.

1. Introduction

Emerging pollutants are a class of fabricated compounds that have been detected in surface water at minute amounts (Wooding et al., 2017; Houtman, 2010; Ealias and Saravanakumar, 2017; Li et al., 2017). They enter aquatic ecosystem through various pathways, for example, release of wastewater from medical clinics or pharmaceutical manufacturing zones, animal wastewater from poultry, aquaculture, etc. (Wang et al., 2018; Lv et al., 2015; Pan and Xing, 2012; Eichert et al., 2008). Among several the pharmaceutical wastes are recently identified as a new class of contaminants those hare having significant eco-toxicity even at a very low concentration (ppb to ppm level) (Diniz et al., 2015; Patel et al., 2019). Due to such environmental significance, efficient removal of these pollutants has drawn substantial attention in recent years (Kumari et al., 2021; Shin et al., 2021; Zhang et al., 2021; Li et al., 2019a). The non-steroid anti-inflammatory drug Diclofenac sodium (DCF) has been used for the osteoarthritis treatment (Xiong et al., 2019). However, it established a significant concern as it is neither biodegradable nor simple to be expelled completely from water by conventional treatment method (Shalauddin et al., 2019; Shao et al., 2017). Among different methods, including ion exchange (Morales-Zarate et al., 2018), precipitation (Li et al., 2019b), advanced oxidation and biological, adsorption is considered to an effective approach for treating emerging pollutants due to its high feasibility, effective efficiency and simplicity over a broad concentration range (Oturan and Aaron, 2014; Azimi et al., 2017; Campo and Di Bella, 2019). There has been rising amount of research on the preparation of suitable adsorbents for removing diclofenac sodium from water (Xiong et al., 2019; Ghavi et al., 2020; Bhadra et al., 2016; Jauris et al., 2016). However, slow adsorption capacity, high cost and low regeneration ability of these adsorbents are still challenges to wide scale operation. Therefore, an inexpensive and effective adsorbent catalyst with high diclofenac removal efficiency is urgent.

Layered double hydroxides (LDH) are a class of layered material having exchangeable anions intercalated between positive charged layers. These materials have been attracted significant attraction in the field of wastewater treatment because of the adsorption, catalytic and electrochemical properties (Rahman et al., 2018; Taviot-Guého et al., 2018; Richetta et al., 2017; Gong et al., 2013; Yang et al., 2019; Laipan

* Corresponding author.
E-mail address: rkdas@thapar.edu (R.K. Das).

https://doi.org/10.1016/j.clay.2021.106119
Received 28 November 2020; Received in revised form 12 April 2021; Accepted 25 April 2021
Available online 7 May 2021

ARTICLE IN PRESS

JID: JTICE

[m5G;August 5, 2021;8:38]

Journal of the Taiwan Institute of Chemical Engineers 000 (2021) 1–10

Contents lists available at ScienceDirect

Journal of the Taiwan Institute of Chemical Engineers

journal homepage: www.elsevier.com/locate/jtice

Enhanced photocatalytic degradation of eco-toxic pharmaceutical waste diclofenac sodium by anion loaded **Cu-Al LDH·Bi_2O_3** composites

Pooja Kumari, Raj Kumar Das, Bonamali Pal*

School of Chemistry and Biochemistry, Thapar Institute of Engineering and Technology, Patiala-147004, Punjab, India, Tel: +91-175-239-3443

ARTICLE INFO

Article History:
Received 16 June 2021
Revised 13 July 2021
Accepted 17 July 2021
Available online xxx

Keywords:
Layered double hydroxide composites
Anion Impregnation
Photocatalysis
Diclofenac sodium degradation
Eco-toxic pharmaceutical waste removal
Wastewater treatment

ABSTRACT

Background: Nowadays, the non-steroidal drug diclofenac sodium (DCF) has emerged as hazardous pollutant due to its eco-toxic nature and its efficient elimination from wastewater is emerging as crucial problem. But, low activity, high cost and instability of the conventional photocatalysts restrain their uses.
Method: In this study, different anion impreganted Cu-Al layered double hydroxides (LDH) and Bi_2O_3 derived heterocomposites have been examined as plausible photocatalysts for degradation of DCF under visible light radiation. These composites have synthesized by simple wet impregnation methods and characterized by several methods such as XRD, HR-TEM, XPS SEM-EDX, XPS, DRS, phototuminescence(PL), BET etc.
Significant Findings: The BET sorption isotherms indicate that the anion loaded composites are having larger specific surface area than the pristine one. Also, upon anion impregnation the zeta potential values shift towards more negative values confirming absorption of anions. They show significantly higher (65% for carbonate and 83% for sulphate) photcatalytic activity compare to the parent hybrid (53%). Here, the anions act as efficient electron scavengers to suppress the electron-hole pair recombination. The individual photocatalytic reactions follow pseudo-first order kinetics. Due to low cost, simpler preparation, enhanced activity and recyclability the anion loaded derivatives can emerge as excellent photocatalyst for eradicating DCF.

1. Introduction

Drugs are micro-pollutants recognized in very small quantities. In spite of this, their harmful effects on the nature cannot be ignored, because these molecules act in living organisms [1-3]. Diclofenac sodium (DCF) is one of the non-steroid anti-inflammatory drug (NSAID) that has been very often utilized to treat various chronic inflammatory and degenerative joint diseases for past few decades [4]. Diclofenac is very common drug found in watery environment because of its large consumption [5-8]. Due to its eco-toxicity, continuous intake of DCF can cause several adverse effects [9-11]. Prolonged exposure of DCF can cause various health hazards such as epilepsy [12], psychiatric disorder [13], Kounis Syndrome [14], hallucination [15] etc. Furthermore, it contains a harmful halogenated aliphatic group that can affect the oxidation steps of Krebs cycle [16-17]. Among various physiochemical approaches electrochemical oxidation [18], adsorption [19-22], photo-Fenton process [23-24] photocatalysis [25-28] are the best method for the removal of different emerging pollutants. Layered double hydroxide (LDH) materials are class of layered clays general formula $[M(II)_{1-x}M(III)(OH)_2]^{x+}[A_{x/n}H_2O]^{x-}$ where M(II) and M(III) are the metal cations and A^{n-} is an intercalated anion. The surface charge of LDH materials can be simply tuned by changing pH of the medium as well as controlling the molar ratio of bivalent and trivalent cations. LDH materials are attracting great interests in the emerging areas such as electrochemistry, adsorption, anion exchange and photocatalysis [29-33]. The preparation of visible light active layered double hydroxide is of great interest because of its enormous practical applications. The flexible properties of LDH plays important role in photocatalysis. In comparison to bulk photocatalysts, layered materials showed higher activity due to high surface area and efficient separation of photogenerated electrons and holes [34-36]. Zhao and co-workers reported that Zn-Al LDH possess superior removal efficiency (74.3%) towards photodegradation of Orange II [37]. Furthermore, the large importance of LDH materials is due to its more water absorbing capacity as these water molecules can interact with inter pore as well as outer surface [38]. However, due to the poor light absorption capacity of LDH materials several studies have been reported by combining the LDH with semiconductor that exhibited different properties. Hou and co-workers reported efficient photocatalytic degradation of rhodamine B by Bi_2MoO_6/Zn-Al LDH heterostructures [39]. TiO_2/LDH clay nanocomposites were shown to possess high photocatalytic activity (>90% efficiency) towards phenol and methylene blue removal [40] with. Similarly, Wang research group described decoration of ZnO nanorods on Mg-Al LDH and demonstrated the adsorption as well as photo catalytic activity of different anionic substrates like acid red [41] with

* Corresponding author.
E-mail address: bpal@thapar.edu (B. Pal).

https://doi.org/10.1016/j.jtice.2021.07.023
1876-1070/

Optical Materials 106 (2020) 109975

Contents lists available at ScienceDirect

Optical Materials

journal homepage: http://www.elsevier.com/locate/optmat

Influence of photodeposition time and loading amount of Ag co-catalyst on growth, distribution and photocatalytic properties of $Ag@TiO_2$ nanocatalysts

Sakshi Bhardwaj, Diksha Sharma, Pooja Kumari, Bonamali Pal*

School of Chemistry and Biochemistry, Thapar Institute of Engineering and Technology, Patiala, 147004, Punjab, India

ARTICLE INFO

Keywords:
Ag co-catalysis
Particle size distribution
Effect of photodeposition time
Salicylic acid
Photocatalytic degradation

ABSTRACT

The activity of different wt% Ag co-catalyst over TiO_2 surface under varying UV illuminations (30, 60 and 90 min) for the photodegradation of salicylic acid has been studied. A considerable red shift in the plasmon band was observed with a significant color change (white to light brown) with increased photodeposition time (30–90 min) of Ag over TiO_2. Further, the elemental mapping confirms a continuous increase in the wt% of Ag with increased deposition time from 30 min (0.21 wt%) to 90 min (1.69 wt%). These 1, 3 and 5 wt% Ag deposited nanocatalysts prepared at 90 min duration showed higher activity for the photodegradation of salicylic acid under UV light irradiation compared to their counter parts of 30 and 60 min. The higher rate constant ($k = 2.73 \times 10^{-2}$ min^{-1}) value shown by (5 wt% $Ag)_{90}@TiO_2$ is appreciably higher compared to (1 wt% $Ag)_{90}@TiO_2$ ($k = 2.29 \times 10^{-2}$ min^{-1}) and (3 wt% $Ag)_{90}@TiO_2$ ($k = 2.33 \times 10^{-2}$ min^{-1}) photocatalyst and followed pseudo first order kinetics. The maximum activity of (5 wt% $Ag)_{90}@TiO_2$ catalyst has been credited to higher size, number and distribution of Ag co-catalyst nanoparticles over TiO_2 surface which greatly vary with change in amount and photodeposition time of Ag nanoparticles.

1. Introduction

The unique optical properties of plasmonic metals (M = Cu, Ag and Au) related to collective oscillations of their surface electrons are known as surface plasmonic resonance (SPR) [1–3]. This property renders these metals greater importance in recent times and have been used in different shapes, sizes [4] and forms to further improve the optical and surface properties of TiO_2 photocatalyst. These metals are when photo deposited (Au, Ag, Cu) create traps to capture the photo-induced electrons leading to the formation of reduced metal species on the surface of TiO_2. The increased absorption capability of these $M@TiO_2$ nanoparticles is a consequence of strong SPR effect which leads to electron transfer from metal to the conduction band (CB) of TiO_2. Among these, Au-TiO_2 photocatalysts have been considered to be efficient for environmental [5], water splitting and other energy storage applications. Since, the SPR band of Au NPs depends largely on morphology, size and chemical environment, therefore modification of any of these properties is considered to affect the frequency of plasmon band [6], surface structural and interfacial properties. In this concern, the Falaras and co-workers reported the degradation of azo-dye (methyl orange) two times faster using Au-TiO_2 thin films [7,8] compared to bare TiO_2. Lu and co-workers also reported the phenol oxidation and chromium reduction using mesoporous Au-TiO_2 nanocomposites by varying Au loading amount [9]. Further, Gupta and co-workers also reported the photocatalytic hydrogen production [10,11] using Au modified TiO_2 NPs. Apart from these, the optical absorption, surface structure and particle size of the metallic species have also been established to play an important role in the photocatalytic activity of TiO_2 under visible-light irradiation [12].

Besides various advantages, the higher cost of Au metal makes its use limited and scarce. On the other hand, Cu and Ag nanocomposites are gaining much attention due to their cost effective precursors, easy availability and suitable reduction potentials ($Cu^{+2} = 0.337$ V and $Ag^{+} = 0.799$ V). Literature reveals that the photodeposited Ag over TiO_2 greatly enhances the co-catalytic activity than in oxidised form (Ag^{+}) such as the degradation of malic acid [13]. Ag-TiO_2 thin films have been proven to decolourize the methyl orange much efficiently [14,15]. Apart from pollutant treatment, Ag-TiO_2/Ag/a-TiO_2 based nanocomposites have also been observed to efficiently degrade *E.coli* bacteria [16]. It was observed that the bactericidal effect of these composites was 5.1 times

* Corresponding author.
E-mail address: bpal@thapar.edu (B. Pal).

https://doi.org/10.1016/j.optmat.2020.109975
Received 28 March 2020; Received in revised form 28 April 2020; Accepted 30 April 2020
Available online 12 May 2020